# UNIVERSITY OF SOUTHAMPTON

FACULTY OF ENGINEERING AND THE ENVIRONMENT

Bioengineering Science


# Computational modelling of amino acid transfer interactions in the placenta

by


**Nuttanont Panitchob**


Thesis for the degree of Doctor of Philosophy

December 2015

UNIVERSITY OF SOUTHAMPTON

ABSTRACT

FACULTY OF ENGINEERING AND THE ENVIRONMENT
Bioengineering Science

Doctor of Philosophy

# COMPUTATIONAL MODELLING OF AMINO ACID TRANSFER INTERACTIONS IN THE PLACENTA

by Nuttanont Panitchob

Placental amino acid transport is essential for fetal development during pregnancy. Impaired transport has been associated with restricted fetal growth that can potentially lead to diseases in later life. However, quantitative understanding of placenta transport remains limited and therefore requires investigation. The aim of this study was to develop a computational framework that can represent the amino acid transport system in the placenta as a whole.

The transfer of amino acid across the placenta is mediated by a broad array of specific membrane transporters. Mathematical models, based on carrier-mediated transport theory, were developed to mechanistically represent these transporters. These include accumulative transporters, which use secondary active transport driven by the sodium electrochemical potential; exchangers (antiporters), which swap one substrate for another on different sides of the membrane; and facilitative transporters, which transport substrate along its concentration gradient. The transporter models were thoroughly investigated and validated with experimental data with respect to their mechanistic characteristics and parameter sensitivity. Overall, the models were demonstrated to be adequate in representing the specific transporter behaviours.

There are 20 amino acids, including 9 essential ones, and over 19 different transporters, all of which act on certain overlapping subsets of these amino acids. All transporters must work interdependently for successful transfer of the required amino acids from the maternal to the fetal side; however, this complex process is not fully understood. A compartmental model of placental amino acid transport incorporating kinetic transporter models was developed and revealed to be able to sufficiently capture the integrated transport system. Modelling results clearly demonstrated how modulating specific transporter activity can increase the transport of certain classes of amino acids, but that this comes at the price of decreasing the transport of others, which could have potential implications for developing new clinical treatment options. This integrated modelling approach along with kinetic models of transporters will help in gaining an improved quantitative understanding of epithelial transport in the placenta and other systems and it is ultimately hoped that this will contribute to the development of clinical applications to intervene or prevent impaired-transport related pathologies.

# Contents

# List of Tables

# List of Figures

# List of Publications

1. Panitchob N, Widdows KL, Crocker IP, Hanson MA, Johnstone ED, Please CP, Sibley CP, Glazier JD, Lewis RM, Sengers BG. Computational modelling of placental amino acid transport as an integrated system. *(in preparation for submission)*

2. Lofthouse EM, Perazzolo S, Brooks S, Crocker IP, Glazier JD, Johnston ED, Panitchob N, Please CP, Sibley CP, Widdows KL, Sengers BG, Lewis RM. Phenylalanine transfer across the isolated perfused human placenta: An experimental and modelling investigation. *(in preparation for submission)*

3. Panitchob N, Widdows KL, Crocker IP, Hanson MA, Johnstone ED, Please CP, Sibley CP, Glazier JD, Lewis RM, and Sengers BG. Computational modelling of amino acid exchange and facilitated transport in placental membrane vesicles. *Journal of Theoretical Biology*, 365:352–364, 2015.

4. Widdows K, Panitchob N, Crocker IP, Please CP, Hanson MA, Sibley CP, Johnstone ED, Sengers BG, Lewis RM, and Glazier JD. Integration of computational modeling with membrane transport studies reveals new insights into amino acid exchange transport mechanisms. *The FASEB Journal*, 29:2583–2594, 2015.

5. Widdows K, Panitchob N, Lofthouse E, Crocker I, Sibley C, Please C, Johnstone E, Sengers B, Lewis R, and Glazier J. Activation by intravesicular amino acids of system L-mediated serine uptake into human placental microvillous plasma membrane vesicles. *Placenta*, 35:A99, 2014.

6. Lofthouse EM, Brooks S, Crocker IP, Glazier J, Hanson MA, Johnstone ED, Panitchob N, Please CP, Sibley CP, Widdows KL, and Sengers BG. The effect of flow on placental amino acid transfer in the isolated perfused placenta. In *Proceeding of the Physiological Society*, London, United Kingdom, 2014.

7. Widdows K, Panitchob N, Crocker IP, Brooks S, Please CP, Sibley C, Johnstone E, Sengers BG, Glazier J, and Lewis RM. Mathematical models to predict exchange and facilitated transport across the microvillous plasma membrane (MVM) of the human placenta. *Placenta*, 34:A46, 2013.

8. Widdows K, Panitchob N, Crocker I, Brooks S, Johnstone ED, Please CP, Sibley C, Sengers BG, Glazier JD, and Lewis RM. Mathematical modelling of amino acid transport across the microvillous plasma membrane of the placental syncytiotrophoblast. *BLOG An International Journal of Obstetrics & Gynaecology*, 120:E11, 2013.

9. Lewis RM, Brooks S, Crocker IP, Glazier JD, Hanson MA, Johnstone ED, Panitchob N, Please CP, Sibley CP, Widdows K, and Sengers BG. Review: Modelling placental amino acid transfer – From transporters to placental function. *Placenta*, 27:S46–S51, 2013.

# Declaration of Authorship

I, **Nuttanont Panitchob**, declare that this thesis and the work presented in it are my own and has been generated by me as the result of my own original research.

**Computational modelling of amino acid transfer interactions in the placenta**

I confirm that:

1. This work was done wholly or mainly while in candidature for a research degree at this University;
2. Where any part of this thesis has previously been submitted for a degree or any other qualification at this University or any other institution, this has been clearly stated;
3. Where I have consulted the published work of others, this is always clearly attributed;
4. Where I have quoted from the work of others, the source is always given. With the exception of such quotations, this thesis is entirely my own work;
5. I have acknowledged all main sources of help;
6. Where the thesis is based on work done by myself jointly with others, I have made clear exactly what was done by others and what I have contributed myself;
7. Parts of this work have been published as shown in the List of Publications.

**Signed:**.....

**Date:**.....

# Acknowledgements

I would like to express my earnest gratitude to all whom made this thesis possible. Firstly, I would like to sincerely thank Dr. Bram Sengers, whose kind guidance, support, and vast insights significantly assisted me through this doctoral experience. I would like to equally thank Dr. Rohan Lewis, whose keen passion and acumens in the field of biology helped guided me through this research.

In addition, I would like to acknowledge collaborators at the University of Manchester including Prof. Colin Sibley, Dr. Jo Glazier, Dr. Ian Crocker, Dr. Ed Johnstone, and especially Dr. Kate Widdows for carrying out the experiments. Appreciation also goes out to Prof. Colin Please at University of Oxford for his mathematical insights.

I also would like to gratefully recognize the funding of Vice Chancellor's studentship from the University of Southampton and research grant from BBRSC (grant number BB/I011315/1 and BB/I011250/1).

Lastly, I would like to dedicate this thesis to my family whom always believe in me. In particular, I would like to thank my parents, Yupa and Dr. Supat Panitchob, for their unwavering support and encouragements that have guided me throughout my life, and also my sister, Dr. Yuwapat Panitchob for her advices and assistance in formatting this thesis.

# List of Abbreviations

| | |
|---|---|
| AIB | $\alpha$-aminoisobutyric acid |
| AcEx | Amino acid group susbtrate to accumulative and exchange transporters |
| AcExF | Amino acid group susbtrate to accumulative, exchange, and facilitative transporters |
| ALA | Alanine |
| ASN | Asparagine |
| BCH | 2-Amino-2-norbornanecarboxylic acid |
| BM | Basal membrane |
| BMEx | Basal membrane amino acid group susbtrate to exchangers |
| BMExF | Basal membrane amino acid group susbtrate to exchange and facilitative transporters |
| CYS | Cystine |
| EVB | Extra-vesicular buffer |
| Ex | Amino acid group susbtrate to exchangers |
| ExF | Amino acid group susbtrate to exchange and facilitative transporters |
| EXP | Experiment |
| GLN | Glutamine |
| HIS | Histidine |
| ILE | Isoleucine |
| IUGR | Intrauterine growth restriction |
| IVB | Intra-vesicular buffer |
| LAT | Large-neutral amino acid transporter |
| LEU | Leucine |
| LYS | Lysine |
| MeAIB | $\alpha$-methylamino-isobutyric |
| MET | Methionine |
| MVM | Microvillous membrane |
| MVMAcEx | Microvillous membrane amino acid group susbtrate to accumulative and exchange transporters |
| MVMEx | Microvillous membrane amino acid group susbtrate to exchangers |
| PHE | Phenylalanine |
| PRO | Proline |

| | |
|---|---|
| SEM | Standard error of the mean |
| SER | Serine |
| SLC | Solute carrier |
| SNAT | Sodium-coupled neutral amino acid transporter |
| TAT | T-type amino acid transporter |
| THR | Threonine |
| TRP | Tryptophan |
| TTTS | Twin-to-twin transfusion syndrome |
| TYR | Tyrosine |
| VAL | Valine |

# Chapter 1

# Introduction

The placenta is vital during pregnancy as it serves as the sole interface connecting the mother to the fetus via the umbilical cord. It is responsible for the supply of fetal nutrients, gas exchange, and removal of waste products which are continuously transferred between the two circulations. In normal fetal development, sustaining regular transport of amino acids across the placenta is an essential process. Amino acids, which are building blocks of proteins, are required for growth and tissue repair. Impaired fetal growth has shown to be associated with inadequate placental amino acid transfer [1–3]. Intrauterine growth restriction (IUGR), which affects about one in every ten pregnancies, serves as the underlying motivation for this thesis. Although the actual pathogenesis of IUGR is not well understood, it generally has been linked to limitations in nutrient availability for the fetus. Since placental transfer serves as the only source of nutrients for the fetus during pregnancy, IUGR is highly likely to be associated with placental transport. Studies suggested reductions in many transporter activities in the placental membranes observed in IUGR pregnancies compared to normal pregnancies [4]. In order to prevent or ameliorate irregularities in fetal development, it is important to understand the complex mechanisms underlying the amino acid transport system in the placenta.

Transfer of amino acids from maternal blood across the placenta and into the fetal blood is a complex process with many potential rate limiting steps, as well as other factors that can affect transport; which may include maternal and fetal blood flow, amino acid transporter expression, or the morphology of the placenta [5]. However, the transport of amino acids across the maternal and fetal facing membranes of the placental syncytiotrophoblast will be central to this process, as these provide the main barriers for amino acid transfer. Transport of amino acids is mediated by specific membrane transport proteins [6]. These include; i) facilitative transporters, which allow amino acids to diffuse in the direction of their gradient, ii) exchangers, which transport one amino acid in exchange of another, and iii) accumulative transporters, which actively transport amino acids against their gradient with the energy derived

from electrochemical (sodium) gradients. The ways in which these transporters interact is complex and hard to predict intuitively, therefore mathematical modelling may be beneficial by providing an integrated quantitative approach to better understand the combined effect of their activity [5].

## 1.1 Aims and objectives

The aim of this thesis is to first exploit mathematical modelling to represent the underlying mechanisms of individual amino acid transporters independently. This will provide novel tools that will allow us to examine for the first time how each transporter type functions mechanistically, which will provide a significant step forwarded compared to the phenomenological approaches currently used by biologists. Then, the second aim of the thesis is to develop a new systematic modelling framework to incorporate these individual transporter models to represent the placenta as a whole functional unit. This will, for the first time, provide a complete integrated overview of the placental transport system in all its complexity. Ultimately, this work will contribute to the field of placental study in terms of providing a better understanding of such complicated transport mechanisms, leading to assessment tools for clinical and experimental data, or aiding the development of prevention measures and treatments for nutrient deficiency disorders like IUGR. In order to achieve these scientific and clinical contributions, the following objectives of this thesis are defined as follows:

- To develop and refine individual transporter models to represent their underlying transport mechanisms
- To design new experimental approaches to validate the transporter models
- To develop an integrated model which incorporates individual transporter models to represent the fundamentals of the complete placental amino acid transport system
- To determine the key influencing factors for the placental transfer of amino acids using the integrative model in order to show the model's immediate implication
- To demonstrate the potential clinical and experimental relevance of both transporter and integrated system models to highlight the significance of this work

## 1.2 Thesis structure

In this thesis, the background description of the placenta is presented first to provide an overview of the complex structure of the placenta. Then, various placental functions

are outlined including in particular the transport of amino acids, which is the main focus of this thesis. Pathological conditions are then described, in addition to IUGR, showing correlations to changes in placental structure and functional characteristics. Experimental approaches for the study of the placenta are then presented to highlight strengths and weaknesses of each strategy. The background concludes by reviewing previous placental modelling efforts, not limited to only amino acid transport. In the next chapter, the transport model for the thermodynamically passive amino acid transport by exchanger or facilitative transporters is presented, followed by extensive model investigation and validation with experimental data. This already illustrates the short-term applications of this modelling approach. In a similar manner, development of a model for the accumulative transporter is presented in the following chapter. This work presents a novel model of the complicated accumulative transporter mechanism and includes a detailed model exploration and validation with previous literature data. Next, the integrated model of the placenta is presented, which incorporates all transporter models introduced in the previous chapters. This includes the systematic exploration of the model from simple cases to physiological cases, demonstrating how computational modelling can be used to address such complex scenarios. In addition, an example of the application of the model is presented for a certain physiological conditions (phenylketonuria) to show its potential real clinical contribution. Lastly, the main conclusions of the work are discussed, including suggestions for future work.

# Chapter 2

# Background

The human body requires twenty distinct types of amino acids, nine of which are essential amino acids which cannot be synthesized by the body. Instead, these essential amino acids must come from dietary intake. The fetus receives nutrients from the mother directly through the placenta. Attached to the maternal uterine wall, the placenta transports nutrients between the maternal and fetal blood circulation. However, the two blood circulations do not mix but rather their contents are exchanged via a membrane barrier, limiting fetal transfer of unwanted substances. Hence, the placenta not only serves as an interface for nutrient transfer but also as a protective mechanism for the fetus.

The details of the placental structure and membrane barrier mentioned are explained in the following section. Furthermore, the principal functions of the placenta are presented, outlining the importance of the placenta during pregnancy. In addition, an overview of placental nutrient transport is given. Next, a review of placental abnormalities leading to pathological conditions that can affect both the mother and the fetus is provided. Finally, experimental approaches for the study of the placenta are reviewed along with previous modelling work.

## 2.1 Structure of the placenta

The human placenta takes on the shape of a disk and grows along with the development of the fetus. A mature placenta is 20–25 cm in diameter and is about 2–3 cm thick, weighing approximately 500 grams [7]. Note that in other mammalian species, the placenta takes a diverse range of structures driven by different evolutionary pressures [8]. In human placenta, the maternal side attached to the uterine wall is called the basal plate. The surface closest to the fetus is called the chorionic plate. A photograph of a delivered placenta is shown in Figure 2.1. The structure between the two sides is a

complex system of vascular tissues, therefore the placenta should not be thought of as a simple permeable membrane. Within this complex tissue, the exchange of nutrients, waste products and gases occurs.

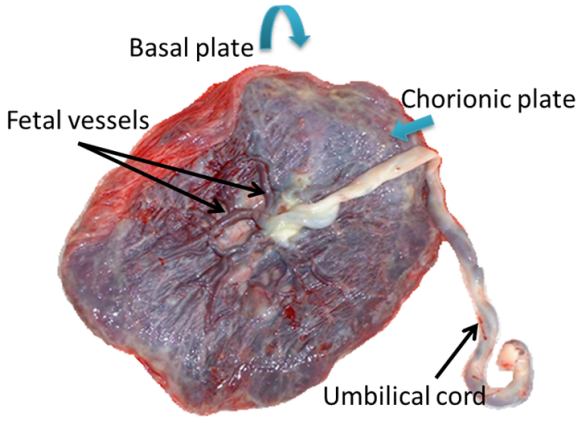


FIGURE 2.1: Photograph of a placenta after delivery, showing the chorionic plate, with the basal plate hidden underneath. The umbilical cord is attached in the middle of the placenta on the chorionic side, and contains two fetal arteries and a vein that branch out to form the villous tree structures in between the chronic and basal plates.

The umbilical cord connects to the placenta typically in the middle of the chorionic plate and contains two arteries and a vein conducting the blood flow from and to the fetus, respectively. On the maternal side, the blood is perfused into the placental intervillous space through spiral arteries and decidua veins on the basal plate. The schematic cross-section of the placental structure is shown in Figure 2.2A. The placenta can be divided into functional subunits called cotyledons which contain 60–70 villous tree structures [7]. A micro-CT image of one cotyledon is shown in Figure 2.3. Villous trees are an extension of the vascular network originating from the umbilical cord forming branching structures within the intervillous space. Placental villi (Figure 2.2B and Figure 2.3) can be categorised by their size and place in the hierarchy. Thus, starting from the fetal vasculature, stem, intermediate, and terminal villi can be distinguished. A terminal villus, which is the smallest branch of the villous tree, is covered by a single layer of cells fused together called the syncytiotrophoblast. The syncytiotrophoblast, which develops from the underlying cytotrophoblast layer, is in contact with the maternal blood in the intervillous space. This barrier layer is the site where the transfer of amino acids and other essential substances into the fetal circulation is controlled [6]. Allowing only certain molecules to pass that are diffusible through lipid membranes, the syncytiotrophoblast protects the fetus from most unwanted molecules. For a molecule to transfer to the fetal side, it needs to travel across both the microvillous membrane (MVM) and the basal membrane (BM) of the syncytiotrophoblast. An immunofluorescence image as shown in Figure 2.4 illustrates the syncytiotrophoblast layer, which contains specific transporter proteins (LAT1 & LAT2) that mediate the transport of substances across both MVM and BM. After having crossed the MVM and BM, the molecule is able to diffuse into

fetal circulation through gaps between the endothelial cell layer. Lastly, between the endothelial and trophoblast (syncytiotrophoblast) cells, the connective stromal tissue provides the structure of the villi. A confocal projection image of terminal villi showing the three distinct placental tissue layers is shown in Figure 2.5.

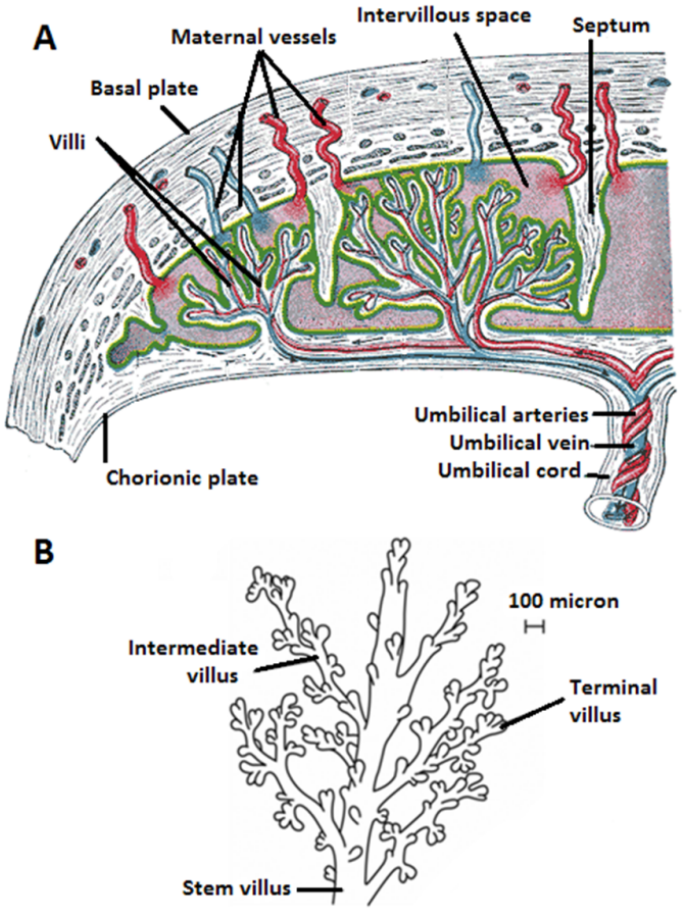


FIGURE 2.2: Morphology of the placenta: (A) Cross-section of the placenta showing the branching structure of the villi that contains fetal capillaries stemming from the umbilical vessels. The villi are surrounded by the maternal blood perfused into the intervillous space from the network of maternal blood vessels (spiral arteries and decidua veins). (B) Placental villous tree hierarchy. Adapted from Gray, 1918 [9] & Sibley *et al.*, 2005 [1].

Although the transport of some small molecules (oxygen/carbon dioxide) is governed by simple diffusion alone; enabling the transfer of certain molecules, such as amino acids, is more complex. The subsequent section provides an overview of the various placental transport processes, including amino acid transport mechanisms which involve protein transporters mediating the transfer.

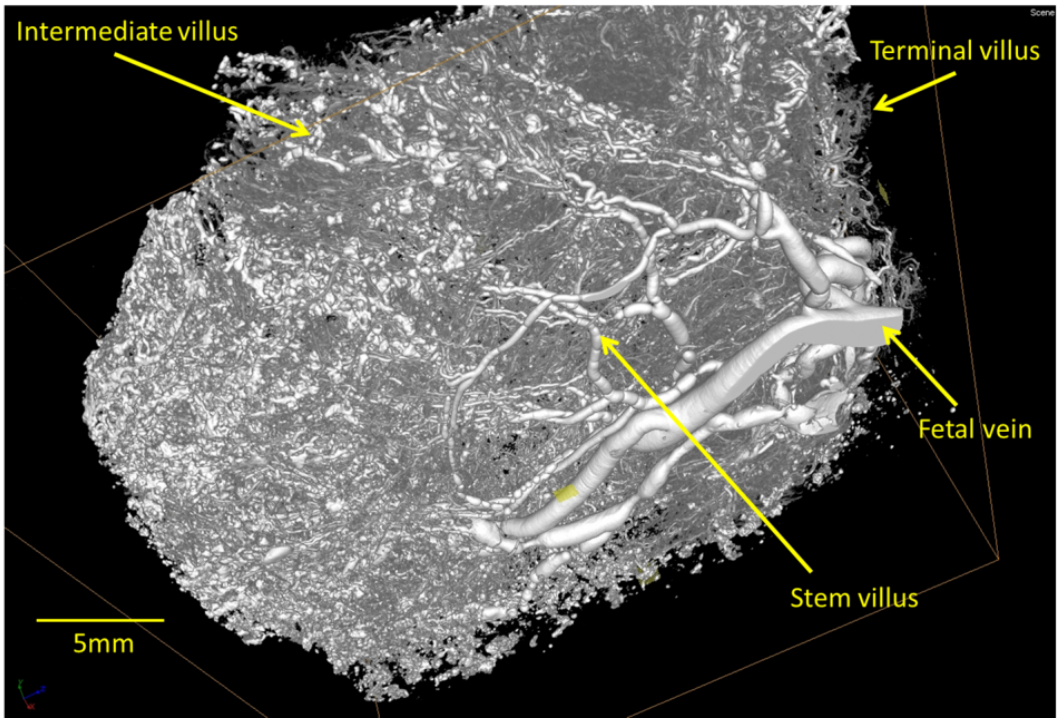


FIGURE 2.3: Micro-CT image of a vascular perfusion of a functional subunit of the placenta (cotyledon) showing the vascular structure of the placental villi branching from the fetal vein to form the stem, intermediate and terminal villi, respectively. Image courtesy of Dr. Rohan Lewis, University of Southampton.

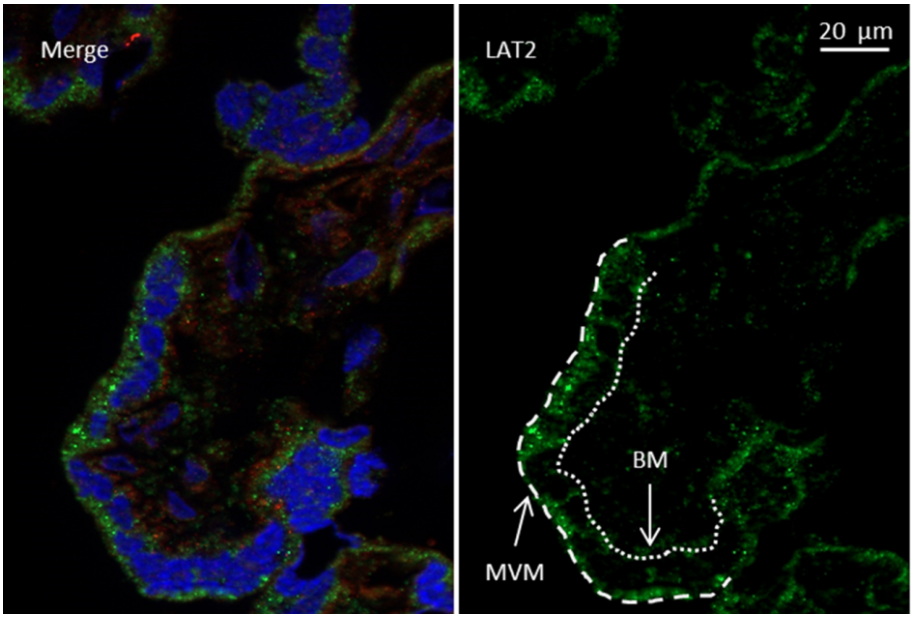


FIGURE 2.4: Immunofluorescence image of a placental villi cross section showing transport protein (transporter) LAT2 localisation (in green) at the microvillous (MVM; dashed) and basal (BM; dotted) membrane of the syncytiotrophoblast layer. Note that LAT1 and nuclei localisation are also shown in red and blue, respectively. Image courtesy of Dr. Kate Widdows, University of Manchester.

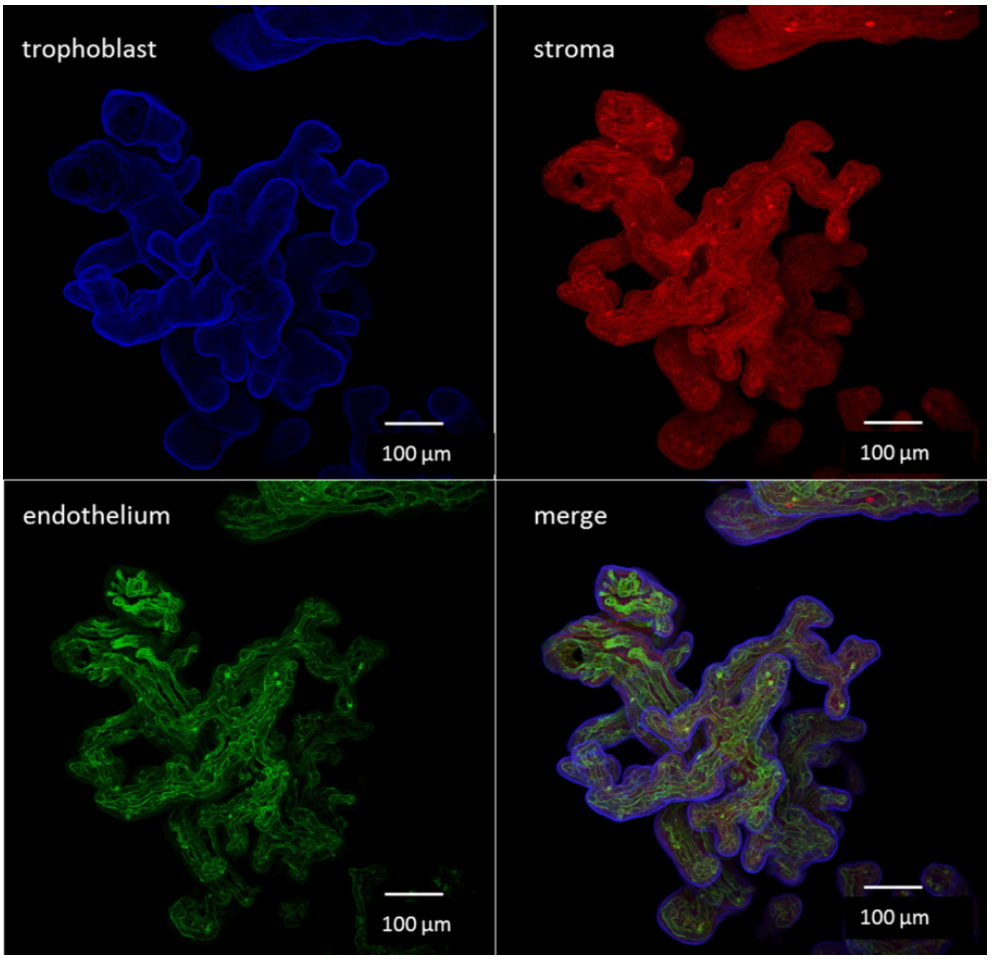


FIGURE 2.5: Confocal 3D projection images of placental terminal villi showing three cell layers: The outer layer trophoblast (in blue) that includes the syncytiotrophoblast where transport proteins are located, connective stroma (in red) that is responsible for structure, and fetal capillary endothelium (in green). Image courtesy of Dr. Rohan Lewis, University of Southampton.

## 2.2 Placental functions

### 2.2.1 Transfer of substances between maternal and fetal sides

Primarily, the placenta supports selective transfer of various types of molecules which include nutrients, gases, and waste products (back to the maternal side). While the placenta transports some molecules to the fetus unaltered, the placenta itself can take up certain molecules, such as glucose or oxygen. In addition, certain molecules can be metabolized by the placenta before being transported to the fetus in another form. The size of the molecule affects the permeability across the syncytiotrophoblast. Smaller molecules are more likely to successfully reach the fetus. Many small molecules are able to passively diffuse through the placental tissue. Passive diffusion of molecules occurs via transcellular and paracellular routes. For example, small molecules like oxygen and carbon dioxide transfer via the transcellular pathway in response to partial pressure

differences. While the concept of a paracellular route is not well defined due to the notion of the syncytiotrophoblast's lack of obvious space between cells, recent studies show evidence of such mechanism in the syncytiotrophoblast [10, 11].

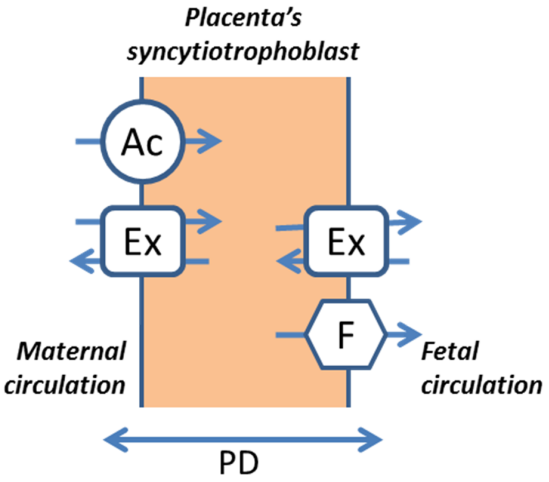


FIGURE 2.6: Schematic diagram depicting the placental amino acid transport interface in the syncytiotrophoblast layer, showing the microvillous membrane facing the maternal circulation and the basal membrane facing the fetal circulation. At the membranes, transport proteins mediating amino acid transport are shown. Categorised by their transport mechanisms, these transport proteins include accumulative transporters (Ac), exchangers (Ex), and facilitative transporters (F). Paracellular diffusion (PD) is also depicted.

TABLE 2.1: Summary of selected placental transport proteins categorised by mechanism, membrane localisation, and amino acid specificity. Note this is not an exhaustive overview.

| Name | System | Mechanism | Localisation | Amino acid substrates | Reference |
|---|---|---|---|---|---|
| LAT1 | L | Exchange | MVM, BM | GLN, HIS, ILE, LEU, MET, PHE, TRP, TYR, VAL | [12] |
| LAT2 | L | Exchange | MVM, BM | ALA, ASN, CYS, GLN, HIS, ILE, LEU, MET, PHE, SER, THR, TRP, TYR, VAL | [12] |
| LAT3 | - | Facilitative | BM | ILE, LEU, MET, PHE, VAL | [13] |
| LAT4 | - | Facilitative | BM | ILE, LEU, MET, PHE | [14] |
| TAT1 | - | Facilitative | BM | ALA, LEU, PHE, TRP, TYR | [12, 13] |
| SNAT1 | A | Accumulative | MVM | ALA, ASN, CYS, GLN, GLY, HIS, MET | [12] |
| SNAT2 | A | Accumulative | MVM | PRO, SER | [12] |
| SNAT4 | A | Accumulative | MVM | ALA, ASN, CYS, GLN, GLY, HIS, LYS | [12] |

Note that amino acid abbreviations can be found in the List of Abbreviations.

Other molecules that are not able to diffuse passively across the syncytiotrophoblast, such as amino acids, are transported via transporter proteins to mediate the placental transfer in both MVM and BM (Figure 2.6). These transporters can function using either energetically active or passive mechanisms. In addition to being characterised by their transport mechanisms, the protein transporters can also be categorised according to their

substrate specificity (*i.e.* specific to each class of amino acids) and localisation on certain membranes [12]. A table summarising the various placental transporters, categorised according to their mechanism, membrane localisation, and substrate specificity is shown in Table 2.1. As shown, this presents a very complex system, involving many interdependent variables, which is difficult to intuitively understand without systematic modelling effort. An overview of the various types of placental transporter mechanisms is presented as follows:

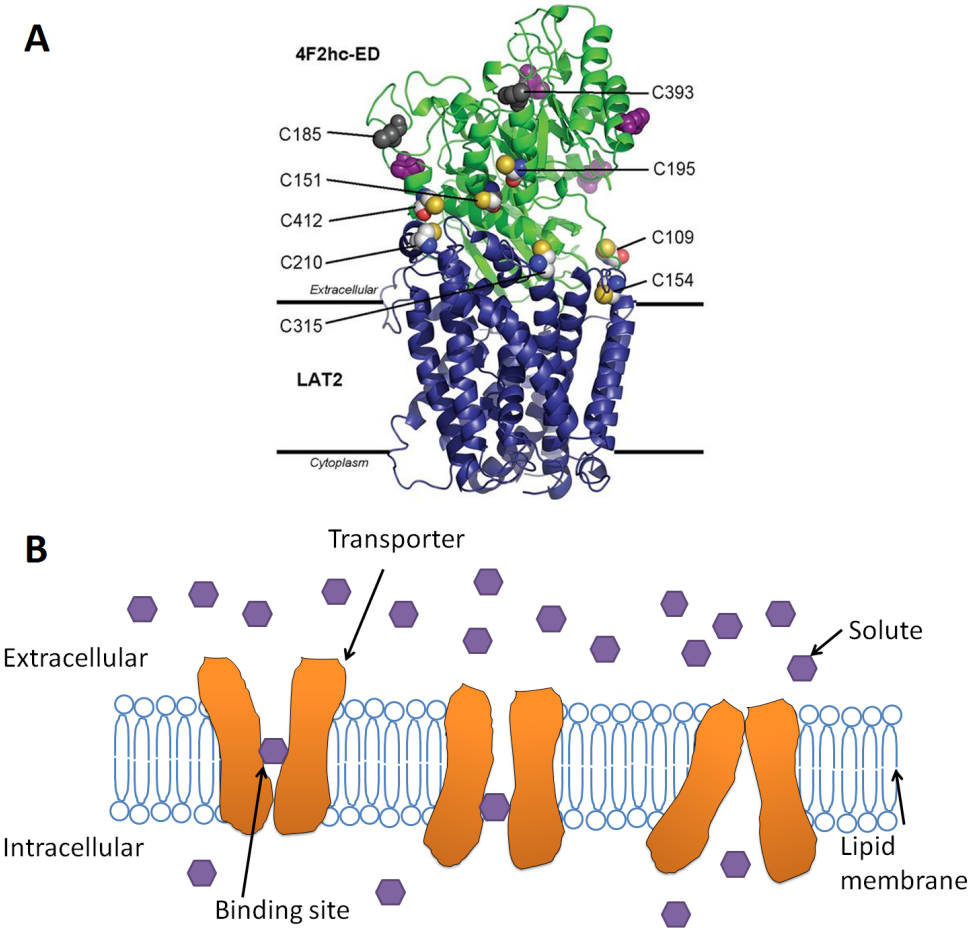


FIGURE 2.7: Transport protein structural representation and conformational changes during transport of solute. A) Structural model of transport protein LAT2 (in blue chains) and its ancillary unit 4F2hc (in green chains) showing molecule binding sites (in spheres). Image reproduced from Rosell *et al.*, 2014 [15]. B) Schematic of transport cycle in a facilitative transport process across lipid bilayer membrane. Transport protein exposes binding site prompting a solute to bind, then undergoes conformational changes that results in unbinding of the solute to the other side.

**Facilitated transporter**: Facilitated diffusion can move molecules down their concentration gradient via carrier proteins or channels. The process is thermodynamically passive because the carriers or channels do not require energy for transport, but instead this is driven by the concentration gradient. For the case of channel transporters, the molecules simply diffuse through the channel once opened. However, for amino acids, carrier mediated transport is thought to be the main

mechanism, rather than channels. In carrier-mediated transport, the molecule binds to the transport protein and is then being transported as a result of conformational changes of the carrier between membrane interfaces. In this process, the solute (substrate) binds to the carrier to the binding site(s) on one side of the membrane. Randomly, the carrier undergoes reversible conformational changes, which exposes the solute-binding sites alternately to either side of the membrane. The carrier can discharge the solute on the side where the binding sites are exposed. Since the transition between the two conformational states occurs randomly and reversibly, more solutes bind to the carrier on the side which has the higher concentration; therefore the net transport of the solute occurs in the direction of the concentration gradient. A sample of transport protein's structural model and schematic of the transport cycle is shown in Figure 2.7. Examples of molecules that exhibit this carrier-mediated transport behaviour are glucose, fatty acids, and amino acids. Facilitated transporters are also found at the BM to enable net amino acid efflux to the fetus.

**Exchange transporter**: Another example of a passive transporter is the exchange transporter, which allows amino acids between different sides of membranes to be swapped. An exchanger takes one amino acid molecule and switches it with another one from the other side of the membrane. Exchange transporters are ubiquitous in both MVM and BM. The exchange processes do not change the absolute amount of the amino acids within the syncytiotrophoblast, but instead only affect the relative composition of each type of amino acid. This is an important regulatory mechanism for the cell that mediates the uptake of required amino acids to be transported inside, but at the same time protects the cell from osmotic effects by transferring another molecule out [6, 16].

**Accumulative transporter**: Additionally, the active uptake of molecules against their concentration gradient can be achieved by specific types of transporters. In the placenta, active processes dominate the overall transport of amino acids across the membranes. This is supported by evidence that the amino acid concentration in fetal plasma is higher than in maternal plasma [6]. The main transporters that actively transport amino acids in the placenta are the accumulative transporters. Accumulative transporters actively regulate the amino acid uptake into the syncytiotrophoblast which leads to an increase in amino acid concentration, against its gradient. This active process relies on the energy that is derived indirectly from the sodium-potassium pump $Na^+/K^+$-ATPase and is driven by the transmembrane electrochemical gradient (secondary active cotransport). The electrochemical potential difference between the two membranes is determined both by the $Na^+$ concentration gradient and the membrane electrical potential. In the case of $Na^+$ dependent transporters, which are present in both MVM and BM, the transmembrane $Na^+$ gradient is sustained higher outside than inside the cell for the transport to work (*i.e.* $Na^+$ going down its gradient allows the amino acid to be transported up). The $Na^+$ gradient is effectively maintained by the primary active $Na^+/K^+$-ATPase transport mechanism.

The transport process for a $Na^+$ dependent transporter of a given amino acid can be described by the following steps as follows [17]:

1. The activator $Na^+$ ion binds to the carrier to favour the transport of the amino acid.
2. The affinity of the extracellular cotransport binding site is increased with the binding of $Na^+$.
3. $Na^+$/amino acid transporter complex is formed.
4. Delivery of the $Na^+$ and amino acid on the other side of membrane.
5. Release from binding site of amino acid and $Na^+$, respectively.
6. $Na^+$ is separately transported out via $Na^+/K^+$-ATPase maintaining low intracellular concentration.

As shown in Figure 2.6, these placental transporters work together to regulate amino acid transfer across the MVM and BM at the syncytiotrophoblast layer. Effectively, the net transport of amino acids across the BM is required to support fetal growth. Exchangers and accumulative transporters cannot individually move all of the amino acids required by the fetus across both MVM and BM (refer to Figure 2.6). Accumulative transporters only move the amino acids into the syncytiotrophoblast and the exchanger can only change composition. Therefore, there must be another mechanism that transfers the amino acids across the BM in the placenta in addition to the accumulator and exchanger. Recent studies suggested the existence of such a mechanism in the form of efflux transporters in the BM [6, 16, 18, 19]. As previously mentioned, the efflux transporter mediates amino acid transport via a facilitated diffusion mechanism.

Thus, while it is clear from the above that all transporters types need to work together, the combined effect is hard to predict intuitively; therefore, individual studies of each type of transporter must be carried out. Specific transporter mechanisms are explored in greater detail to derive each mathematical models, which are presented in Chapter 3 (facilitative and exchange transporters) and Chapter 4 (accumulative transporter).

### 2.2.2 Endocrine function

In addition to mediating transfer of nutrients and other substances, the placenta also has other important functions during pregnancy. For instance, it is an endocrine organ, secreting hormones into both the maternal and fetal circulations. These hormones are important during pregnancy as they adapt maternal physiology to support the pregnancy and allow development of the fetus. For example, estrogen, which causes breast enlargement for preparation for lactation and uterine growth for the fetus, is being produced by the placenta [20].

### 2.2.3 Immune function

Moreover, the placenta also acts as an immune barrier for the fetus. The placenta protects the fetus from being infected with diseases such as sexually transmitted diseases by providing a protective interface between the two blood circulations without mixing. This, however, does allow some infective agents to be transmitted to the fetus, thus the protection offered is not always complete. For instance, transmission of HIV from infected mother occurs in 14.4%–39% of pregnancies [21]. The reason for this occurrence is still largely unknown.

## 2.3 Placental pathology

It is important for the placenta to be operating normally during pregnancy to ensure positive neonatal outcomes. During pregnancy, the fetus requires adequate nutrition for growth and development, while nutrient deficiency or surplus supply may result in diseases for the baby postpartum. Anomalies in the placenta structure and characteristics have been reported in relation to these pathological conditions. For instance, in IUGR, which affects 10 percent of all pregnancies, the placenta is reported to be under-perfused [22], small in overall size [23], with reduced cell volumes in all placental tissues [24], decreased intervillous space and villous surface area [25], and abnormal villous angiogenesis [22]. These conditions contribute to reduced overall fetal transfer of nutrition (*e.g.* amino acids) and oxygen (hypoxia) causing retardation of fetal growth in IUGR that can result in disease such as impaired neurological development after birth. Conversely, oversupply of nutrition may occur in diabetic pregnancies where the glucose level is too high can drive fetal overgrowth. Structural indications in the placenta that promote high transfer of glucose were shown in case of diabetic infants. For instance, increased intervillous space volume, while no change in villous surface area was apparent [26]. This suggested that the transfer could be increased for larger intervillous spaces, which reduces the flow resistance (assumed to be flow limited). Moreover, pathological disorders can also occur to the mother. For example, maternal anemia and preeclampsia were reported to be related to under-perfused placentas that also have low villous surface area [27]. Lastly, disorders related to abnormal (usually low) perfusion as a result of twin-to-twin transfusion syndrome (TTTS) in multiple pregnancy are also reported to be related to the placental perfusion and distribution of the blood between the fetuses [28]. A complete overview of the placental alterations in relation to these disorders mentioned is summarised in Table 2.2.

TABLE 2.2: Summary of placental morphological conditions reported per pathological disorders.

| Disorder | Cause | Perfusion | Trophoblast thickness | Stroma thickness | Endothelium thickness | Vascular branching | Intervillous volume | Size/Weight | Villous surface area | Lesion | Thrombosis | Reference |
|---|---|---|---|---|---|---|---|---|---|---|---|---|
| IUGR | Fetal hypoxia, hypoglycemia, malnutrition | – | – | – | – | i | – | – | – | y | y | [22–25, 29] |
| Diabetes (type 1) | Hyperglycemia | | + | | + | | + | + | = | | | [26, 27, 30] |
| Preeclampsia | Uncertain placental anomaly | – | = | = | = | + | | – | – | | | [24, 27, 31] |
| Maternal anemia | Insufficient red blood cells, hypoxia | – | – | | = | = | | = | – | | | [27] |
| TTTS | Disproportionate perfusion | i/– | | | | i | | | i | | | [28, 32] |

IUGR: intrauterine growth restriction, TTTS: twin-to-twin transfusion syndrome.
+ denotes increase, – denotes decrease, = denotes unchanged.
i denotes irregular, and y denotes affected.

TABLE 2.3: Transport activity of various substrates under certain pathologies observed at placental syncytiotrophoblast microvillous (MVM) and basal (BM) membrane. Adapted from Jansson *et al.*, 2007 [4].

| | System A | | Lysine | | Leucine | | Glucose | | |
|---|---|---|---|---|---|---|---|---|---|
| Disorder | MVM | BM | MVM | BM | MVM | BM | MVM | BM | Reference |
| IUGR | – | = | = | – | – | – | = | = | [33–35] |
| Diabetes | + | = | = | = | + | = | = | + | [36, 37] |

+ denotes increase, – denotes decrease, = denotes unchanged.

Moreover, impaired transfer has been shown to be associated with IUGR and in animal models impaired amino acid transfer precedes the onset of IUGR suggesting causation. IUGR and diabetes, which largely involve the disproportionate transfer of nutrients, can be related to the transport capacity of the transport proteins [2]. In Table 2.3, a summary of several substrate transport activities that were altered at both placental membranes for each disorder is presented [4]. This report suggested reductions in most amino acid transport activities at both MVM and BM, but unchanged activity for glucose [33–35]. In addition, increased glucose activity is mostly observed at the BM in the case of diabetes [36, 37].

In conclusion, as shown in this brief summary, placental morphology can affect the transport of substances that may result in immediate and future diseases for the baby or the mother. Related factors will be considered and explored further when the placental transport model is being developed. It is hoped that this body of work can contribute to developing treatments or prevention of these complications.

## 2.4 Experimental approaches for placental transfer studies

For the study of amino acid transport in biological systems, various experimental techniques can be performed to investigate transport at different levels of observation. Depending on the question of interest and suitability, each technique possesses various advantages and disadvantages [17]. These techniques include:

1. *In vivo* flux technique which measures the net effect on amino acid concentrations from blood samples
2. Regional perfusion which measures an organ in isolation, *ex vivo*.
3. Cultured cell methods, which investigate the transport regulation separated from other cells and other endocrine influences.
4. Membrane vesicle techniques which observe the behaviour of the spherical cell membranes prepared from the tissue of an organ.

While each method has its own strengths and weaknesses, three of the techniques are particularly relevant for the study of placental transfer in relation to computational modelling. While the *in vivo* flux method may provide the information closest to the normal operating conditions, the result from the sample may be affected by other physiological systems and it is difficult to extract the placenta-specific information. In contrast, in regional perfusion, we can observe the placenta independent of all other organs in an *ex vivo* setting. By varying the input and output flow of the placenta, we can observe the transport by the organ in response to the flow. Modelling of the perfusion experiments can be done at the organ scale with a compartmental representation of the placenta coupled to the flow on the maternal and fetal side [16, 38]. Time-dependent data can be recorded on the scale of minutes up to hours. Though information from perfusion experiments is important, the placenta still represents a 'black box' to some extent and information at the cellular membrane level is equally essential to complement these studies. Hence, the cultured cell methods and membrane vesicle techniques are preferred for the cellular transport studies at a smaller time scale. These experiments can provide parametric data for the kinetic response of specific individual transporter as well as time-dependent information due to changes in the concentrations.

In particular, *Xenopus* oocyte cells are commonly used for observing the transport at the cell level. Oocytes, which are induced to overexpress specific human transporter proteins, are used for observing uptake of substrate into the cells from the external environment while maintaining normal intracellular cell operations (*e.g.* metabolism and intracellular concentrations). These influences can be avoided using the membrane vesicle technique where only the plasma membrane is isolated from epithelia and formed into a vesicle suspension. Therefore membrane vesicle studies can be appropriate for exploring placental transport , with the advantage of eliminating confounding influences such as the effects of placental structure and metabolism at the cellular level and offering improved control over intracelluar concentrations.

In vesicle studies, placental MVM vesicles have been used to investigate amino acid uptake activity [39, 40]. The MVM vesicles were prepared from isolated syncytiotrophoblast layer using centrifugation to form membrane pellets that can then be resuspended to form vesicles, with the same membrane orientation as *in vivo* [41]. The transporters embedded in the MVM vesicles were preserved in the method. However, the regulation by intracellular components was absent due to the nature of the technique in which the cell organelles were eliminated. This gave the freedom to measure the specific activity of the transporters without prior knowledge or involvement of the cellular regulation of transporter expression. Intra-vesicular and extra-vesicular buffer solutions were added to maintain a normal environment for the membrane vesicles as well as to pre-set the desired experimental conditions. Radiolabelled amino acid substrate was then utilized for tracing the transport activity, which was measured by method of liquid scintillation counting. Additionally, transporter specific inhibitors can be added to isolate the particular transporter's activity. For instance, in observing the uptake of serine, $\alpha$-methylamino-isobutyric acid (MeAIB) can be added as an inhibitor in order to isolate the System A transport component, which uses the accumulative transport mechanism [39]. In addition, the System L component believed to use the exchange mechanism can be isolated by using 2-Amino-2-norbornanecarboxylic acid (BCH) as inhibitor. In some transporters where ionic molecules are required for the cotransport of the substrate, the isolation of such transporter activity can be achieved by the absence of that ionic molecule in the experiment. For example, the accumulative transporter's activity can be eliminated by not adding the required sodium ions in the experiments.

By having the ability to extract transporter specific uptake data, vesicle studies are a suitable method to independently investigate individual models for each transporter mechanism. Moreover, other cellular influences (*e.g.* metabolism) are omitted which reduce the complexity of the interpretation of the experimental data.

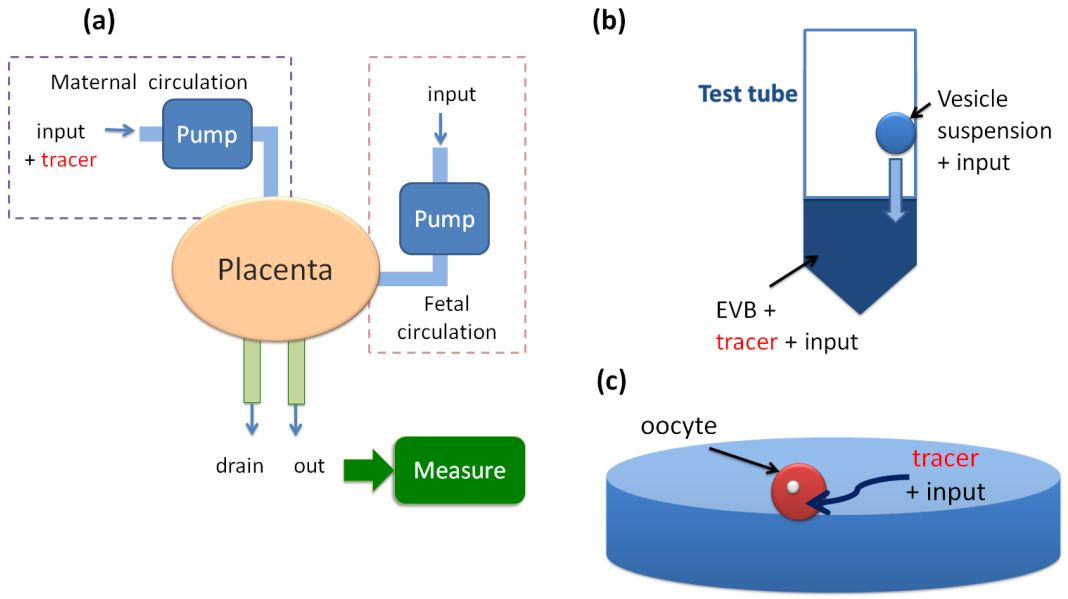


FIGURE 2.8: Schematic diagram of experimental techniques used for the study of placental transport: (a) *Ex vivo* perfusion method, which controls flows and input concentrations; (b) Isolated membrane vesicle experiment with controlled conditions in the extravesicular buffer (EVB) and inside the vesicles; (c) Cultured cell method using oocytes overexpressing human transporter proteins to measure tracer uptake or efflux.

## 2.5 Review of placental modelling

In this section, the literature on previous placental modelling efforts is reviewed. Investigators have developed modelling interests that ranged from the macroscopic system, such as blood flow in placenta, to transport at the microscopic scale and individual transporter kinetics. Additionally, transporters can be modelled at the molecular level to understand the dynamics of the changes in molecular structure during transport. Previous placental modelling studies have mainly focussed on the topics of blood flow, oxygen/gas transfer, and solute transport by simple diffusion (as summarised by [42]). On the other hand, outside the area of placental transport, there have been numerous studies specifically on membrane transporters, which could be equally relevant to placental amino acid transport. These studies encompass many different physiological applications; such as, thyroid hormone transport in the brain [43, 44], drug transport mediated by ATP-binding cassette transporters [45, 46], or renal transport of nutrients [19, 47, 48]. Numerous studies in the past have used carrier type models to obtain an improved insight in transporter mechanisms and activity, for instance; choline transport in erythrocytes [49], glucose transport in the kidney [50], or the transport of monosaccharide in tumour cells [51].

Conclusively, the review was intended to show the progression of modelling efforts building up to the current studies of amino acid transport modelling in the placenta. In the next sections, several key studies are highlighted and explained in more detail.

### 2.5.1 Placental blood flow

Blood flow is an important factor for tissue perfusion. For the placenta, the flow characteristics are commonly thought to be limiting factors in the quantity of nutrients being delivered by blood perfusion. Therefore, many efforts have been made to obtain a better understanding of the flow pattern in the placenta. In the past, experimental methods of investigation that were based on radiography and casting techniques were used to graphically mimic the flow pattern in the branching villous structure of the placenta [52, 53]. However, quantitative information on the villous morphology has been in dispute, thus the authors suggested random distribution of the venous outflow openings [42]. Earlier studies simply modelled the maternal spatial flow pattern in the cotyledon of the placenta as a 2D squared-shape porous medium using the principles from Darcy's law, which assume a linear relationship of the flow velocity to the blood pressure and porosity of the medium [54]. More recent work made an improved representation of the cotyledon as a hemispherical volume with a branching villous tree structure that comprises of veins, an artery, and a cavity [42]. In addition, recent models have suggested a stream-tube flow configuration that models maternal flow between the villi [55, 56]. The study suggested that the resulting heterogeneous maternal blood flow pattern, which in the past has been simplified to a homogeneous pattern, can have different relative effects on the transport of substances. The model also addressed the combined effects of the complex flow, uptake kinetics, and solute distribution patterns, which together could influence the efficiency of a given transport system (*e.g.* for oxygen transfer, as reviewed in the next section). In summary, the findings of blood flow characteristics are insightful and may be useful when considering the modelling of amino acid transport coupled to physiological flow conditions.

### 2.5.2 Oxygen transport

Oxygen is one the most important substances to be transported by the placenta, as the placenta is the only source of oxygen for the fetus. The placental oxygen transfer can be summarised as a three-step process [57]. Firstly, from the maternal side, the oxygenated blood enters the placenta via arteries from the basal plate and occupies the intervillous space. The blood comes in contact with the terminal villi which act as a barrier for the flow, prompting the decrease in flow rate from the basal plate to the chorionic plate. Secondly, the oxygen diffuses across the villous membrane to the fetal capillaries. This passive process relies on the oxygen gradient between each interface to drive the transport, which is suggested to be flow limited as flow maintains the *trans*-placental gradient [58, 59]. Lastly, the oxygen enters into the fetal blood circulation and is being used by the fetus.

While many attempted to model the gas exchange process, these studies proved to be difficult due to the high variability of the placental structures involved. For instance, the

placenta's oxygen exchange was modelled at the most basic level with non-dimensional parameters [60]. Fick's law for diffusion was implemented, which states that the flux of oxygen is proportional to the gradient of the oxygen level at the maternal-fetal interfaces. This work demonstrated basic transport theory without geometric considerations. However, since oxygen transport is thought to be flow-limited, the placental morphology should also be accounted for in models as it directly influences the flow rates. In more recent studies, the oxygen transport was modelled at a single capillary with gas exchange at the wall [61], which suggested that the oxygenation was strongly influenced by the thickness of the capillary (proportionally) and the thickness of the wall (oppositely). Further development was made in another recent study that considers the effects of various terminal villi shapes [57]. The model was based directly on 2D digital photomicrographs of cross sections of the placenta, which were used to represent the geometry of the villous-capillary interfaces at the terminal villous. It was suggested that crowded capillaries in the placental microstructure reduce the oxygenation efficiency. In addition, the studies of flow mentioned in the previous section suggested that when considering the overall macro scale, the optimal configuration of the villi within the cotyledon should be neither too dense nor too sparse for optimal oxygen transfer [55, 56]. In general, these studies have demonstrated that diffusion of oxygen molecules (and also other gases) is highly dependent on the geometry of the placental morphology, which greatly varies from one to another. The morphology of the placenta is closely related to the blood flow characteristic which is shown to be a limiting factor for gas exchange. From these oxygen transport studies we can relate the effect of the microscopic structures to the macro-scale transfer, which could be applied to amino acid transport studies. However, it is generally thought that the uptake of amino acids is not flow limited since it requires transport against the overall higher concentrations in the syncytiotrophoblast than the maternal side [5]. Hence for amino acids, this implies the focus on the transporter system rather than flow and structure in detail. Nonetheless, once the transmembrane transport model is realised, flow models that consider placental structural features can be combined with the membrane transport models to represent transport at the macroscopic scale.

### 2.5.3 Membrane transport of nutrients

There have been efforts in modelling the membrane transport of biologically relevant solutes across various epithelia. These studies include transport in kidney, liver or intestines, in addition to the placenta. It is beneficial to review these previous works in other organs, as the underlying principles of membrane transport are universal and it can provide additional modelling tools to the placental study. The studies are summarised as follows:

Membrane nutrient transport experiments are often carried out under the assumption

that transport can be described as a Michaelis-Menten process due to the simplicity of this approach [47, 50, 62]. Experimentalists carry out studies to determine the Michaelis-Menten kinetic parameters by measuring the initial uptake rates across a range of substrate concentrations, without considering the underlying transport mechanisms or specific experimental conditions that may result in experimental variations [43, 44]. Most commonly, the configuration of these past experiments, does not include time-course data [44, 62], which can provide more detailed information on the transporter response than just initial uptake rates. Hence, it is important to relate these kinetic experiments to more mechanistic models while considering timecourse data (in addition to kinetic data based on initial uptake rates). This was evident in previous studies, for example, carrier-mediated modelling approaches have been used to explain the transport of various nutrients [17, 50, 63, 64], which was then related back to the interpretation of transport as a simple Michaelis-Menten process. In carrier-mediated transport, the substrate is assumed to bind to a carrier (transporter) in order to transport from one side of the membrane to another. In general, this process is parameterised in terms of the carrier's translocation rates across the membrane and its substrate binding/unbinding activity (*i.e.* binding affinity). For each transporter type, the basic theory for carrier mediated transport can be further expanded to represent each transport mechanism.

For instance, in a cotransport model, substrate transport requires an additional ion (sodium) to be transported simultaneously by the carrier. In past studies, experimentalists have represented cotransport based on Michaelis-Menten type equations to carry out membrane transport studies, for instance, in vesicle amino acid uptake experiments using rabbit intestinal epithelium [62] and rat fibroblasts [47]. Both of these studies demonstrated the dependency of transport on sodium, represented by a phenomenological Michaelis-Menten kinetic model. In another study as continuation of [47], the amino acid proline was investigated by observing uptake in renal brushborder membrane vesicles [48]. The model assumed the flux of the uptake could be represented by two superimposed Michaelis-Menten processes, one for each of the sodium-dependent and -independent components. Notably, the time-dependent experimental results in the studies of [47, 48] showed an overshoot in the uptake of substrate before reaching the equilibrium value, which was shown to be related to presence of the sodium gradient. However, the fitted Michaelis-Menten parameters were not uniquely determined as only the ratios of such parameters were successfully obtained. This revealed the limitations of the Michaelis-Menten kinetic representation; since such overshoot phenomena are essentially dependent on time and internal concentration. Moreover, these studies did not take electrochemical effects into consideration, as the transport of the ions (sodium) would change the potential difference which could affect the transport process. A representative list of the equations used in the literature to model the nutrient transport across various epithelial membranes is presented in Table 2.4.

TABLE 2.4: Nutrient membrane transport equations as modelled in literature.

| Model equation | Description | Reference |
|---|---|---|
| $J_A = \frac{V_{max}[A]^I}{\frac{K_A K_{Na}}{[Na]^I} + [A]^I}$ | Cotransport: Flux $J_A$ is a Michaelis-Menten process dependent on external concentration $[A]^I$ with maximum transport rate $V_{max}$ and half-saturation constant as the ratio of the product of dissociation constants $K_A$ and $K_{Na}$ over the external concentration of the cotransported solute sodium $[Na]^I$. | [62] |
| $J_A = \frac{V_{max}[A]^I}{\frac{K_A K_{Na}}{[Na]^I} + [A]^I} - \frac{V_{max}[A]^{II}}{\frac{K_A K_{Na}}{[Na]^{II}} + [A]^{II}}$ | Cotransport: Flux $J_A$ is the difference of two Michaelis-Menten processes governed by the external $[A]^I$ and internal $[A]^{II}$ concentration as described in [62]. | [47, 48] |
| $J_A = \frac{V_{app}[A]^I}{K_{app} + [A]^I}$<br>$ln\frac{[A]^I}{[A]^{II}} \leq ln\frac{[Na]^{II}}{[Na]^I} + \frac{F\Delta\psi}{RT}$ | Cotransport: Flux $J_A$ is an apparent Michaelis-Menten process as a function of external concentration $[A]^I$. Equilibrium thermodynamics relation between the concentrations of substrate $A$ and sodium $Na$ given by an inverse logarithmic relationship in combination with the effect of the electric potential difference $\Delta\Psi$. | [50, 64] |
| $J_A = V_{max}\left(\frac{[A]^I}{K_A + [A]^I} - \frac{[A]^{II}}{K_A + [A]^{II}}\right)$ | Facilitative transport model: Flux $J_A$ from side $I$ to $II$ is driven by the difference in concentration between the two sides. The net flux is modelled as the difference of two Michaelis-Menten equations. | [63, 65] |
| $J_A = V_{max}\left(\frac{[A]^I}{K_A + [A]^I}\right)\left(\frac{[A]^{II}}{K_A + [A]^{II}}\right)$ | Exchanger: Flux $J_A$ from side $I$ to $II$ is the product of two Michaelis-Menten processes on the two sides. | [16] |

In order to consider all driving forces for cotransport (accumulative transporter), in addition to the chemical driving force arising from the concentration gradients, the effects of the electric-potential on the ion must be taken into consideration. This was seen in an improved mechanistic investigation of the cotransport system, which was conducted on sodium-dependent glucose transport in the rabbit brush border membrane vesicles [50] and in a similar oocytes study expressing small intestine transporters [64]. The latter model described all the individual transport parameters for each carrier state (*e.g.* bound *vs* empty carrier), including exponential relationships for the effect of the

membrane potential. For investigating the effects of membrane potential, the chemical 'voltage clamping' principle was suggested for the purpose of chemically adjusting the membrane potential. This is expected to be useful when designing the experiments for investigating the accumulative transporter. Moreover, the overshoot phenomenon was confirmed by the results, based on which it was argued that it was driven by the sodium gradient, rather than just a dependency on the absolute concentration level [50]. This was illustrated by an example of the uptake profile; where the curve of solute uptake for the case where sodium ions were present but in equilibrium showed no overshoot effect, whilst another curve for the case where an initial sodium gradient was present displayed the overshoot phenomenon. The author also introduced the different approaches used in vesicle experiments, for example by setting different concentrations on each side of membrane, in contrast to the common practice of only measuring the zero-*trans* case (*i.e.* zero initial concentration inside the vesicles). The zero-*trans* condition is often implicitly assumed and coupled with Michaelis-Menten analysis in vesicles and oocyte uptake experiments without consideration of any effects resulting from the potential presence of endogenous (*trans*) concentrations inside the vesicle/cell. This was presumed to be a source of variation in the apparent kinetic parameters determined from these experiments, which needs to be explored by the model. Interestingly, the authors described the sodium-dependent carriers as being initially negatively charged and to have the propensity to undergo charge neutralisation with positively charged sodium ions [50]. From the findings, it was observed that as the membrane potential was made more negative, the transmembrane translocation of the empty carrier was faster and the sodium ion's dissociation rate became more rate-limiting.

In addition, to the cotransport model representing the accumulative transport mechanism, energetically passive nutrients transporters have been investigated, specifically with respect to the exchange transporters. Although, there were several reported apparent Michaelis-Menten kinetic parameters values in placental transporter studies, their values showed high variation [19, 66, 67]. Again, this is presently hypothesised to be caused by the implicit assumption of zero-*trans* conditions, ignoring any effects of internal concentrations when performing kinetic experiments. In theory, the exchanger requires the substrate(s) to be present on both sides of the membrane for the transporter to operate, hence, logically no transport should occur under zero-*trans* conditions, contrary to common experimental observations in vesicle studies [39, 68]. This apparent contradiction needs to be explored further, which requires a better mechanistic model other than just simple Michaelis-Menten kinetics that cannot account for internal concentrations. A previous study on placental transport has applied a phenomenological model for the exchanger as the product of two Michaelis-Menten processes for each side of the membrane [16]. However, the mechanistic basis for the exchanger model and its application to experimental data requires further examination.

### 2.5.4 Molecular structural modelling

In addition to the kinetic studies, modelling of the transport protein can be done at the molecular structural level as demonstrated in the study of glucose transporters [69], which described the conformational changes of the protein during transport and binding of solutes. While the kinetic models focused on the overall transport mechanism and the molecular structural models consider the physiochemical behaviour of the transport protein that influences transport, neither approach can be ruled as superior to another as they provide complementary information. Hence, combining knowledge from both modelling approaches is deemed to be beneficial to obtain a better representation of the transport mechanism in the end.

### 2.5.5 Organ-scale modelling

The idea of modelling various placental functions has been presented [70], which reviewed multiple basic and phenomenological models for (diffusive) transfer of different nutrients. While this serves as good stepping stone for the effort towards a 'virtual' placenta, many nutrients transport systems – such as for amino acid – require more sophisticated mechanistic models. Furthermore, morphological considerations should be addressed for each transport system that may contribute to the efficiency of transfer.

### 2.5.6 Compartmental modelling

Finally, the work by Sengers *et al.*, 2010 on modelling of the amino acid transfer in the placenta had served as the starting point of the current research [16]. The investigators developed amino acid transporter specific models based on assumptions for their transport kinetics and used these to construct an integrated compartmental model. *Ex vivo* perfusion experiments of human placenta were used to test the model. While the work gave excellent insights in how placental transport could work as an integrated system, the transporter models itself were however largely phenomenological. Therefore, potential work could be done to account for a more complex mechanistic representation of the biophysical transport processes.

## 2.6 Conclusion

From the body of literature reviewed, it can be inferred that improved quantitative understanding of placental amino acid transfer is essential for possible clinical applications to treat fetal conditions. Particularly, a systematic computational modelling approach is crucial in understanding such complex transport interactions for the placenta

as a whole. However, individual transport components by each transporter must be investigated and developed first due to the current lack of mechanistic models. By developing a novel integrative computational-experimental framework building on recent studies [16, 39], the current work as outlined in the following chapters will ultimately contribute to the development of a 'virtual' placenta to aid the interpretation of experiments and clinical interventions.

# Chapter 3

# Exchange and facilitated transporter – model development and application to placental membrane vesicles studies[1]

## 3.1 Introduction

Amino acid transfer across the placenta is an important determinant of fetal growth [68, 71, 72]. It is well known that placental amino acid transport is mediated by a broad array of specific membrane transporters with overlapping substrate specificity. However, it is not fully understood how these transporters function, both individually and as an integrated system. Recent study introduced integrated approach for the placental transport system [16]; however, an improved mechanistic model is needed for a better understanding for potential clinical applications such as preventing intrauterine growth restriction.

Transfer of amino acids from the maternal blood, across the placenta and into the fetal blood, is a complex process in which amino acids need to cross both the maternal facing microvillous plasma membrane (MVM) and the fetal facing basal plasma membrane (BM) of the placental syncytiotrophoblast [6, 73]. Transport of amino acids is mediated by specific membrane transporter proteins. These include: (i) Accumulative transporters, which can transport amino acids against their gradient using secondary active transport driven by the sodium electrochemical gradient, thereby building up high concentrations in the syncytiotrophoblast [74]. (ii) Exchangers (antiporters), which transfer one amino acid from outside of the plasma membrane in exchange for an amino

[1]This work has been published as Panitchob *et al.*, 2015 and Widdows *et al.*, 2015 as shown in the List of Publications.

acid from inside. (iii) Facilitated transporters, which enable facilitated diffusion of amino acids down the concentration gradient, from the placental syncytiotrophoblast into the fetal circulation, resulting in net transport. As a result, exchangers play an important role in altering the composition of amino acids, but not the net amount, which is the responsibility of the facilitative transporters. Transport proteins expressed at the placental membranes that are thought to function via the exchange mechanism include LAT1 and LAT2 from the SLC7 gene family, of which the transport activity is often referred to as system L – the sodium-independent transport of large (LAT1 and LAT2) and small (LAT2) neutral amino acids [14, 75]. These transporters are common in cells of various other tissues and their substrates include many amino acids. For transport proteins displaying the facilitative transport mechanism, LAT3 and LAT4 from the SLC43 family are expressed at the placental basal membrane [14]. Although, LAT3 and LAT4 share the same Na-independent transport mechanism as LAT1 and LAT2, their substrate specificity is more restricted, *i.e.* they have a lower number of substrates.

While LAT2 is believed to be an obligatory exchanger (strict one-to-one exchange) [19, 66], one study has reported a non-obligatory (facilitative) component [67]. Sodium-independent transport of serine, which can be primarily attributed to the transporter protein LAT2 [39], was used to investigate such transport behaviour that can be found in the placenta. Experiments using isolated plasma membrane vesicles prepared from human placental MVM or BM are commonly used to measure *in vitro* amino acid uptake, allowing for transporter activity to be studied under controlled conditions. In previous placental vesicle studies, sodium-independent serine uptake has been observed when amino acids were initially nominally absent inside the vesicle (zero-*trans* experiment) [39]. However, this is incompatible with the concept of obligatory exchange, which requires amino acid to be present on both sides of the membrane in order for exchange to occur. Therefore, this gives rise to two alternative hypotheses: (i) That sodium independent transport of serine may not be fully obligatory, or alternatively (ii), there is an initial level of endogenous amino acids present inside the vesicle, which could then enable obligatory exchange.

To investigate these possibilities, a mathematical model for tracer uptake was developed based on carrier-mediated transport, which can represent either facilitated transport or obligatory exchange. *In vitro* measurements of serine uptake by placental microvillous membrane vesicles were carried out and the model applied to interpret the results based on the measured apparent Michaelis-Menten parameters $K_m$ and $V_{max}$. In order to relate the model to biological experiments, in which the well-known Michaelis-Menten equation is most commonly applied to describe saturable transport processes [39, 66, 76]. However, this equation does not fully represent many important transport phenomena, for instance facilitated diffusion and exchange transporters, which are intrinsically dependent on substrate concentrations on both sides of the plasma membrane. Thus,

while this approach is useful to describe apparent transport properties under specific conditions (*e.g.* initial uptake rates), more complex mechanistic models are required to capture transporter behaviour under various physiological conditions. Therefore, subsequently, model predictions based on this data were used to inform and design an additional series of time-course experiments to provide a more comprehensive analysis of transporter behaviour.

## 3.2 Methods

### 3.2.1 Transporter model: General carrier model

It was assumed that the kinetics of amino acid transport across the placental membrane could be described by a carrier-mediated process [50, 63, 77]. An amino acid cannot traverse the cell membrane on its own, but needs to bind to a specific transport protein [6]. Once the amino acid is bound, the transporter (carrier) can undergo a conformational change, exposing the substrate binding site to the other side of the plasma membrane to allow for transport across. Depending on the assumptions made, the carrier model can represent both amino acid transport mediated by obligatory exchangers, as well as non-obligatory (facilitative) transporters. Note that an extensive treatment of carrier models can be found in the reference work by Stein [63].

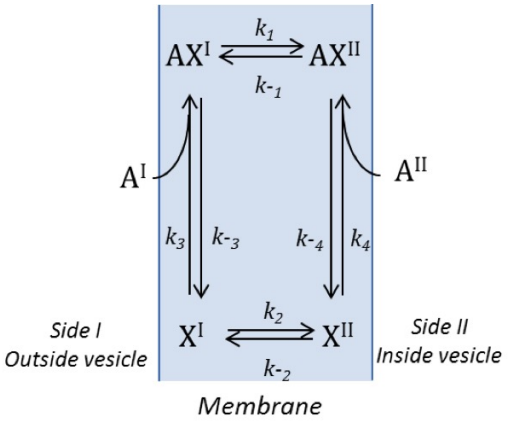


FIGURE 3.1: General carrier model for a single substrate. Schematic including the different transporter states and the various binding and translocation rate constants. Transporter $X$ can bind to substrate $A$ to form a complex $AX$. Depending on parameters, $X$ can translocate between the outside ($I$) and inside ($II$) of the vesicle in either loaded or unloaded form.

A general carrier model (schematic diagram shown in Figure 3.1) is realised based on the following assumptions: The transporter, designated as unbound carrier $X$, is constrained in the membrane and can adopt two alternative states $I$ and $II$, with binding sites exposed on either side of the membrane. The amino acid $A$ can reversibly bind to the transporter $X$ to form the bound carrier complex $AX$, which can also alternate between

two different states on either side of the membrane. It is assumed that each carrier can only bind a single molecule of amino acid. Translocation or chemical reaction between each of the four states in Figure 3.1 is governed by the rate constants $k_i$ (unit of $s^{-1}$ or l $mol^{-1}s^{-1}$). $[A]^i$, $[X]^i$, $[AX]^i$ represent the concentration of solute $A$, carrier $X$, or carrier-solute complex $AX$, where $i$ represents the membrane surface with side $I$ or side $II$. Note that concentration has the unit of mole per litre.

The net flux $J_{AX}$ of the substrate-transporter complex $AX$ directed from side $I$ to side $II$, can be represented as the net effect of the forward and backward directed fluxes. The same applies for the net flux $J_X$ of unbound transporter $X$ from side $I$ to $II$.

From Figure 3.1, the fluxes can be written as follows:

$$J_{AX} = k_1[AX]^I - k_{-1}[AX]^{II} \tag{3.1}$$

$$J_X = k_2[X]^I - k_{-2}[X]^{II} \tag{3.2}$$

Each flux component is the product of the appropriate linear rate constant and concentration. Note that the fluxes take the unit of the rate constants and the concentrations, therefore have the unit of mole per litre per second (mol $l^{-1}$ $s^{-1}$).

Rapid equilibrium is assumed, *i.e.* amino acid binding is fast compared to translocation across the membrane, which implies that bound and unbound concentrations are considered to be at equilibrium at each side of the membrane [78, 79]. Therefore, the rate constants for binding can be replaced by the following dissociation constants ($K_I$ and $K_{II}$), given by:

$$K_I = \frac{[A]^I[X]^I}{[AX]^I} = \frac{k_{-3}}{k_3} \tag{3.3}$$

$$K_{II} = \frac{[A]^{II}[X]^{II}}{[AX]^{II}} = \frac{k_{-4}}{k_4} \tag{3.4}$$

$K_I$ and $K_{II}$ , therefore, by definition have the same unit as the concentration. Note that this corresponds to the binding ($k_3$, $k_4$) and unbinding rate constants ($k_{-3}$, $k_{-4}$) have the dimensions of mol $l^{-1}$ $s^{-1}$ and $s^{-1}$, respectively.

Within the membrane, the transporters are assumed to be conserved [62–64]. Hence, the total number of transporters $x_T$ is given by:

$$[X]^I + [X]^{II} + [AX]^I + [AX]^{II} = x_T \tag{3.5}$$

Quasi-steady state transport is assumed, *i.e.* the time scale of binding and translocation is fast compared to any changes in concentration within the compartments [80]. Thus quasi-steady state transport implies that the sum of the fluxes of bound and unbound carrier must be zero [62–64], *i.e.* they must be equal and opposite for the transport cycle to continue:

$$J_X + J_{AX} = 0 \tag{3.6}$$

Substrate $A$ can only cross the cell membrane bound to the transporter, therefore $J_A = J_{AX}$. Then by rearranging these equations, the general equation for describing the flux of substrate $A$ into the cell is given by:

$$J_A = \frac{(k_{-2}k_1K_{II}[A]^I - k_2k_{-1}K_I[A]^{II})x_T}{(k_1+k_{-1})[A]^I[A]^{II} + (k_{-2}+k_1)K_{II}[A]^I + (k_2+k_{-1})K_I[A]^{II} + (k_2+k_{-2})K_{II}K_I} \tag{3.7}$$

**Michaelis-Menten interpretation**: In experimental vesicle studies, uptake is usually reported in terms of apparent Michaelis-Menten parameters. Considering only the initial flux $J_{A_0}$, then all initial concentrations are known and for the case of zero-*trans* uptake, Equation 3.7 reduces to:

$$J_{A_0} = \frac{k_{-2}k_1[A]_0^I x_T}{(k_{-2}+k_1)[A]_0^I + (k_2+k_{-2})K_I} \tag{3.8}$$

Therefore, the apparent Michaelis-Menten parameters can be expressed as follows [49, 78]:

$$K_{app} = \frac{k_2+k_{-2}}{k_{-2}+k_1}K_I \tag{3.9}$$

$$V_{app} = \frac{k_{-2}k_1x_T}{(k_{-2}+k_1)} \tag{3.10}$$

Thus $K_{app}$ is a function of the external substrate dissociation constant $K_I$, as well as the transporter translocation rates, while $V_{app}$ is a function of the translocation rates of the bound and unbound carrier.

**Parameter reduction**: For the transporter model, *e.g.* Equation 3.7, the number of kinetic parameters in the model can be reduced to lower the complexity of the model when applied to the experiments. These simplifying steps were made in first instance to derive the simplest possible model that can still adequately represent the specific transporter mechanism, only adding further complexity as necessary based on

the comparison with the experimental data. The rationale for each step is described as follows:

1. *Equal translocation rate*: First, it was assumed that the forward ($k_i$) and backward ($k_{-i}$) translocation occurs at the same rate. However, note that different rates could apply for the carrier substrate complex $AX$ and the unbound transporter $X$. The translocation rates as defined in Figure 3.1 can be expressed as follows:

$$k_1 = k_{-1} = k \tag{3.11}$$

$$k_2 = k_{-2} = hk \tag{3.12}$$

Here $k$ represents the translocation rate constant for the bound carrier-substrate complex $AX$ in either direction. Thus, $h$ denotes the translocation rate of the unbound carrier $X$ as a fraction of that of the carrier-substrate complex (*i.e.* the relative unbound-to-bound translocation rate). Therefore, the fluxes of the bound and unbound carrier become:

$$J_{AX} = k([AX]^I - [AX]^{II}) \tag{3.13}$$

$$J_X = hk([X]^I - [X]^{II}) \tag{3.14}$$

2. *Microscopic reversibility*: The transport mechanisms considered here are passive in nature, driven by concentration gradients only, without any energy input in the form of *e.g.* ATP. Therefore, the principle of microscopic reversibility implies that, for a cyclic transport process, the product of the clockwise rate constants is equal to the product of the anti-clockwise rate constants, Equation 3.15 [64, 81] (*i.e.* based on the equilibrium of each step in the transport cycle at steady state and the known internal and external concentrations at equilibrium):

$$k_1 k_{-4} k_{-2} k_3 = k_{-1} k_{-3} k_2 k_4 \tag{3.15}$$

Under the assumption of rapid equilibrium Equation 3.15 reduces to:

$$\frac{k_1}{k_{-1}} = \frac{k_2}{k_{-2}} \frac{K_I}{K_{II}} \tag{3.16}$$

Thus if the translocation rate constants in both directions are assumed to be equal (Equation 3.11–Equation 3.12), then the substrate dissociation constants on both sides of the membrane also necessarily have to be equal ($K_I = K_{II} = K$). Conversely, Equation 3.16 also implies that if the dissociation constants were

assumed to be different on both sides, then all translocation rates cannot be equal. Consequently, based on these assumptions, the model as given by Equation 3.7 reduces to:

$$J_A = \frac{2V_{J_A}hK([A]^I - [A]^{II})}{2[A]^I[A]^{II} + K(h+1)([A]^I + [A]^{II} + K)} \tag{3.17}$$

where, $V_{J_A} = \frac{kx_T}{2}$.

Here $h$ is dimensionless, $K$ has unit of concentration ($\mu$mol l$^{-1}$) and $V_{J_A}$ is in $\mu$mol m$^{-2}$ min$^{-1}$. The rate of change of the concentration within the vesicle $\frac{d[A]^{II}}{dt}$ can be obtained by multiplying the flux $J_A$ by the area to volume ratio of the vesicle. In this form, Equation 3.17 represents transport of only a single substrate. A similar procedure as described above can be adopted for the transport of multiple substrates. The resulting expression for two substrates is given in Equation 3.25.

Thus, based on these two considerations described above, the number of the model's kinetic parameter was cut in half, from 6 to 3. However, any potential asymmetry in these parameters can affect the transient behaviour of the model, which will be explored further as outlined in Section 3.2.3.

### 3.2.2 Exchange/facilitative transporter model: Application of the model

With the carrier-model realised in the previous section, further model development is required to apply the model to the experimental conditions, which are described in Section 3.2.4. In particular the model needs to be extended to account for multiple substrates. An overview of the model is presented in Figure 3.2. Radiolabelled substrate was used experimentally to measure uptake, while unlabelled substrate can either be present inherently, or added as part of the experimental design. Therefore, radiolabelled substrate $A$ and unlabelled substrate $B$ were distinguished explicitly in the model. The transporter, designated as unbound carrier $X$, can adopt two alternative states $I$ and $II$, with a binding site exposed either on the outside $I$ or inside $II$ of the membrane. Amino acids $A$ and $B$ can bind reversibly to the transporter $X$ to form a bound substrate-carrier complex, $AX$ or $BX$, which itself can also alternate between the outside and inside of the plasma membrane (Figure 3.1). It was assumed that each carrier could only bind a single amino acid molecule at any one time [82].

A number of simplifying assumptions were made to reduce the number of parameters to the lowest possible to represent the main features of the proposed transport mechanism. The radiolabelled amino acid $A$, and unlabelled amino acid $B$ were assumed to have identical transport characteristics. The translocation rate constants for the loaded transporter complex were assumed to be equal in forward and backward directions,

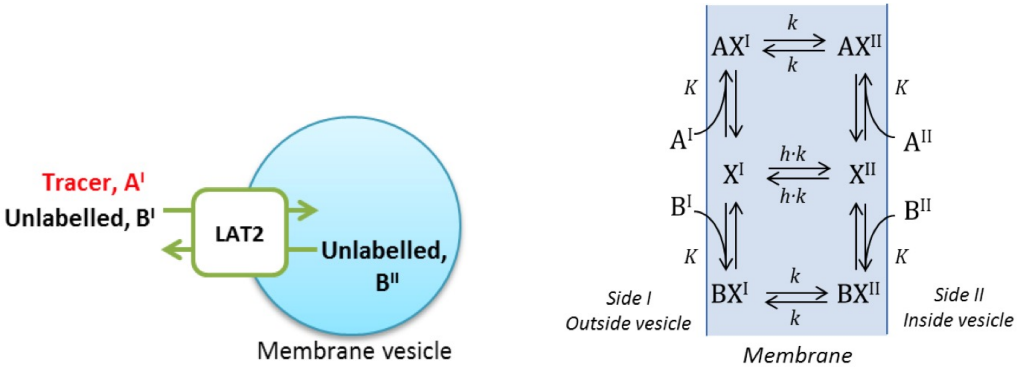


(a) (b)

FIGURE 3.2: Overview of the exchanger/facilitative experimental system and transporter model. a) Transporter activity was evaluated by measuring the uptake of a radiolabelled tracer $A$ into placental microvillous membrane vesicles. b) Transporter model, schematic showing the different transporter states. Transporter $X$ can bind to either tracer $A$ or unlabelled substrate $B$ to form a complex $AX$ or $BX$, which can then translocate between the outside ($I$) and inside ($II$) of the vesicle plasma membrane. Transporter $X$ can also translocate on its own, depending on the parameter $h$. The case $h = 0$ corresponds to an obligatory exchanger, while for $h \neq 0$ the transporter will display facilitative diffusion.

both given by the rate constant $k$. This then also implied the same binding affinity on the inside and outside of the membrane, *i.e.* equal dissociation constants $K$, based on thermodynamic arguments (Equation 3.3–Equation 3.4). The bound and unbound carriers do not necessarily transfer at the same rate. Therefore, in addition, a parameter $h$ was introduced to represent the relative mobility of the unbound carrier $X$ with respect to the bound carrier complex $AX$ or $BX$. This is shown as followed:

From Figure 3.2b, the fluxes can be written as:

$$J_{AX} = k([AX]^I - [AX]^{II}) \tag{3.18}$$

$$J_{BX} = k([BX]^I - [BX]^{II}) \tag{3.19}$$

$$J_X = hk([X]^I - [X]^{II}) \tag{3.20}$$

This parameter $h$ is critical in distinguishing obligatory exchange from non-obligatory transport. As can be observed from Figure 3.2b, for $h = 0$, the unbound carrier does not move on its own and only the bound carrier complex can translocate. Therefore transport is a perfectly obligatory exchange process in which $A$ needs to be exchanged for $B$ on a 1:1 basis for any net transport to occur. In contrast, if $h$ is not zero then

the unbound carrier can move on its own. Therefore the process is non-obligatory, as no substrate is required on the other (*trans*) side of the membrane in order for the carrier to return and continue the transport cycle. Thus for $h > 0$ this can give rise to facilitated diffusion.

As described in previous section, rapid equilibrium is assumed. Therefore, the rate constants for binding can be replaced by the following dissociation constants $K$, which are assumed the same for both species $A$ and $B$ on both side of the membrane, given by:

$$K = K_I = \frac{[A]^I[X]^I}{[AX]^I} = \frac{[B]^I[X]^I}{[BX]^I} \tag{3.21}$$

$$K = K_{II} = \frac{[A]^{II}[X]^{II}}{[AX]^{II}} = \frac{[B]^{II}[X]^{II}}{[BX]^{II}} \tag{3.22}$$

$K$, therefore, by definition has the same unit as the concentration. Note that this corresponds to the binding ($k_3$, $k_4$) and unbinding rate constants ($k_{-3}$, $k_{-4}$) have the dimensions of l mol$^{-1}$ s$^{-1}$ and s$^{-1}$, respectively.

Using conservation of the total number of transporters $x_T$ is given by:

$$[X]^I + [X]^{II} + [AX]^I + [AX]^{II} + [BX]^I + [BX]^{II} = x_T \tag{3.23}$$

In a similar manner as in the previous section, quasi-steady state transport is assumed, which implies that the sum of the fluxes of the bound and unbound carrier must be zero:

$$J_X + J_{AX} + J_{BX} = 0 \tag{3.24}$$

Based on the assumptions described earlier, the following equation can be derived for the uptake of radiolabelled substrate $A$ into the vesicle:

$$\frac{d[A]^{II}}{dt} = \frac{2V\left([A]^I([B]^{II} + Kh) - [A]^{II}([B]^I + Kh)\right)}{2[Tot]^I[Tot]^{II} + K(h+1)([Tot]^I + [Tot]^{II}) + 2hK^2} \tag{3.25}$$

where,

$$[Tot]^i = [A]^i + [B]^i, \quad \text{for } i = I, II.$$

$$[A]_0^I = A_1,\ [B]_0^I = B_1,\ [A]_0^{II} = 0,\ [B]_0^{II} = B_2$$

Here $h$ is dimensionless, $K$ has unit of concentration ($\mu$mol l$^{-1}$) and the uptake rate $V$ is in $\mu$mol l$^{-1}$ min$^{-1}$. Note that $V$ is in concentration per unit time as it incorporates the vesicle volume (*i.e.* flux in mol min$^{-1}$ divided by vesicle volume). Note that the initial conditions for each substrate can vary depending on the experimental designs, which are explained in Section 3.2.4 and 3.2.5. Thus from Equation 3.25, obligatory exchange and non-obligatory or facilitative transport are essentially based on the same model, depending on the value of $h$. Note that the uptake of unlabelled substrate $B$ can be expressed in a similar manner as $A$ by the following equation:

$$\frac{d[B]^{II}}{dt} = \frac{2V\left([B]^{I}([A]^{II} + Kh) - [B]^{II}([A]^{I} + Kh)\right)}{2[Tot]^{I}[Tot]^{II} + K(h+1)([Tot]^{I} + [Tot]^{II}) + 2hK^2} \tag{3.26}$$

where,

$$[Tot]^{i} = [A]^{i} + [B]^{i}, \quad \text{for } i = I, II.$$

$$[A]_0^I = A_1,\ [B]_0^I = B_1,\ [A]_0^{II} = 0,\ [B]_0^{II} = B_2$$

However in the Results, the uptake of $B$ is not shown as substrate $A$ is the only variable of interest.

**Michaelis-Menten interpretation**: In most experimental vesicle studies only the initial uptake rate is measured, with no amino acids added inside the vesicle (zero-*trans* conditions). Assuming Michaelis-Menten kinetics, uptake is then usually quantified in terms of the parameters $V_{max}$ and $K_m$, *i.e.* the maximum uptake rate and half maximum rate concentration, respectively. If we now consider Equation 3.25 with no tracer inside at the start of the experiment $[A]_0^{II} = 0$, then the initial rate of tracer uptake can be written in the following form:

$$\frac{d[A]^{II}}{dt}_{(t=0)} = \frac{V_{app}[A]_0^I}{[Tot]_0^I + K_{app}} \tag{3.27}$$

where,

$$V_{app} = \frac{2V([B]_0^{II} + Kh)}{2[B]_0^{II} + K(h+1)} \tag{3.28}$$

$$K_{app} = \frac{K(h+1)[B]_0^{II} + 2hK^2}{2[B]_0^{II} + K(h+1)} \tag{3.29}$$

Thus, for initial uptake the model reduces indeed to a Michaelis-Menten relationship, where $V_{app}$ and $K_{app}$ are the apparent Michaelis-Menten parameters. However, critically it can be observed from Equation 3.28–3.29 that these apparent Michaelis-Menten

parameters depend directly on the value of the parameter $h$, as well as the concentration of any unlabelled substrate $[B]_0^{II}$ that may be present inside the vesicle. Therefore, Equation 3.27 can be applied to interpret apparent uptake parameters for either obligatory or non-obligatory exchange.

### 3.2.3 Asymmetry of the transport parameters in exchanger/ facilitative transporter model

In this section the implications of asymmetry in transport parameters for the model is explored further. The schematic of the extended model with explicit translocation rate and dissociation constants is shown in Figure 3.3. The corresponding model equation, derived based on the same assumptions as in Equation 3.18–3.24, is given in Equation 3.30.

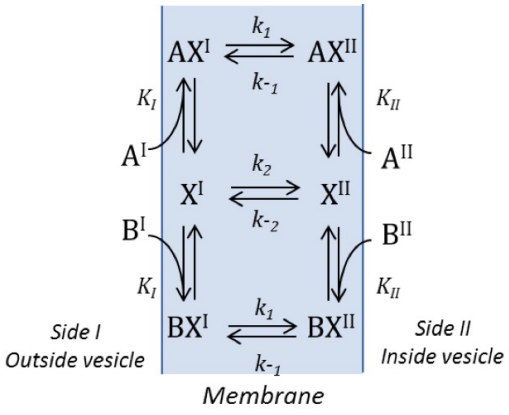


FIGURE 3.3: Extended exchanger/facilitative transporter model for two substrates ($A$ is radiolabelled, and $B$ is unlabelled). Schematic including the different transporter states and the various dissociation and translocation rate constants. Transporter $X$ can either bind to substrate $A$ or $B$ to form a complex $AX$ or $BX$. $X$ can translocate between the outside ($I$) and inside ($II$) of the vesicle in either loaded or unloaded form with different translocation rate constants in each direction.

$$J_A = \frac{(k_1 k_{-1}([A]^I[B]^{II} - [A]^{II}[B]^I) + k_{-2}k_1 K_{II}[A]^I - k_2 k_{-1} K_I [A]^{II})x_T}{(k_1 + k_{-1})[Tot]^I[Tot]^{II} + (k_{-2} + k_1)K_{II}[Tot]^I + (k_2 + k_{-1})K_I[Tot]^{II} + (k_2 + k_{-2})K_{II}K_I} \tag{3.30}$$

where,

$$[Tot]^i = [A]^i + [B]^i, \quad \text{for } i = I, II.$$

$$[A]_0^I = A_1,\ [B]_0^I = B_1,\ [A]_0^{II} = 0,\ [B]_0^{II} = B_2$$

**Asymmetric bound translocation rate and dissociation constants**: If asymmetry in the translocation rate constants of the bound transporters ($k_1 \neq k_{-1}$)

is assumed, then the other model parameters must be adjusted in accordance with the thermodynamic constraint for a passive process as given in Equation 3.16. If symmetry in the unbound translocation rate constants ($k_2 = k_{-2} = hk$) is assumed, then Equation 3.16 becomes:

$$\frac{K_{II}}{K_I} = \frac{k_{-1}}{k_1} \tag{3.31}$$

Let $c = K_{II}/K_I$ be the ratio between internal and external dissociation constants, with $K_{II} = cK$ and $K_I = K$, then:

$$\begin{aligned} k_{-1} &= ck \\ k_1 &= k \end{aligned} \tag{3.32}$$

$c$ is then, by definition, the factor that governs the asymmetry in the translocation rates constants. Note that $c$ is unity when symmetry is assumed.

**Asymmetric unbound translocation rate and dissociation constants**: In addition, asymmetry in the translocation rate constants of the unbound transporter ($k_2 \neq k_{-2}$) was explored, with symmetric bound translocation rate constants ($k_1 = k_{-1} = k$). Equation 3.16 then becomes:

$$\frac{K_{II}}{K_I} = \frac{k_2}{k_{-2}} \tag{3.33}$$

Let $c = K_{II}/K_I$ again be the ratio between internal and external dissociation constants, with $K_{II} = cK$ and $K_I = K$, then define:

$$\begin{aligned} k_2 &= chk \\ k_{-2} &= hk \end{aligned} \tag{3.34}$$

**Asymmetric bound and unbound translocation rate constants, with equal dissociation constants**: Furthermore, the case of asymmetry in the translocation rate constants ($k_1 \neq k_{-1}$ and $k_2 \neq k_{-2}$) was explored, with symmetric dissociation constants ($K_I = K_{II} = K$), Equation 3.16 then becomes:

$$\frac{k_1}{k_{-1}} = \frac{k_2}{k_{-2}} \tag{3.35}$$

Let $c = k_1/k_{-1}$ be the ratio between forward and backward translocation rate constants of the bound transporters with $k_1 = ck$ and $k_{-1} = k$, then define:

$$\begin{aligned} k_2 &= chk \\ k_{-2} &= hk \end{aligned} \tag{3.36}$$

### 3.2.4 Experimental design: Experimental kinetics of $^{14}$C-serine uptake into MVM vesicles

Experiments were conducted by Dr. Kate Widdows, Institute of Human Development, University of Manchester. Placentas were obtained following written informed consent with approval of the Central Manchester Research Ethics Committee (REC 12/NW/0574) from uncomplicated singleton pregnancies at term (38–40 weeks gestation) delivered by Caesarean section. MVM vesicles were isolated from each placenta using $Mg^{2+}$ precipitation and differential centrifugation [41, 83]. The final pellet was resuspended in intravesicular buffer (IVB; 290 mmol $l^{-1}$ sucrose, 5 mmol $l^{-1}$ HEPES, 5 mmol $l^{-1}$ Tris, pH 7.4). MVM fragments were vesiculated by passing 15 times through a 25-gauge needle and stored at -80$^o$C prior to use. $^{14}$C-serine uptake (zero-*trans*) experiments were performed under sodium free conditions as previously described [39]. MVM vesicles (diluted to a protein concentration of 10 mg/ml with IVB) were equilibrated to room temperature (21–25$^o$C) prior to uptake. Uptake of $^{14}$C-serine into MVM vesicles was initiated by the addition of 20 $\mu$l MVM vesicle suspension to 20 $\mu$l extravesicular buffer (EVB; 5 mmol $l^{-1}$ HEPES, 5 mmol $l^{-1}$ Tris, 145 mmol $l^{-1}$ KCl, pH 7.4) containing $^{14}$C-serine. An extravesicular tracer concentration of 7.5 $\mu$mol $l^{-1}$ $^{14}$C-serine after dilution was used throughout the study. Uptake of 7.5 $\mu$mol $l^{-1}$ $^{14}$C-serine was confirmed to be linear for up to 15 s for additional unlabelled serine concentrations of (0, 10, 50, 100, 1000 and 2000 $\mu$mol $l^{-1}$), consistent with previous reports [39], while uptake for higher concentrations was not significantly different from zero. To determine the initial uptake rate, tracer uptake into the vesicles was measured at $t = 15$ s. The experiment was stopped by the addition of 2 ml ice-cold Krebs buffer (130 mmol $l^{-1}$ NaCl, 10 mmol $l^{-1}$ $Na_2HPO_4$, 4.2 mmol $l^{-1}$ KCl, 1.2 mmol $l^{-1}$ $MgSO_4$, 0.75 mmol $l^{-1}$ $CaCl_2$, pH 7.4) and filtered through a 0.45 $\mu$m nitrocellulose filter under vacuum. Filters were washed with 10 ml Krebs buffer and the filter-associated radioactivity was determined by liquid scintillation counting. To determine the kinetics of $^{14}$C-serine uptake into MVM vesicles, uptake of (extravesicular, $[A]^I$) 7.5 $\mu$mol $l^{-1}$ $^{14}$C-serine was determined in the presence of increasing extravesicular concentrations of unlabelled serine $[B]^I$ (0.2 $\mu$mol $l^{-1}$–20 mmol $l^{-1}$). For each placenta ($n = 4$), individual measurements were performed at 23 different serine concentrations within this range.

TABLE 3.1: Experimental design matrix (EXP 1–7, 4b) for vesicle exchange experiments, showing the various initial intravesicular and constant extravesicular unlabelled serine concentrations used while measuring the uptake of 7.5 $\mu$mol l$^{-1}$ $^{14}$C-serine tracer ($[A]^{II}$). Note that the initial intravesicular tracer concentration $[A]_0^{II}$ is zero.

| | | Intravesicular unlabelled $[B]_0^{II}$ ($\mu$mol l$^{-1}$) | | |
|---|---|---|---|---|
| | | 0 | 250 | 1000 |
| Extravesicular unlabelled $[B]^I$ ($\mu$mol l$^{-1}$) | 0 | EXP 1 | | |
| | 50 | | | EXP 4b |
| | 250 | EXP 2 | EXP 3 | EXP 4 |
| | 1000 | EXP 5 | EXP 6 | EXP 7 |

In addition, time series experiments were conducted by measuring tracer uptake for placentas ($n = 3$) at specific time points (0, 5, 10, 15, 20, 60, 120, 300, 600 s), for extravesicular concentrations of unlabelled serine $[B]^I$ of 0, 250 and 1000 $\mu$mol l$^{-1}$ (no initial intravesicular concentrations, *i.e.* $[B]_0^{II} = 0$). These experiments were aimed to test if any uptake activity would be observed, and to distinguish if such uptake would then suggest that there was either a facilitative transport component or initial internal endogenous exchangeable serine to enable obligatory exchange.

### 3.2.5 Extended experimental design: Additional time course $^{14}$C-serine uptake vesicle experiments with intravesicular concentrations

Additional time course experiments were designed to comprehensively map the uptake activity behaviour over a range of conditions for different internal as well as extravesicular unlabelled serine levels (0, 250, 100 $\mu$mol l$^{-1}$). As shown in the experimental design matrix in Table 3.1, four extra experimental conditions were included, in which initial intravesicular unlabelled serine $[B]_0^{II}$ was present at 250 and 1000 $\mu$mol l$^{-1}$, to observe possible *trans*-stimulation and/or saturation effects. In addition, an extra condition was added at 50 $\mu$mol l$^{-1}$ external unlabelled serine with 1000 $\mu$mol l$^{-1}$ initial intravesicular unlabelled serine concentrations (EXP 4b) to observe the uptake at a higher outwards directed gradient (compared to EXP 4).

### 3.2.6 Numerical implementation

Model equations were implemented in Matlab (R2013a). To predict the concentration within the vesicle over time, time series were generated by integrating Equation 3.25 using the 'ode45' function (Runge-Kutta (4th, 5th) method) using variable time step with relative and absolute tolerances of $10^{-4}$ and $10^{-6}$, respectively. Note that the integration step was performed with the initial conditions as presented in Table 3.1 and that extravesicular concentrations were assumed constant due to the large volume of the buffer. Apparent Michaelis-Menten parameters were determined by fitting Equation 3.27 to the averaged experimental uptake rate measurements, using the 'fminsearch' minimisation function (Nelder-Mead simplex method) with the cost function defined as the residual sum of squares of errors between the model simulations and experimental measurements as described below:

$$RSS = \sum_{i=1}^{n} \left( \frac{[A]_i^{II,Model} - [A]_i^{II,Exp}}{[A]_i^{II,Exp}} \right)^2 \tag{3.37}$$

To account for the difference in absolute values between experimental conditions, for each data point the difference between model prediction and experiment was normalised first by the experimental value, squared and then summed over all points to yield the overall error criterion. Note that the initial guess values for the fitted parameters that were used by the 'fminsearch' minimisation function were chosen within the same order of magnitude of physical and/or experimentally reported values. Multiple initial guess values were attempted to confirm that the fitting algorithm converged to a unique solution. Note that the sample size of the experimental data may be increased (*e.g.* from $n = 3$ as in outlined in Section 3.2.4) to confidently determine the standard deviation in the data. Variation in the standard deviation of the data can then also be weighted accordingly in the cost function for the fitting procedure, however this was not done presently.

An intravesicular volume of 1.6 $\mu$l mg protein$^{-1}$ was used to convert tracer uptake from units of mol per mg protein to concentration in mol per unit volume. This volume conversion factor was based on the previously measured equilibrium $Na^+$ uptake (at 60 min) of 1.60±0.20 nmol mg protein$^{-1}$ (mean±SEM, $n = 6$), at a $Na^+$ substrate concentration of 1 nmol $\mu$l$^{-1}$, obtained using MVM vesicles prepared by the same method [83].

The same procedure was used to fit the time course experiments. A single set of parameters $h$ and $V$ was fitted to represent all experimental conditions, as specified further in the results. Parameter $K$ was also fitted in the complete time course experiments in addition to $h$ and $V$. The list of parameters for estimation is presented in Table 3.2.

A sensitivity analysis was carried out to determine the impact of individual parameters on the fit quality by fixing these parameters at a range of different levels and then repeating the full parameter estimation procedure for each case. A relative normalised error was computed by dividing the total error for each parameter variation case (as given by the cost function in Equation 3.37) by the reference error determined from the best-fitted case (*e.g.* the normalised error takes value of 1 and over, since the reference error for the best fit case is the lowest). Note that the ranges of each parameter variation were chosen to cover the entire range of concentrations or feasible parameter values for the experiments.

TABLE 3.2: Summary of model parameters estimated using the fitting algorithm.

| Symbol | Name | Unit | Description |
|---|---|---|---|
| $V$ | Uptake rate | $\mu$mol l$^{-1}$ min$^{-1}$ | Maximal transport rate |
| $K$ | Dissociation constant | $\mu$mol l$^{-1}$ | Substrate binding parameter |
| $h$ | Unloaded carrier mobility transporter | - | Ratio of unbound-to-bound translocation rate |

## 3.3 Results

### 3.3.1 Model behaviour – initial uptake rate

Generic model behaviour (Equation 3.27) is illustrated in Figure 3.4 for parameters $V = 1$ and $K = 0.5$. Note that for the purpose of showing clearly the fundamental behaviour of the transport model, all variables and parameters were used in dimensionless form, *i.e.* implying normalisation. It can be observed that both non-obligatory and obligatory exchange can give rise to Michaelis-Menten-type behaviour (*i.e.* linear uptake for low and constant uptake for high external concentrations at saturation), depending on conditions. For the non-obligatory model in Figure 3.4a, the initial uptake rate of tracer $A$ was calculated under zero-*trans* conditions, *i.e.* internal concentrations were set to zero $[A]_0^{II} = 0$ and $[B]_0^{II} = 0$. In addition, for clarity the external unlabelled concentration was also set to zero $[B]_0^{I} = 0$. Under these conditions, uptake as a function of external tracer concentration $[A]_0^{I}$ displayed Michaelis-Menten behaviour depending on the value of $h$. The case $h = 0$ corresponds to obligatory exchange and therefore did not show any uptake in the absence of internal concentrations, as expected. Similarly, in Figure 3.4b, results are reported for the case of obligatory exchange ($h = 0$), but now assuming the presence of different concentrations of unlabelled concentrations $[B]_0^{II}$ inside the vesicle, as an internal concentration of amino acids is a prerequisite for obligatory exchange ($[A]_0^{II} = 0$ and $[B]_0^{I} = 0$, as before). It can be seen that the initial uptake rate as a function of external concentration displayed a strong dependence on internal concentration, with a significant uptake rate already reached for relatively low internal

concentrations, *e.g.* $[B]_0^{II} = 0.1$. Again, for the case $[B]_0^{II} = 0$ no uptake took place, as would be expected for an obligatory exchanger.

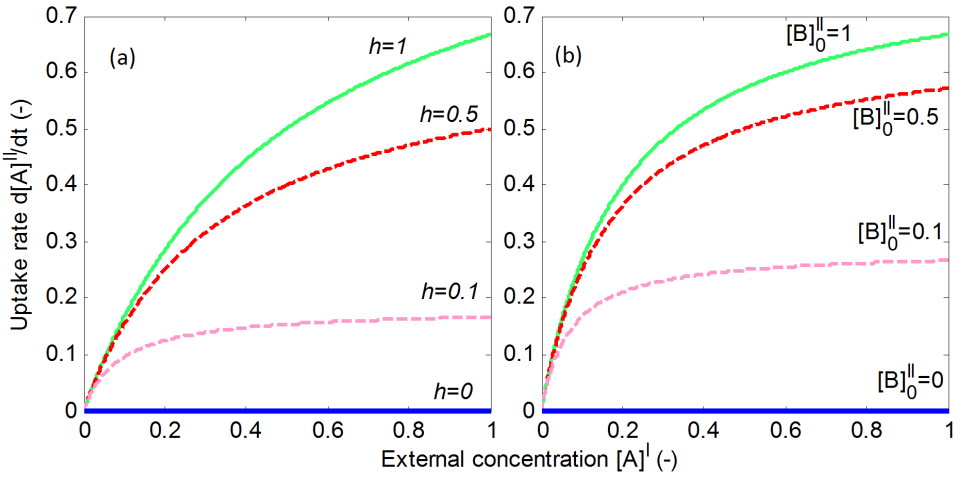


FIGURE 3.4: Exchange/facilitative model simulations: Initial uptake rate of tracer $A$ as a function of its external concentration $[A]^I$. a) Non-obligatory transport for different values of $h$, with zero internal substrate. b) Obligatory exchanger ($h = 0$) for different concentrations of unlabelled substrate $[B]^{II}$ inside the vesicle (arbitrary units). Both hypotheses display qualitatively similar Michaelis-Menten type behaviour.

### 3.3.2 Model behaviour – time series

In order to differentiate non-obligatory *vs* obligatory exchange behaviour, a potential time series experiment was simulated (Figure 3.5), for a combination of different values of $h$ and internal concentration levels $[B]_0^{II}$. It was assumed the extravesicular buffer volume is large enough so that external concentrations could be assumed constant. Therefore, a fixed value of external tracer $[A]^I = 1$ and unlabelled concentration $[B]^I = 0$ were used in Equation 3.25, with the same parameters $V = 1$ and $K = 0.5$. The initial tracer inside the vesicle $[A]_0^{II} = 0$. Figure 3.5a shows that in the absence of initial internal concentrations ($[B]_0^{II} = 0$), uptake followed a facilitated diffusion process, in which the predicted tracer concentration within the vesicle rises up to an equilibrium level equal to the external concentration. The rate at which this equilibrium is reached increases with increasing $h$, while no uptake is observed for the obligatory exchanger ($h = 0$), as before.

However, Figure 3.5b shows that no difference between the obligatory and non-obligatory models could be observed for the case ($[B]_0^{II} = 1$) where the initial internal concentration is equal to the external tracer concentration. Furthermore, predictions were not sensitive to the value of $h$, *i.e.* note that all lines in the figure overlap.

In contrast, Figure 3.5c shows clear differences between the obligatory and non-obligatory model for the case of high internal concentrations ($[B]_0^{II} = 5$). For the obligatory exchanger ($h = 0$) the tracer concentration increases monotonically until an

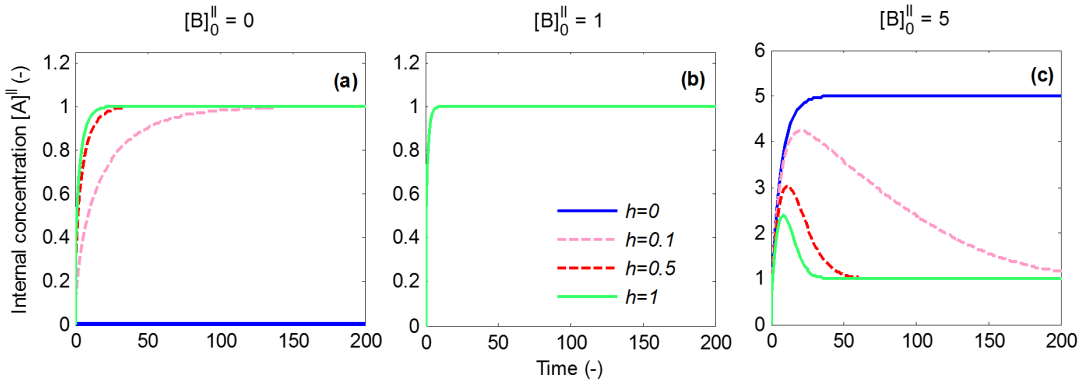


FIGURE 3.5: Theoretical model behaviour for obligatory exchange ($h = 0$) and facilitated transport ($h > 0$). Time series for different values of $h$ (relative mobility of the unloaded transporter) and initial concentrations $[B]_0^{II}$ inside the vesicle (arbitrary units). The external concentration of tracer $[A]^I = 1$ in all cases. a) Zero initial substrate inside; note that no uptake takes place for obligatory exchange. b) Equal internal and external concentrations; note all lines overlap. c) Higher internal concentration; note the overshoot dependent on the value of $h$, with $h = 0$ corresponding to obligatory exchange and $h > 0$ to facilitated diffusion.

equilibrium is reached, which is higher than the external concentration. This is because at the end of the experiment all internal unlabelled substrate present initially ($[B]_0^{II}$) has been replaced by tracer $[A]^{II}$ (*i.e.* as a result of continued 1:1 exchange with only tracer present externally and unlabelled substrate assumed to dilute out, $[B]^I = 0$ as stated previously).

More complex transient behaviour is observed for the non-obligatory model ($h \neq 0$) in Figure 3.5c. The large outwardly directed gradient of unlabelled substrate initially drives tracer uptake via exchange, resulting in a substantial overshoot, which then goes back to the diffusive equilibrium as the outwardly directed gradient dissipates. The rate at which the tracer concentration returned to the diffusive equilibrium depended directly on the value of $h$, *i.e.* the mobility of the unloaded carrier. Thus for low values of $h$ the transporter primarily behaved as a 1:1 exchanger initially, before returning to equilibrium more slowly via facilitated diffusion.

### 3.3.3 Model interpretation of serine uptake experiment

Next, to relate the model to the experimental data, the tracer uptake measurements were fitted using Equation 3.27 as outlined in the Methods (Figure 3.6), resulting in $K_{app} = 87$ $\mu$mol l$^{-1}$ and $V_{app} = 131$ $\mu$mol l$^{-1}$ min$^{-1}$. Subsequently, Equation 3.28 and Equation 3.29 were used to determine the actual values of the model parameters $K$ and $V$ that would correspond to these apparent Michaelis-Menten parameters for different values of $h$ and $[B]_0^{II}$, (Table 3.3). In general $K$ and $V$ were higher than the apparent parameters $K_{app}$ and $V_{app}$, but values decreased for increasing internal serine concentration present. Increasing $h$ also reduced $K$ and $V$, and in addition decreased

the sensitivity to the internal serine concentration. For $h = 1$ the model parameters became independent of any internal serine concentration present, and moreover $K$ and $V$ corresponded directly to the apparent Michaelis-Menten parameters $K_{app}$ and $V_{app}$.

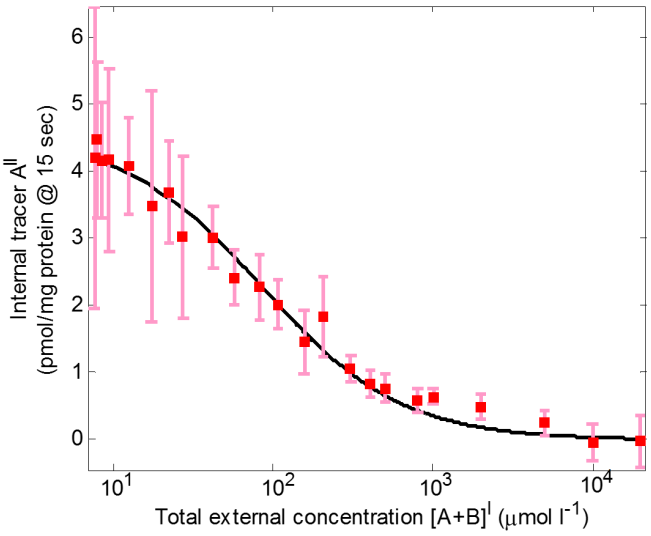


FIGURE 3.6: Results of vesicle exchange experiments: Initial tracer uptake as a function of the total external concentration (labelled + unlabelled substrate). 7.5 $\mu$mol $l^{-1}$ tracer ($^{14}$C-serine) was used throughout, while the concentration of unlabelled serine was increased. Data presented as mean and standard deviation ($n = 4$). Experimental results were fitted using Equation 3.27 (solid black line, $R^2 = 0.98$).

### 3.3.4 Model predictions based on experimental parameters

Subsequently, the model was used to predict the uptake behaviour that could be expected if the experiment were continued beyond the initial phase. Figure 3.7 shows the time series results generated using the model parameters derived in Table 3.3 for the corresponding initial conditions and values of $h$. For the obligatory exchanger ($h = 0$) tracer concentrations continued to rise to very high values, until equilibrium was reached at the level of the initial unlabelled concentration present inside $[B]_0^{II}$ (*i.e.* all unlabelled substrate replaced by labelled on a 1:1 basis). For non-zero $h$ in all cases, internal tracer concentrations eventually reached a diffusive equilibrium equal to the external tracer concentration of 7.5 $\mu$mol $l^{-1}$. For zero initial internal concentration ($[B]_0^{II} = 0$), the tracer concentrations rose monotonically, while for non-zero initial concentrations $[B]_0^{II}$, first an overshoot was produced due to *trans*-stimulation before decreasing again to the diffusive equilibrium level. In addition, the peak height and rate at which the concentration returned to equilibrium were determined by the value of $h$, *i.e.* the relative mobility of the unloaded transporter.

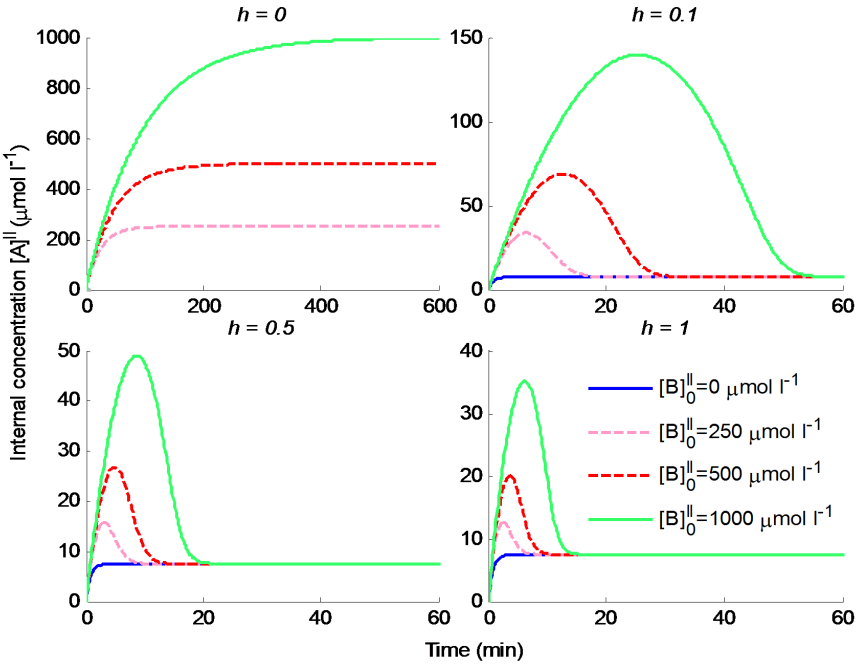


FIGURE 3.7: Exchange/facilitative transporter model predictions based on the experimental initial uptake data. Time series were generated for the various scenarios, including different values of $h$, internal substrate concentrations $[B]_0^{II}$ and model parameters based on the experimental measurements (Table 3.3). Note the difference in timescale for $h = 0$ (top left).

TABLE 3.3: Exchange/facilitative transporter model parameters (Equation 3.25) corresponding to the measured apparent Michaelis-Menten parameters, for different unloaded carrier mobility $h$ and internal concentration $[B]_0^{II}$.

| | $[B]_0^{II} = 0$ | $[B]_0^{II} = 250$ | $[B]_0^{II} = 500$ | $[B]_0^{II} = 1000$ | $\mu$mol l$^{-1}$ |
|---|---|---|---|---|---|
| $h = 0$ | no uptake* | $K = 266$ | $K = 210$ | $K = 190$ | $\mu$mol l$^{-1}$ |
| | | $V = 201$ | $V = 159$ | $V = 144$ | $\mu$mol l$^{-1}$min$^{-1}$ |
| $h = 0.1$ | $K = 478$ | $K = 198$ | $K = 177$ | $K = 167$ | $\mu$mol l$^{-1}$ |
| | $V = 722$ | $V = 175$ | $V = 152$ | $V = 141$ | $\mu$mol l$^{-1}$min$^{-1}$ |
| $h = 0.5$ | $K = 130$ | $K = 119$ | $K = 118$ | $K = 117$ | $\mu$mol l$^{-1}$ |
| | $V = 197$ | $V = 144$ | $V = 138$ | $V = 135$ | $\mu$mol l$^{-1}$min$^{-1}$ |
| $h = 1$ | $K = 87$ | $K = 87$ | $K = 87$ | $K = 87$ | $\mu$mol l$^{-1}$ |
| | $V = 131$ | $V = 131$ | $V = 131$ | $V = 131$ | $\mu$mol l$^{-1}$min$^{-1}$ |

*The case $h = 0$ corresponds to an obligatory exchanger and therefore cannot represent uptake in the absence of $[B]_0^{II}$.

### 3.3.5 Time course experiments

The results of the time course experiments are presented in Figure 3.8. Uptake of tracer alone (EXP 1 from Table 3.1) displayed a rapid rise in internal concentrations up to constant steady state level. Given the experimental variability, the existence of a small overshoot could neither be confirmed nor excluded. The internal tracer concentration at equilibrium (based on the volume conversion factor of 1.6 $\mu$l mg protein$^{-1}$) was

approximately equal to the external tracer concentration of 7.5 $\mu$mol l$^{-1}$.

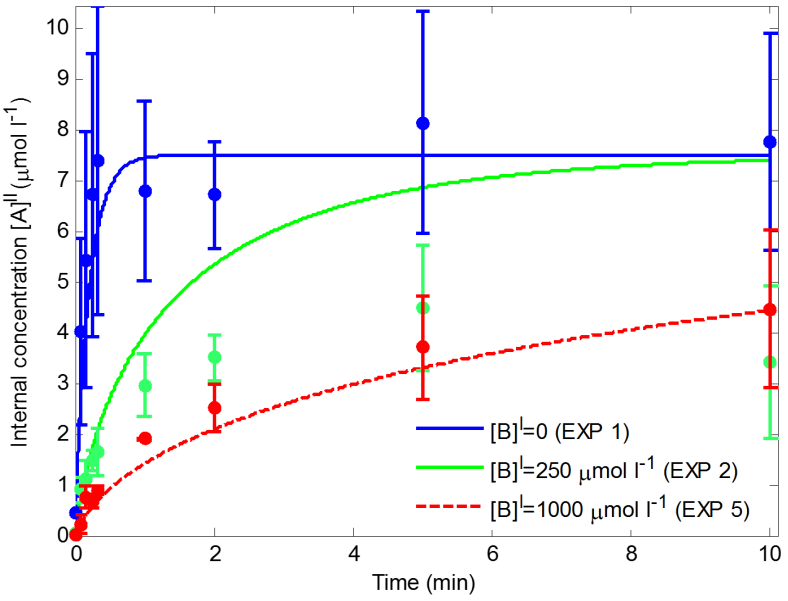


FIGURE 3.8: Exchange experimental results and model fittings. Time course results for the uptake of 7.5 $\mu$mol l$^{-1}$ tracer $[A]^I$ ($^{14}$C-serine) in the vesicle for various concentrations of additional external unlabelled serine $[B]^I$. Experimental data is presented as mean and standard deviation ($n = 3$). Lines represent the model fit ($R^2 = 0.80$) for a facilitated diffusion transport process ($h > 0$) in the absence of initial internal concentrations in the vesicle ($[B]_0^{II} = 0$). Note that facilitated diffusion implies that at steady state the tracer concentrations inside and outside the vesicle are equal.

To further probe the transport behaviour, additional experiments were performed in which either 250 or 1000 $\mu$mol l$^{-1}$ of unlabelled substrate was added to the extravesicular buffer (EXP 2&5 from Table 3.1). As can be observed from Figure 3.8, addition of external unlabelled substrate resulted in a marked inhibition of the initial rate of tracer uptake, dependent on the amount of substrate added. After the initial phase, intravesicular tracer levels in the presence of either 250 or 1000 $\mu$mol l$^{-1}$ external substrate continued to rise at a decreasing rate, but did not reach the level observed for tracer alone within the time frame of the study.

### 3.3.6 Model analysis of time course experiments

First, it was evaluated how well the model could represent the experimental data in absence of internal endogenous substrate ($[B]_0^{II} = 0$). A single set of parameters $h$ and $V$ was fitted, while $K$ was derived using Equation 3.29 from the value of $K_{app} = 87$ $\mu$mol l$^{-1}$ determined previously in Section 3.3.4.

The model results in Figure 3.8 show a good overall representation of the initial tracer uptake for the various external concentrations of unlabelled substrate ($[B]^I = 0$, 250 and 1000 $\mu$mol l$^{-1}$). Furthermore, the time course for 0 and 1000 $\mu$mol l$^{-1}$ was captured

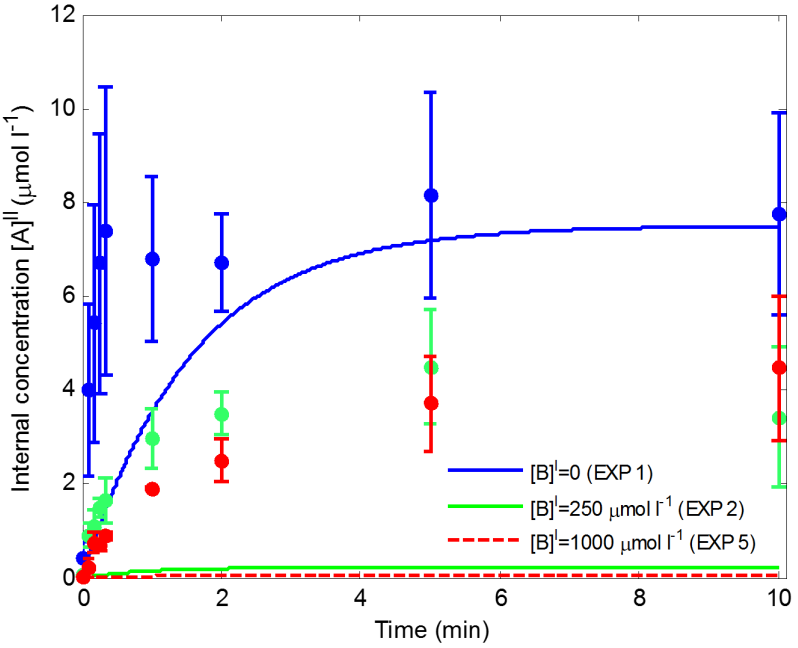


FIGURE 3.9: Exchange experiment time course results and model fittings for an obligatory exchanger ($h = 0$). Lines represent the model fit ($R^2 = -0.18$) in the presence of initial internal substrate $[B]_0^{II} = 7.5$ $\mu$mol l$^{-1}$. Experimental data (same as in Figure 3.8) is presented as mean and standard deviation ($n = 3$). Note that while the experimental equilibrium tracer level for zero external unlabelled serine ($[B]^I = 0$) could be matched, the model predicted a disproportional reduction in uptake for additional external unlabelled serine of 250 and 1000 $\mu$mol l$^{-1}$.

adequately. The main discrepancy observed is the considerable overprediction of uptake for 250 $\mu$mol l$^{-1}$ unlabelled substrate from 60 s onwards.

In addition, the possibility was investigated of obligatory exchange ($h = 0$) in the presence of a small internal level of substrate $[B]_0^{II} = 7.5$ $\mu$mol l$^{-1}$, equal to the external tracer concentration. Only the parameter $V$ was fitted, while $K$ was kept the same value as determined before in Figure 3.8. The results (Figure 3.9) show that while obligatory exchange could match the equilibrium level for tracer alone, it could not simultaneously represent the effect of adding unlabelled external substrate, as this would result in disproportionally low levels of intravesicular tracer.

To provide a more complete overview, the results of the sensitivity analysis of the parameter estimation procedure, as described in Section 3.2.6, are presented in Figure 3.10. The model fit as in Figure 3.8 was repeated, but now for various levels of initial internal substrate $[B]_0^{II}$ ranging from 0 to 1000 $\mu$mol l$^{-1}$ (parameters $h$ and $V$ were fitted, with $K$ determined from Equation 3.29 as before). Overall, the relative error increased with increasing internal substrate concentration (Figure 3.10a). A very small dip in the error criterion could be observed for $[B]_0^{II} = 50$ $\mu$mol l$^{-1}$, however investigation of the predicted time course already displayed an overshoot not present in the experiment (results not shown). Next the sensitivity of the parameter estimation

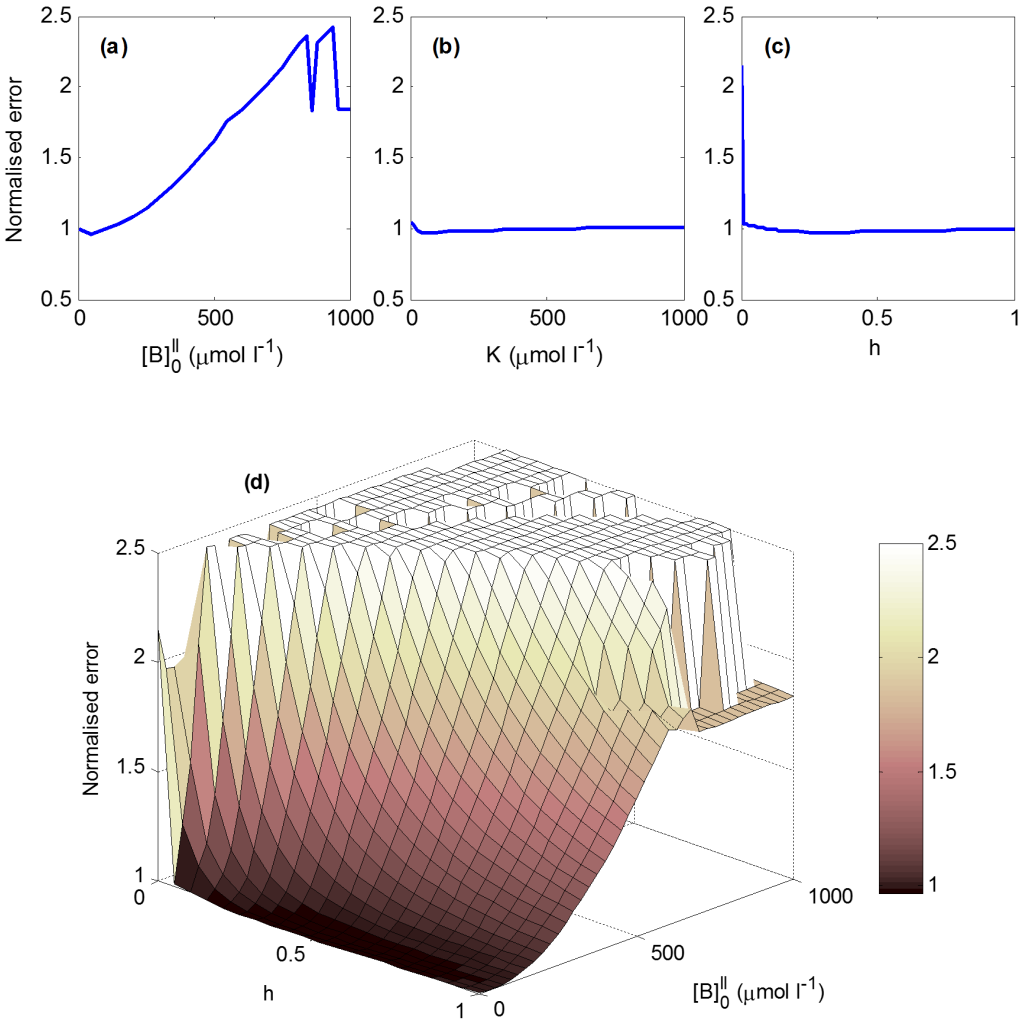


FIGURE 3.10: Exchange/facilitative transporter model sensitivity analysis. The model fit was repeated for a range of fixed parameters and the overall error expressed relative to the fit in Figure 3.8a) Effect of initial internal concentration $[B]_0^{II}$, b) dissociation constant $K$, and c) relative mobility of the unloaded transporter $h$. Note the sharp peak for $h = 0$, while the error is approximately constant for any $h > 0$. d) Combined effect of $h$ and $[B]_0^{II}$ on the fit quality (values $> 2.5$ have been omitted). Note the error is more sensitive to $[B]_0^{II}$ for low values of $h$.

to the dissociation constant $K$ was investigated over the range of 0 to 1000 $\mu$mol l$^{-1}$ (parameters $h$ and $V$ were fitted with $[B]_0^{II} = 0$ $\mu$mol l$^{-1}$). The results in Figure 3.10b demonstrated that the overall error was not significantly affected by $K$. Finally, the effect of the unbound carrier mobility was explored in Figure 3.10c by repeating the fit for various fixed values of $h$ from 0 to 1 (only the parameter $V$ was fitted with $[B]_0^{II} = 0$ $\mu$mol l$^{-1}$, while $K$ was kept the same value as determined before in Figure 3.8). This demonstrated that $h$ did not have a significant impact on the overall error, with the notable exception of a sharp peak at $h = 0$. Looking closer at the estimated parameters revealed that low values of $h$ resulted in high values of $V$ and vice versa, but the shape of the curves was qualitatively similar for any $h > 0$ (results not shown). The combined

effect of $h$ and $[B]_0^{II}$ on the fit quality is displayed in Figure 3.10d, and shows that the overall error is more sensitive to $[B]_0^{II}$ for low values of $h$. For high concentrations the error is highly variable as the fitted time courses cannot represent the experimental data (results not shown). Note that the results of the sensitivity analysis relate to both the model as well as the fitting algorithm, since the fitting was repeated with each parameter fixed in turn. For example, Figure 3.10 shows that for low $[B]_0^{II}$, $h$ cannot be uniquely determined from the error criteria since the error was effectively identical for all non-zero value of $h$.

### 3.3.7 Extended time course experiments and model fitting

The model as given in Equation 3.25 was fitted to the extended time course experimental results, which spanned the eight experimental conditions, to obtain the model parameters ($h$, $V$, and $K$), as the model should be able to represent the system for all experimental conditions. Complete time course uptake experiments (with experimental conditions given in Table 3.1) and model fitting results are shown in Figure 3.11. The model fits suggested non-obligatory behaviour with $h$ parameter value of 0.16, which translated to having a 16% facilitative component when compared to the exchange activity. In addition, a dissociation constant $K$ of 121 $\mu$mol l$^{-1}$ and $V$ of 84 $\mu$mol m$^{-2}$ min$^{-1}$ were fitted ($R^2 = 0.69$). Note that a revised intravesicular volume of 1.3 $\mu$l mg protein$^{-1}$ was used to convert tracer uptake from units of mol per mg protein to concentration in mol per unit volume, which was based on the mean value obtained from previous experiments that used similar buffer conditions [84, 85]. The obligatory exchange model was also attempted but could not represent the experimental data (results not shown). Note that individual data sets were also fitted to observe the variation in the model parameters, however this did not show significant disparity compared to the fitting results of the mean values (results not shown).

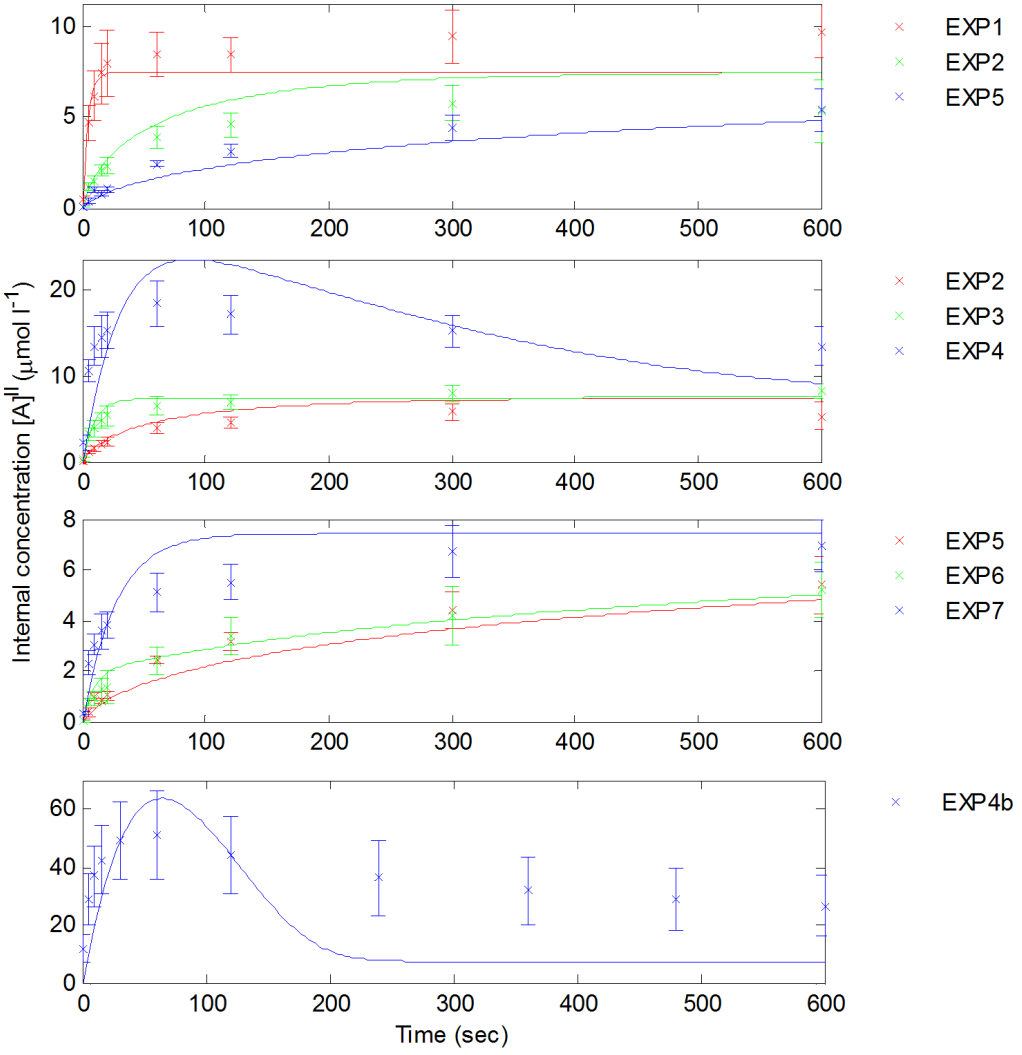


FIGURE 3.11: Extended exchange vesicle experiment; time course results (x) and model fits (solid lines; $R^2 = 0.69$) for a range of internal and external concentrations of unlabelled serine according to the experimental design given by Table 3.1. Note that error bars represent standard deviation of the data ($n = 5$ for EXP1–7, $n = 9$ for EXP4b). A single set of model parameters was used to represent all experimental conditions.

### 3.3.8 Simulations of the asymmetry in model parameters

To investigate the potential impact of asymmetry in transport parameters, the reduced exchanger/facilitative model, which was applied to the experiments, was explored further by explicitly including the different individual rate constants $k$ in both directions and dissociation constants $K$ on each side of the membrane. According to the models developed in Section 3.2.3, the results of the simulations can be shown for three different asymmetry assumptions as follows:

**Asymmetric bound translocation rate and dissociation constants ($k_1 \neq k_{-1}$):** The resulting theoretical predictions for the obligatory exchange model ($h = 0$) and non-obligatory (facilitated) transporter model (for the case $h = 1$) are shown in Figure 3.12, using the parameter values of $k = 1$, $x_T = 1$ and $K = 0.5$ (arbitrary units).

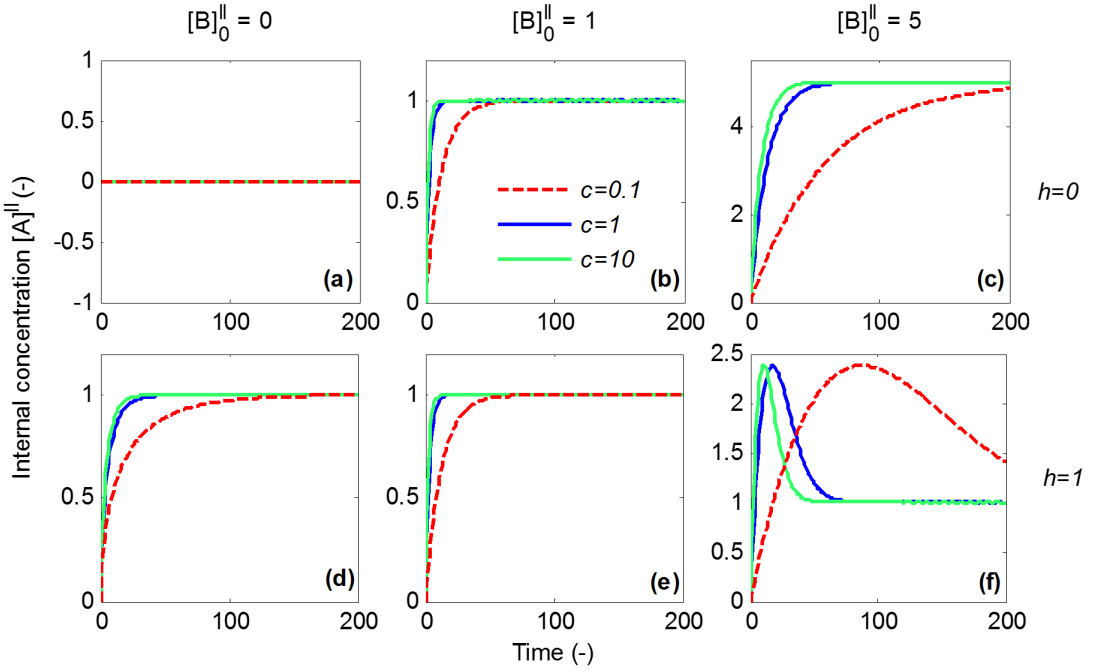


FIGURE 3.12: Effects of asymmetry in bound transporter ($AX$ and $BX$) translocation rate ($k_1 \neq k_{-1}$) and dissociation constants ($k_I \neq k_{II}$) according to Equation 3.31–Equation 3.32. (a–c) Results for obligatory exchange, $h = 0$. (d–f) Results for the non-obligatory model, with $h = 1$. Time series for different values of the asymmetry factor $c$ and initial concentrations $[B]_0^{II}$ inside the vesicle (arbitrary units). The external concentration of tracer $[A]^I = 1$ in all cases. a, d) Zero initial substrate inside. b, e) Equal internal and external concentrations. c, f) Higher internal concentration.

From the results in Figure 3.12 it can be observed that a higher reverse translocation rate constant for the bound transporter ($k_{-1}$) has minimal effect on the model predictions for tracer uptake ($c = 10$), while a lower uptake rate constant ($c = 0.1$) leads to slower uptake for the cases considered. Notably, the value of $c$ shifts the position of the overshoot in time and affects the peak width, but does not affect the peak height (Figure 3.12f).

**Asymmetric unbound translocation rate and dissociation constants** ($k_2 \neq k_{-2}$): The resulting theoretical predictions for the obligatory and non-obligatory models are shown in Figure 3.13, using the same parameters as before.

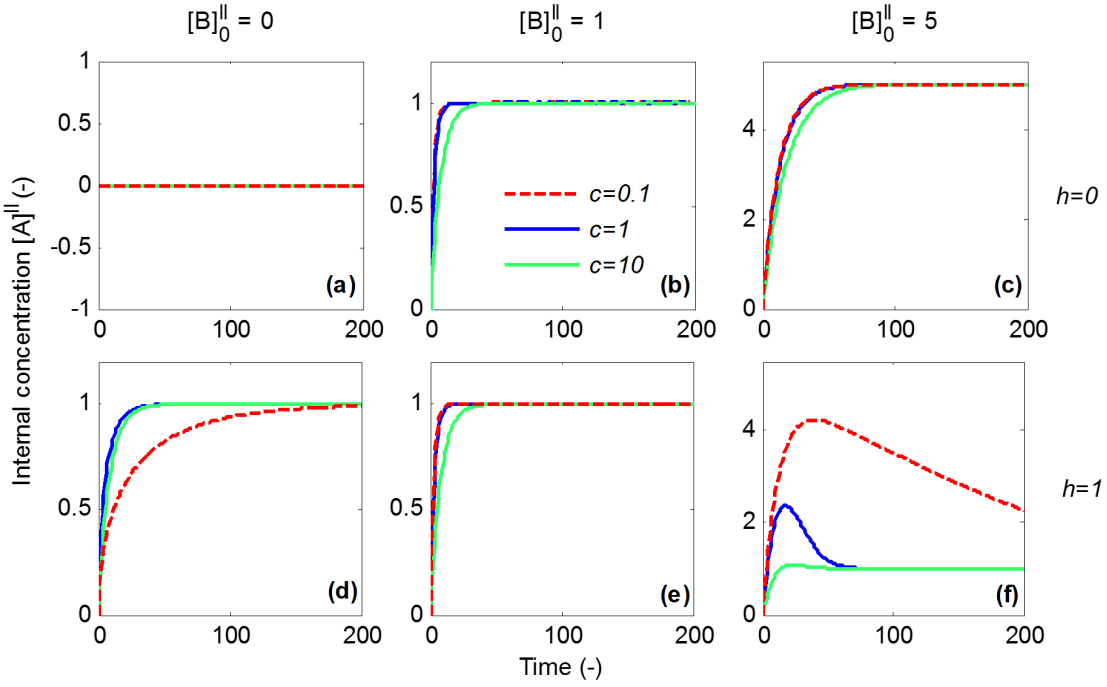


FIGURE 3.13: Effects of asymmetry in unbound transporter ($X$) translocation rate ($k_2 \neq k_{-2}$) and dissociation constants ($k_I \neq k_{II}$) according to Equation 3.33–Equation 3.34. (a–c) Results for obligatory exchange, $h = 0$. (d–f) Results for the non-obligatory model, with ($h = 1$). Time series for different values of $c$ and initial concentrations $[B]_0^{II}$ inside the vesicle (arbitrary units). The external concentration of tracer $[A]^I = 1$ in all cases. a, d) Zero initial substrate inside. b, e) Equal internal and external concentrations. c, f) Higher internal concentration.

For the non-obligatory (facilitative) model, Figure 3.13d shows that in absence of internal substrate, a higher forward translocation rate constant for the unbound transporter ($k_2$) has minimal effect on the model predictions for tracer uptake ($c = 10$), while a lower uptake rate constant ($c = 0.1$) leads to slower uptake. Figure 3.13e shows that this effect of $c$ is reversed in the presence of an initial internal substrate concentration equal to the external tracer concentration. In addition, for this situation there is no difference between the obligatory and non-obligatory model (Figure 3.13b, e). In contrast, marked differences arise for high initial internal substrate concentrations. The obligatory exchange model in Figure 3.13c displays only minor effects, which are due to the difference in dissociation constants depending on $c$, as unbound translocation rates are zero because $h = 0$. However, for the non-obligatory (facilitative) model in Figure 3.13e, a low value of $c$ leads to a higher peak, which decreases more slowly. On the other hand, a high value of $c$ almost completely eliminates the overshoot, since the fast unbound forward translocation rate bypasses tracer uptake in the transport cycle during efflux of initial internal substrate.

**Asymmetric bound and unbound translocation rate constants, with equal dissociation constants** ($k_1 \neq k_{-1}$ and $k_2 \neq k_{-2}$): The resulting theoretical predictions for the obligatory exchange and non-obligatory (facilitated) transport models are shown in Figure 3.14, using the same parameters as before.

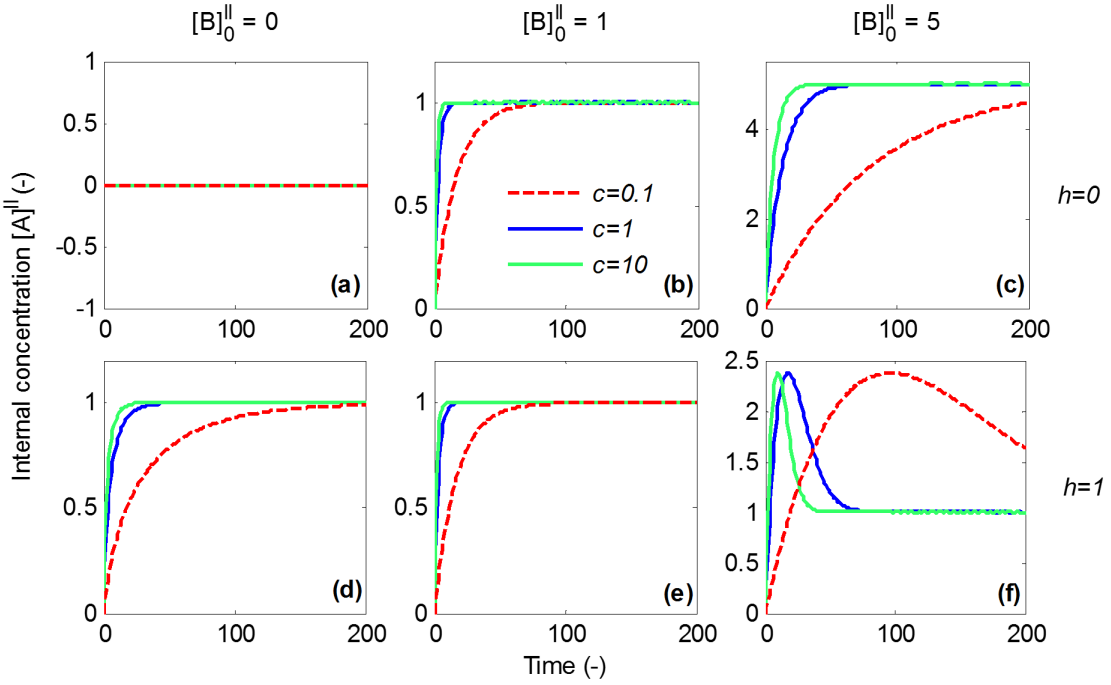


FIGURE 3.14: Effects of asymmetry in bound transporter ($AX$ and $BX$) and unbound transporter ($X$) translocation rate constants ($k_1 \neq k_{-1}$ and $k_2 \neq k_{-2}$), with equal dissociation constants ($K_I = K_{II}$), according to Equation 3.35–Equation 3.36. Time series for different values of $c$ and initial concentrations $[B]_0^{II}$ inside the vesicle (arbitrary units). The external concentration of tracer $[A]^I = 1$ in all cases. a, d) Zero initial substrate inside. b, e) Equal internal and external concentrations. c, f) Higher internal concentration.

It can be observed that the results in Figure 3.14 are very similar to those in Figure 3.12, but note that $c$ has the opposite effect in Equation 3.32 and Equation 3.35, acting either on the forward or reverse bound translocation rate constants $k_1$ and $k_{-1}$. However, this has the same effect on the overall transport cycle where $A$ is exchanged for $B$ (Figure 3.3).

## 3.4 Discussion

Placental membrane vesicle experiments are used routinely for the study of exchanger transporters [33, 39, 86, 87]. However, these experiments consistently display substrate uptake under zero-*trans* conditions, which is incompatible with the concept of an obligatory exchanger mechanism and remains currently unexplained. Therefore, mathematical modelling was applied to clarify how these experimental observations could relate to the behaviour of the transporter under investigation. Importantly, for clarity

and to facilitate biological interpretation the number of parameters in the model was kept to the minimum required to represent the key transporter mechanisms at play.

Both non-obligatory and obligatory exchanger models could explain the observed initial rate of serine tracer uptake under sodium free conditions, depending on the initial substrate concentration inside the vesicle. Previous evidence for an obligatory exchanger, as opposed to facilitated diffusion, is provided by the 1:1 ratio between amino acid influx and efflux, combined with the observation that no significant amino acid depletion was detected in oocytes maintained in amino acid free buffer [66]. However, for an obligatory exchanger to function this would necessarily imply the presence of initial substrate within the vesicle. In this respect, the dependency of apparent Michaelis-Menten parameters on internal substrate concentration derived in the current study (Equation 3.28, 3.29), could potentially help explain variation in reported $K_m$ values for $Na^+$-independent serine uptake in the literature (116–675 $\mu$mol $l^{-1}$) [39, 67]. However, the internal concentrations cannot affect the apparent $K_m$ if the unloaded and loaded transporters have equal mobility ($h = 1$) in the carrier model (Equation 3.29, Table 3.3; *i.e.* since binding of internal substrate would not affect the return rate of the carrier in the transport cycle).

### 3.4.1 Time course experiments

Since a standard uptake experiment did not allow non-obligatory and obligatory exchange to be distinguished based on initial rate alone (Figure 3.4a, b), the possibility of continuing the experiment as a time series was explored first theoretically and then tested experimentally. Based on the model predictions in Figure 3.7, the lack of a pronounced overshoot observed in the experimental time course (Figure 3.8) indicated the absence, or only low levels, of internal substrate within the vesicles. In addition, equal internal and external tracer concentrations at steady state were observed in the experiment (Figure 3.8), which provided a strong indication for non-obligatory transport leading to diffusive equilibrium. Furthermore, tracer uptake could be completely inhibited (Figure 3.6), demonstrating that uptake was transporter mediated as opposed to simple diffusion, within experimental accuracy. However, similar concentrations on both sides of the membrane are not conclusive proof of facilitated diffusion, as an obligatory exchanger would give the same result in the case where internal and external concentrations were equal (Figure 3.5b). In addition, the vesicle volume conversion factor used here to determine internal concentration levels may not be known precisely in many cases. Therefore, the time course experiment was repeated in the presence of additional external unlabelled serine. This showed that the experimental data could be captured reasonably well by the model based on facilitated diffusion (Figure 3.8), while obligatory exchange would predict a disproportionate reduction in steady state concentrations (Figure 3.9). This is because at equilibrium, obligatory exchange would result in equal ratios of tracer

to unlabelled substrate inside and outside the vesicle, and 7.5 $\mu$mol l$^{-1}$ tracer represents only a very small fraction compared to either 250 or 1000 $\mu$mol l$^{-1}$ unlabelled substrate.

Overall, the results of this study supported the existence of a facilitative transport component in placental MVM vesicles. However, while $h$ was clearly non-zero in the model, the results of the sensitivity analysis demonstrated that it was not possible to ascertain the precise value of $h$ with confidence. This is because for a facilitative transporter, in absence of significant internal concentrations, the tracer uptake depends on the combined velocity of the unloaded and loaded transporter in the transport cycle, thus $h$ and $V$ could not be determined independently. Based on previous exchange and efflux experiments in oocytes one would expect $h$ to be low [66]. A relatively slow unloaded transporter (small $h$) would increase the potential for *trans*-stimulation of the initial uptake rate by internal substrate [88] and display a larger overshoot (Figure 3.7). Thus further opportunities to determine $h$ could be provided by developing experimental protocols in which additional high concentrations of substrate are added within the vesicle. In addition, the presence of an overshoot in such an experiment would directly demonstrate a non-obligatory transport mechanism (Figure 3.5, Figure 3.7). This is because a high outwardly directed substrate gradient would promote an overshoot response for non-obligatory transport (Figure 3.7b–d), while an obligatory exchanger would be expected to equilibrate at different levels directly dependent on the concentration added inside the vesicle (Figure 3.7a). Time course data for the sodium independent uptake of system L substrates in non-preloaded MVM vesicles displayed a small overshoot for tryptophan, as indicated by the drop in tracer level at 45 min [86], while in contrast, no overshoot was observed for leucine [33].

### 3.4.2 Model fitting of extended time course experiments

The extended time course experiments were shown to be in agreement with the non-obligatory transport behaviour as well, which confirmed the earlier results in the zero-*trans* case (*i.e.* EXP 1-2-5). Importantly, overall transport behaviour over a wide range of internal and external concentration could be represented by the model using a single limited set of parameters. Notably, the model was able to describe the overshoot response in EXP 4, in accordance with the experimental data, although the experimental results showed a much slower rate of decrease after the peak. The overshoot in the uptake of radiolabelled serine (substrate $A$) was due to the initially high outward-directed gradient of total serine levels, which was confirmed further in EXP 4b, by increasing this gradient even more, resulting in a higher peak. Note neither responses in zero-*trans* conditions, nor the overshoot response can be represented by the obligatory model; hence suggesting that the transport system is likely to have a non-obligatory mechanism. Though, this facilitated component was likely to be low, with the relative mobility of the unloaded transporter $h$ estimated at 16% of the loaded transporter.

### 3.4.3 Asymmetry in model parameters

A number of simplifying assumptions were made in the application of the model. In particular the transport parameters in the model were assumed to be symmetric. However, in *Xenopus* oocyte studies asymmetric apparent affinities have been found [66]. This could be explained by different translocation rates and dissociation constants according to Equation 3.9 & Equation 3.16. Nonetheless, importantly, relaxing these model assumptions would not affect the equilibrium substrate concentrations for a passive transport process. Note, membrane potential was not included as LAT2 is a sodium independent transporter of neutral amino acids and not known to be electrogenic [19, 89–91]. The effect of asymmetry on the model predictions was explored further in Section 3.3.8. This confirmed that the presence of an overshoot would indicate a non-obligatory as opposed to an obligatory exchange mechanism; however the reverse is not true as such an overshoot depends both on model parameters and internal concentrations (Figure 3.13). The model assuming asymmetry in parameters values were also fitted to the extended time course experimental data; however, this did not result in an improvement to the fits when compared to the reduced symmetric model.

### 3.4.4 Vesicle size distribution

An average vesicle volume conversion factor was used to determine intravesicular tracer concentrations, while vesicles in suspension appear heterogeneous in size [83] and thus would display a range of area to volume ratios, potentially smoothing out the response. In addition, the vesicle volume was assumed to be constant over time, while any changes in volume might for example contribute to explaining the overprediction observed for 250 $\mu$mol $l^{-1}$ external unlabelled serine in Figure 3.8. A brief investigation of the effect of the vesicle suspension having a non-uniform size distribution can be found in Appendix A, the results of which suggested that larger-sized vesicles contribute more to the overall uptake behaviour.

### 3.4.5 Parallel transport components

Based on current understanding, a single transporter (LAT2) was proposed to represent the sodium independent transport of serine, and all known $Na^+$ independent serine transport systems are exchangers. However, if multiple transport mechanisms were to be present (*e.g.* a previously unidentified facilitative serine transporter) this would give rise to a mixed response which would be more difficult to interpret, *e.g.* an obligatory exchanger in combination with an unknown diffusive transport route in parallel could give rise to a qualitatively similar response as a non-obligatory transporter.

### 3.4.6 Timescle for the model behaviour

The transport model can be analysed analytically on both a short term and long term basis. In this chapter, the exchanger model was explored in terms of the Michaelis-Menten equation looking at the initial transport rates. In addition, thermodynamic equilibrium was considered in the model which determines the concentrations and their ratios at steady state.

## 3.5 Conclusion

Mathematical modelling was applied to better understand the underlying mechanisms of how transporters mediate placental amino acid transport, which is important in clinical applications to prevent or treat impaired fetal growth during pregnancy. It was also shown that the carrier-based transport model could be used to analyse the transport behaviour of transport proteins by contributing to the design and interpretation of experiments. In this study the sodium-independent transport of serine by the LAT2 protein was suggested to agree better with the non-obligatory exchange mechanism. Moreover, the interpretation of vesicle experiments such as those with placental MVM in reality may be complicated by non-zero internal substrate concentrations. In addition, actual transporter behaviour may deviate from idealised behaviour such as perfectly obligatory exchange. Modelling could allow quantification of these effects in order to reveal their impact. New experimental procedures using comprehensive time series uptake experiments were proposed and implemented in place of the common Michaelis-Menten setup, which does not provide a complete description of transport phenomena.

An iterative approach has proven to be vital, in which the model is used to predict various potential transport scenarios, which can then be tested experimentally, leading to model refinement and new experiments. In this way, modelling could help to interpret and design uptake experiments and contribute to a more complete understanding of the behaviour of specific transport systems. Lastly, this study served as robust foundation for subsequent studies incorporating multiple transporters to investigate placental transport as a whole system, which is presented in Chapter 5.

### 3.5.1 List of contributions

Summary of novel contributions made in this chapter:

- A new combined exchange/facilitative transporter model was developed with only a single parameter distinguishing between each mechanism

- The model can give rise to different apparent Michaelis-Menten constants as a function of internal concentration, which could explain the variation in parameters found in previous experimental literature
- The transport model clearly suggests a non-obligatory exchange mechanism for LAT2 (with a slow facilitative component), while up to now LAT2 has been commonly thought to be an obligatory exchanger

# Chapter 4

# Accumulative transporter – a development of cotransport model

## 4.1 Introduction

During pregnancy, essential nutrients such as amino acids required for fetal development, are supplied from the mother via the placenta. The maternal blood perfused in the placental intervillous space surrounds the villi containing the fetal capillaries, with the syncytiotrophoblast layer acting as an interface between the two circulations. The transport of amino acids across the placental syncytiotrophoblast is regulated by different transport proteins (or transporters) which can be found at the maternal-facing microvillous (MVM) and fetal-facing basal membranes (BM). As categorised by transport mechanism, the transport proteins that work together in mediating amino acid transfer across epithelia include; accumulative transporters which actively pump amino acids across the MVM, exchangers which swap one amino acid for another, and facilitative transporters which transport amino acids along their concentration gradients [6, 73]. Particularly in the placental transport system, the accumulative transporters are important for getting amino acids to the fetus as these transporters can actively transfer against the concentration gradient, as fetal levels are normally higher. Thus, without the accumulative transporters, the fetus cannot maintain high levels of amino acids required for fetal growth, as the other two transporter types are passive – therefore do not transport against the concentration gradient. The accumulative transporters expressed at the placental epithelia belong to the SLC38 gene family and include the proteins SNAT1 and SNAT2. These accumulative transporters and their activities in general are often referred to as system A, because of their substrate preference for alanine and other similar small neutral amino acids [92]. Not limited to placental tissue alone, these transport proteins are also present at other epithelia that fulfil specific regulatory functions such as in the brain and liver [19].

The accumulative transporters inherently have a more complex transport mechanism compared to other passive transporters, as it requires the amino acid substrate to be co-transported with a sodium ion with a 1:1 stoichiometry [93–95]. As a result, the substrate movement together with a positively charged sodium ion also causes an electrical current. Hence, the accumulative transporters are electrogenic and amino acid transport is coupled to the driving forces of both the chemical and electrical gradient of sodium.

In this chapter, first the electrochemical effects on transport in general are explored with a simple carrier model. Next, a cotransport model is developed to represent the mechanism of the accumulative transporter, which is then extended to incorporate the effects of electrical potential. Finally, the validation of the model is performed with literature data, followed by discussion.

## 4.2 Methods

Transport by the accumulative transporter has been shown to be dependent on sodium. Therefore, the electro-chemical potential effects due to the charged sodium ion must be considered. The following section first illustrates the potential dependency for transport of a charged solute for a simple carrier model, which can then be applied to the sodium cotransport model to account for the electro-chemical potential effects due to sodium.

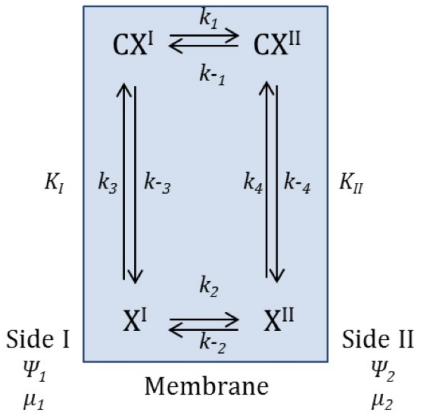


FIGURE 4.1: Carrier model schematic showing the transport of charged substrate $C$ by carrier $X$ across the membrane.

For transmembrane carrier mediated transport of a charged substrate $C$ from membrane side $I$ to $II$ at the electrical potentials $\psi_1$ and $\psi_2$, respectively, with respect to a reference potential, the driving force for transport of the solute is given by

$$\mu_2 - \mu_1 = RT(ln[C]^{II} - ln[C]^{I}) + zF(\psi_2 - \psi_1) \tag{4.1}$$

where $\mu_i$ denotes electrochemical potential of side $i$, and $[C]^i$ is the concentration of charged substrate $C$ at side $i$. Note that $R$ is the gas constant, $T$ is temperature, and $F$ is Faraday constant. z denotes the electrical charge of the charged solute.

Hence, when the electrochemical potential difference is zero at equilibrium, the charged solute concentration ratio is given by the following expression:

$$\frac{[C]^{II}_{eq}}{[C]^{I}_{eq}} = e^{\left(\frac{-zF}{RT}(\psi_2 - \psi_1)\right)} \tag{4.2}$$

Now consider the carrier model in Figure 4.1. When the net flux of the charged substrate is zero at equilibrium, then the ratio of the concentrations can be expressed in terms of substrate translocation rates and dissociation constants as:

$$\frac{[C]^{II}_{eq}}{[C]^{I}_{eq}} = \frac{k_1 k_{-2} K_{II}}{k_{-1} k_2 K_I} \tag{4.3}$$

where, $K_I = \frac{k_{-3}}{k_3}$, and $K_{II} = \frac{k_{-4}}{k_4}$.

Therefore, combining Equation 4.2 and Equation 4.3 yields;

$$\frac{k_1 k_{-2} K_{II}}{k_{-1} k_2 K_I} = e^{\left(\frac{-zF}{RT}(\psi_2 - \psi_1)\right)} \tag{4.4}$$

From Equation 4.4, the electrochemical potential is shown to affect the transport process as a whole. When the electrical gradient is zero, the ratio of the translocation rates and dissociation constants is unity. However, one may assume that only conformational changes of the carrier that move charges across the membrane are potential dependent [63]. Hence, the only translocation rates governing such step, $k_1$ and $k_{-1}$, are affected by the potential gradient term. Hence, the following statement can be assumed for the ratio of the translocation rates of the charged substrate:

$$\frac{k_1}{k_{-1}} = \frac{k^0_1}{k^0_{-1}} e^{\left(\frac{-zF}{RT}(\psi_2 - \psi_1)\right)} \tag{4.5}$$

Here $k^0_1$ and $k^0_{-1}$ denote reference rates in absent of membrane potential.

Furthermore, if one assumes a parameter $\beta$ to define the transmembrane potential effects, explicitly, to the translocation rates in each direction ($k_1$ and $k_{-1}$), the following statements can be made about the individual translocation rates:

$$k_1 = k^0_1 e^{\left(\frac{-\beta zF}{RT}(\psi_2 - \psi_1)\right)} \tag{4.6}$$

$$k_{-1} = k_{-1}^{0} e^{\left(\frac{(1-\beta)zF}{RT}(\psi_2 - \psi_1)\right)} \tag{4.7}$$

### 4.2.1 Cotransport model

As it was shown that the transmembrane potential effect can be explicitly identified as part of the translocation rates for the case of the transport of a charged solute, the same principle can be applied to the cotransport model to describe the active sodium-dependent accumulative transport mechanism of a neutral solute. Firstly, a cotransport model is explored without considering the electric potential, to show only the driving force due to the chemical (concentration) gradient of the co-solute. Then, in the following section, the effect of electrical potential is incorporated.

In the cotransport model, the substrate is transported together with the sodium ion in a 1:1 stoichiometry [93, 94, 96]. The cotransport model also assumes that the sodium ion binds prior to the solute [17, 19]. The schematic of the carrier model for co-transport of a neutral substrate $A$ with a sodium ion is shown below in Figure 4.2.

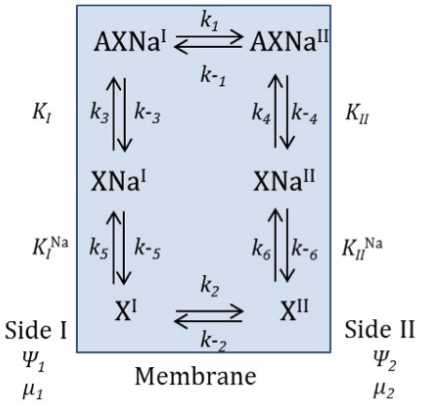


FIGURE 4.2: Carrier model of sodium-dependent accummulative transporter for a neutral substrate with explicit translocation rates and dissociation constants for each binding/unbinding step. Transporter, $X^i$ requires a Na ion to form $XNa^i$ before binding to amino acid $A$ to allow translocation in the form of transporter-sodium-amino acid complex, $AXNa^i$

Consistence with the general rationale on the carrier model, the following assumption can be made:

1. Rapid equilibrium at both sides of the membrane: It is assumed that amino acid reversible binding/unbinding is instantaneous. This implies that bound and unbound concentrations are at equilibrium at each side of the membrane [78, 79]. Therefore, the rate constants for binding can be replaced by the following dissociation constants $K$, given by:

$$K_I^{Na} = \frac{[Na]^I[X]^I}{[XNa]^I} = \frac{k_{-5}}{k_5} \tag{4.8}$$

$$K_{II}^{Na} = \frac{[Na]^{II}[X]^{II}}{[XNa]^{II}} = \frac{k_{-6}}{k_6} \tag{4.9}$$

$$K_I = \frac{[A]^I[XNa]^I}{[AXNa]^I} = \frac{k_{-3}}{k_3} \tag{4.10}$$

$$K_{II} = \frac{[A]^{II}[XNa]^{II}}{[AXNa]^{II}} = \frac{k_{-4}}{k_4} \tag{4.11}$$

$K$, therefore, by definition has the same unit as the concentration. Note that this corresponds to the binding ($k_3$, $k_4$, $k_5$, $k_6$) and unbinding rate constants ($k_{-3}$, $k_{-4}$, $k_{-5}$, $k_{-6}$), which have the dimensions of l mol$^{-1}$ s$^{-1}$ and s$^{-1}$, respectively.

2. Conservation of transporters: Within the membrane, the transporters are assumed to be conserved [62, 63]. Hence, the transporters are always in one of the six states. The total number of transporters contained in the membrane, $x_T$, is given by:

$$[X]^I + [X]^{II} + [XNa]^I + [XNa]^{II} + [AXNa]^I + [AXNa]^{II} = x_T \tag{4.12}$$

3. Quasi-steady state applies since the time scale of binding and translocation is relatively fast compared to any changes in the concentration within the compartments [80]. Thus quasi-steady state transport implies that the sum of the fluxes of bound and unbound carrier must be zero (*i.e.* the rate of transporters going forward across the membrane must be the same as for those returning, in order for the transport cycle to continue) [62, 63].

$$J_X + J_{AXNa} = 0 \tag{4.13}$$

4. The net flux $J_{AX}$ of the substrate-transporter complex $AXNa$ directed from side $I$ to side $II$, can be represented as the net effect of the forward and backward directed fluxes. The same applies for the net flux $J_X$ of unbound transporter $X$ from side $I$ to $II$.

$$J_{AX} = k_1[AXNa]^I - k_{-1}[AXNa]^{II} \tag{4.14}$$

$$J_X = k_2[X]^I - k_{-2}[X]^{II} \tag{4.15}$$

By definition, the solute of interest, amino acid $A$, can only cross from side $I$ to $II$ in the form of transporter-sodium-amino acid complex $AXNa$; therefore the flux of $A$, $J_A$, is essentially equal to the flux of $AXNa$, $J_{AXNa}$. By substitution from Equation 4.8 to Equation 4.15, the flux equation $J_A$ of a cotransport model can be expressed in terms of solute and ion concentrations as:

$$J_A = \frac{(k_1 k_{-2}[A]^I[Na]^I K_{II} K_{II}^{Na} - k_2 k_{-1}[A]^{II}[Na]^{II} K_I K_I^{Na}) x_T}{Denom}$$

where,

$$\begin{aligned} Denom = {} & [Na]^I[Na]^{II}\left\{(k_1 + k_{-1})[A]^I[A]^{II} + (k_1 K_{II}[A]^I + k_{-1} K_I[A]^{II})\right\} \\ & + \left(k_{-2} K_{II}^{Na}[Na]^I + k_2 K_I^{Na}[Na]^{II}\right) K_{II} K_I + (k_1 + k_{-2})[A]^I[Na]^I K_{II} K_{II}^{Na} \\ & + (k_{-1} + k_2)[A]^{II}[Na]^{II} K_I K_I^{Na} + (k_2 + k_{-2}) K_I K_{II} K_I^{Na} K_{II}^{Na} \end{aligned} \tag{4.16}$$

$$[A]_0^I = A_1,\ [Na]_0^I = Na_1,\ [A]_0^{II} = 0,\ [Na]_0^{II} = Na_2$$

From Equation 4.16, equilibrium of the net flux of substrate co-transported with sodium ion yields:

$$\frac{[A]^I}{[A]^{II}} = \frac{[Na]^{II}}{[Na]^I}\left(\frac{k_{-1} k_2}{k_1 k_{-2}} \frac{K_I K_I^{Na}}{K_{II} K_{II}^{Na}}\right) \tag{4.17}$$

This illustrates that the transport process, will reach equilibrium when the sodium gradient becomes thermodynamically balanced by the amino acid substrate gradient [50, 63]. Fundamentally, to achieve accumulation in the cotransport system, the co-solute gradient must be coupled in opposite direction to that of the amino acid substrate.

### 4.2.2 Transmembrane potential effects in the cotransport model

When the transmembrane potential difference is included in the cotransport model, the same opposite coupling applies between the amino acid substrate and co-solute ion. At equilibrium, the transmembrane electrochemical potential difference must be equal but opposite for the solute and co-solute. Hence, the electrochemical potential difference of the substrate $A$ and sodium ion can be expressed as [63]:

$$\begin{aligned} \Delta\mu_A &= \Delta\mu_{Na} \\ \mu_{A^I} - \mu_{A^{II}} &= \mu_{Na^{II}} - \mu_{Na^I} \end{aligned} \tag{4.18}$$

where $\mu_{S^i}$ represents the electrochemical potential of solute $S$ at side $i$.

Then, the corresponding electrochemical potentials for substrate and sodium at each side of the membrane, as defined in Equation 4.1, can be substituted in Equation 4.18 as follows:

$$\begin{aligned} RT(ln[A]^I - ln[A]^{II}) + z_A F(\psi_1 - \psi_2) &= RT(ln[Na]^{II} - ln[Na]^I) + z_{Na} F(\psi_2 - \psi_1) \\ ln\left(\frac{[A]^I[Na]^I}{[A]^{II}[Na]^{II}}\right) &= \frac{F}{RT}(z_{Na} + z_A)(\psi_2 - \psi_1) \\ \frac{[A]^I}{[A]^{II}} &= \frac{[Na]^{II}}{[Na]^I} e^{\left(\frac{(z_{Na}+z_A)F}{RT}(\psi_2 - \psi_1)\right)} \end{aligned} \tag{4.19}$$

where $z_{Na}$ is the charge of sodium and $z_A$ is the charge of substrate $A$. However, for substrate $A$ – a neutral amino acid – the charge is zero.

Hence from Equation 4.19, for zero transmembrane potential difference (*i.e.* $\psi_2 - \psi_1 = 0$), the substrate and sodium are directly coupled without the electrical driving force. For negative potential difference (*i.e.* $\psi_2 - \psi_1 < 0$), the exponential term is positive and less than one, which means that the transport of both substrate and sodium are coupled in favour of the transport to side $II$. Oppositely, for positive transmembrane potential difference, the transport of the substrate and sodium is coupled in favour of the transport to side $I$.

By combining the equilibrium condition in Equation 4.17 with the electrochemical potential coupling equation in Equation 4.19, the thermodynamic constraint for the cotransport model with transmembrane potential difference can be found as follows:

$$\frac{k_{-1}k_2}{k_1k_{-2}} \frac{K_I K_I^{Na}}{K_{II} K_{II}^{Na}} = e^{\left(\frac{z_{Na}F}{RT}(\psi_2 - \psi_1)\right)} \tag{4.20}$$

As shown in Equation 4.20, the electro potential bias term is equal to the ratios of the translocation rates and the dissociation constants of the substrate and sodium. However, if it were assumed that the dissociation constants are not electrogenic, then the electrical bias term is applied to the ratios of the translocation rates only. However, in order to specify the electrical bias term explicitly and relate this to the translocation rates, another assumption on the transporter charge must be made. The following section shows two different transporter charge assumptions and how they affect different sets of translocation rates as a function of the electrical gradient term:

**Transporter has negative charge**: From the cotransport model schematic in Figure 4.2, if we assume the transporter is negatively charged, which then binds to

sodium neutralising the charge, and then binds to neutral substrate; then only affected translocation rates by the transmembrane potential are $k_2$ and $k_{-2}$. Therefore, the ratio of the translocation rates affected by the potential difference can be expressed as:

$$\frac{k_2}{k_{-2}} = \frac{k_2^0}{k_{-2}^0} e^{\left(\frac{z_{Na}F}{RT}(\psi_2 - \psi_1)\right)} \tag{4.21}$$

where $k_2^0$ and $k_{-2}^0$ denote the translocation rates at zero potential difference.

Now, let $\beta$ be the parameter to explicitly define the transmembrane potential effects for the translocation rates in each direction, the following statements can be defined for the individual translocation rates:

$$k_2 = k_2^0 e^{\left(\frac{\beta z_{Na}F}{RT}(\psi_2 - \psi_1)\right)} \tag{4.22}$$

$$k_{-2} = k_{-2}^0 e^{\left(\frac{(\beta-1) z_{Na}F}{RT}(\psi_2 - \psi_1)\right)} \tag{4.23}$$

**Transporter charge is neutral**: However, if it were to be assumed that the transporter is neutral instead and then binds with the positively charged sodium and then the neutral substrate, this would lead to the formation of a positively charged complex overall. Therefore, the only translocation rates affected by the transmembrane potential are $k_1$ and $k_{-1}$, according to Figure 4.1. The ratio of the translocation rates affected by the potential difference can then be expressed as:

$$\frac{k_{-1}}{k_1} = \frac{k_{-1}^0}{k_1^0} e^{\left(\frac{z_{Na}F}{RT}(\psi_2 - \psi_1)\right)} \tag{4.24}$$

where $k_1^0$ and $k_{-1}^0$ denote the translocation rates at zero potential difference.

Then, let $\beta$ be the parameter to explicitly define the transmembrane potential effects to the translocation rates in each direction, the following statements can be made about the individual translocation rates:

$$k_{-1} = k_{-1}^0 e^{\left(\frac{\beta z_{Na}F}{RT}(\psi_2 - \psi_1)\right)} \tag{4.25}$$

$$k_1 = k_1^0 e^{\left(\frac{(\beta-1) z_{Na}F}{RT}(\psi_2 - \psi_1)\right)} \tag{4.26}$$

As a result, depending on the transporter charge assumption, the electrical potential bias terms could be specified for either the empty transporter or substrate-bound transporter translocation rates.

### 4.2.3 Model parameter reduction for application

As we have now established all aspects of the active cotransport model, including explicitly specifying the electrical contributions to the translocation rates, the next step is for the model to be simulated and explored. Further simplifying assumptions are made for the model application in order to reduce the number of parameters. For each transporter charge hypothesis, the following assumptions were adopted:

**Equal zero-potential translocation rates and dissociation constants**: Firstly, the translocation rates $k$ at zero potential difference and electrically unaffected translocation rates are assumed to be equal. In addition, the substrate dissociation constants are treated to be equal at the each side of the membrane. The same also applies for sodium dissociation constants. These assumptions were justified in first instance since it was demonstrated in the previous chapter that any asymmetry in both translocation rate and dissociation constants would only affect the transient response of the uptake and would not fundamentally change the underlying transport mechanism.

**Electro potential bias terms definition**: Let $\varepsilon$ and $\varepsilon^{'}$ represent the electrical potential bias terms for the affected translocation rates in opposite direction, defined as [97]:

$$\varepsilon = e^{\left(\frac{\beta z_{Na} F}{RT}(\psi_2 - \psi_1)\right)} \tag{4.27}$$

$$\varepsilon^{'} = e^{\left(\frac{(\beta-1) z_{Na} F}{RT}(\psi_2 - \psi_1)\right)} \tag{4.28}$$

Hence, with these assumptions for model application, the flux equation from Equation 4.16 of substrate $A$ co-transported sodium ion can be expressed as shown in Table 4.1 for each case of transporter charge assumptions.

### 4.2.4 Michaelis-Menten interpretation

The apparent Michaelis-Menten interpretation of the cotransport model can be derived by assuming zero-*trans* conditions. From Equation 4.16, the instantaneous flux of solute $A$ is then as follows:

$$J_{A_0} = \frac{k_1 k_{-2} x_T [A]^I [Na]^I}{k_{-2} K_I [Na]^I + (k_1 + k_{-2})[A]^I [Na]^I + (k_2 + k_{-2}) K_I K_I^{Na}} \tag{4.29}$$

Therefore, the apparent Michaelis-Menten parameters of the solute $A$ can be derived from Equation 4.29 as the follows:

TABLE 4.1: Reduced parameter model for application of the cotransport model for each of the two transporter charge assumptions.

| | Negatively charged transporter assumption | Neutral transporter assumption |
|---|---|---|
| Electro potential bias terms definition | $k_2 = k_2^0\varepsilon$<br>$k_{-2} = k_{-2}^0\varepsilon^{'}$ | $k_{-1} = k_{-1}^0\varepsilon$<br>$k_1 = k_1^0\varepsilon^{'}$ |
| Equal zero-potential translocation rates and equal dissociation constants | $k_1 = k_{-1} = k_2^0 = k_{-2}^0 = k$<br>$K_I = K_{II} = K$<br>$K_I^{Na} = K_{II}^{Na} = K^{Na}$ | $k_{-1}^0 = k_1^0 = k_2 = k_{-2} = k$<br>$K_I = K_{II} = K$<br>$K_I^{Na} = K_{II}^{Na} = K^{Na}$ |
| Cotransport flux equation of solute $A$ | $J_A = \frac{kx_T(\varepsilon^{'}[A]^I[Na]^I + \varepsilon[A]^{II})[Na]^{II})}{D}$<br>$D = \frac{1}{K^{Na}}[Na]^I[Na]^{II}\left\{[A]^I + [A]^{II} + \frac{2}{K}[A]^I[A]^{II}\right\}$<br>$+(\varepsilon^{'}[Na]^I + \varepsilon[Na]^{II})K + (1+\varepsilon^{'})[A]^I[Na]^I$<br>$+(1+\varepsilon)[A]^{II}[Na]^{II} + (\varepsilon+\varepsilon^{'})KK^{Na}$ | $J_A = \frac{kx_T(\varepsilon^{'}[A]^I[Na]^I + \varepsilon[A]^{II})[Na]^{II})}{D}$<br>$D = \frac{1}{K^{Na}}[Na]^I[Na]^{II}\left\{\varepsilon^{'}[A]^I + \varepsilon[A]^{II} + \frac{(\varepsilon+\varepsilon^{'})}{K}[A]^I[A]^{II}\right\}$<br>$+([Na]^I + [Na]^{II})K + (1+\varepsilon^{'})[A]^I[Na]^I$<br>$+(1+\varepsilon)[A]^{II}[Na]^{II} + 2KK^{Na}$ |
| Michaelis-Menten parameters of solute $A$ | $V_{max}^A = \frac{\varepsilon^{'}kx_T}{(\varepsilon^{'}+1)}$<br>$K_m^A = \frac{K}{(\varepsilon^{'}+1)}\left(\varepsilon^{'} + (\varepsilon^{'}+\varepsilon)\frac{K^{Na}}{[Na]^I}\right)$ | $V_{max}^A = \frac{\varepsilon^{'}kx_T}{(\varepsilon^{'}+1)}$<br>$K_m^A = \frac{K}{(\varepsilon^{'}+1)}\left(1 + 2\frac{K^{Na}}{[Na]^I}\right)$ |
| Michaelis-Menten parameters of solute sodium | $V_{max}^{Na} = \frac{\varepsilon^{'}kx_T}{(\varepsilon^{'}+1)+\varepsilon^{'}\frac{K}{[A]^I}}$<br>$K_m^{Na} = \frac{(\varepsilon^{'}+\varepsilon)K^{Na}}{\varepsilon^{'}+(\varepsilon^{'}+1)\frac{[A]^I}{K}}$ | $V_{max}^{Na} = \frac{\varepsilon^{'}kx_T}{(\varepsilon^{'}+1)+\varepsilon^{'}\frac{K}{[A]^I}}$<br>$K_m^{Na} = \frac{2K^{Na}}{1+(\varepsilon^{'}+1)\frac{[A]^I}{K}}$ |

$$J_{A_0} = \frac{k_1 k_{-2} x_T [A]^I}{k_{-2} K_I + (k_1 + k_{-2})[A]^I + (k_2 + k_{-2}) \frac{K_I K_I^{Na}}{[Na]^I}}$$

$$\therefore V_{max}^A = \frac{k_1 k_{-2} x_T}{(k_1 + k_{-2})}, \tag{4.30}$$

$$\therefore K_{max}^A = \frac{K_I}{(k_1 + k_{-2})} \left[ k_{-2} + (k_2 + k_{-2}) \frac{K_I^{Na}}{[Na]^I} \right]$$

Similarly, the Michaelis-Menten interpretation can be derived for the coupled sodium molecule. From Equation 4.29, the instantaneous flux of sodium and the corresponding apparent Michaelis-Menten parameters are then given by:

$$J_{Na_0} = J_{A_0} = \frac{k_1 k_{-2} x_T [A]^I [Na]^I}{(k_{-2} K_I + (k_1 + k_{-2})[A]^I)\,[Na]^I + (k_2 + k_{-2}) K_I K_I^{Na}}$$

$$\therefore V_{max}^{Na} = \frac{k_1 k_{-2} x_T}{(k_1 + k_{-2}) + k_{-2} \frac{K_I}{[A]^I}} \tag{4.31}$$

$$\therefore K_{max}^{Na} = \frac{(k_2 + k_{-2}) K_I^{Na}}{k_{-2} + (k_1 + k_{-2}) \frac{[A]^I}{K_I}}$$

### 4.2.5 Numerical implementation

The transporter models as presented in Table 4.1 were implemented in Matlab (R2013a) to simulate the concentrations of amino acids by time integration of the flux equations, which were non-linear ordinary differential equations. The 'ode45' function (Runge-Kutta (4th, 5th) method) was used for time integration, which uses a variable time step with relative and absolute tolerances of $10^{-4}$ and $10^{-6}$, respectively. Note that time integration was performed with various initial conditions (of substrate $A$ and $Na$) depending on the experimental conditions and that all extravesicular concentrations were assumed constant due to the large volume of buffer.

### 4.2.6 Parameter estimation

An automated parameter estimation algorithm was applied to find the best-fitting combination of the cotransport model parameters, which included the total transport rate ($kx_T$), electrical bias parameter ($\beta$), and dissociation constants of substrate ($K$) and sodium ($K_{Na}$). The model parameters were fitted based on the relative (normalised) error between the model predictions and characteristic literature data of alanine uptake into oocytes expressing the accumulative transporter SNAT2 [98]. Oocytes are

commonly used for uptake experiments because of their ability to overexpress human transporter proteins and their large size, which allows them to be injected easily. The fitting procedure was implemented using the 'fminsearch' function in Matlab (Nelder-Mead method) with the cost function defined as the residual sum of squares of errors between model simulations and experimental measurements (all data points equally weighted) as described below:

$$RSS = \sum_{i=1}^{n} \left( \frac{[A]_i^{II,Model} - [A]_i^{II,Literature}}{[A]_i^{II,Literature}} \right)^2 \tag{4.32}$$

To account for the difference in absolute values between experimental conditions, for each data point the difference between model prediction and literature was normalised first by the literature value, squared and then summed over all points to yield the overall error criterion. Note that the initial guess values for the fitted parameters that were used by the 'fminsearch' minimisation function were chosen within the same order of magnitude of physical and/or experimentally reported values. Multiple initial guess values were attempted to confirm that the fitting algorithm converged to a unique solution.

## 4.3 Results

Simulations of the cotransport model implementation are presented below. This includes the examination of the cotransport model dependencies on the sodium driving force due to the chemical gradient and electrical charge gradient. Lastly, the model parameter fitting of previous literature data are presented. Note that the results of both transporter charge assumptions are offered in contrast where applicable.

### 4.3.1 Cotransport model simulation

Firstly, the simple cotransport model dependent on only the chemical gradient of sodium was explored. Figure 4.3 shows the uptake rate of solute $A$ (fixed at 1) from outside (side $I$) to inside (side $II$), as given by the flux equation in Equation 4.16, co-transported with different levels of sodium ($Na$) over a range of external concentrations of $A$. Figure 4.3a shows the simulation results for the case of zero-*trans* where there was nothing on the inside with various levels of sodium externally, whereas Figure 4.3b shows results for when the sodium level was fixed at 1 outside with various level of sodium internally. Note that all transport rate and dissociation constants (of both $A$ and $Na$) were set to 1. In addition, for the purpose of showing clearly the fundamental behaviour of the transport model, each variable and parameters were used in dimensionless form, implying normalisation. Both plots suggested Michaelis-Menten behaviour where saturation occurred at maximum concentrations. The results show that the uptake of substrate

$A$ is higher when the sodium gradient is high. This illustrates that in the cotransport model, co-solute and substrate are directly coupled. It was also shown that although sodium is required for transport, it is not required at both sides of the membrane, only externally.

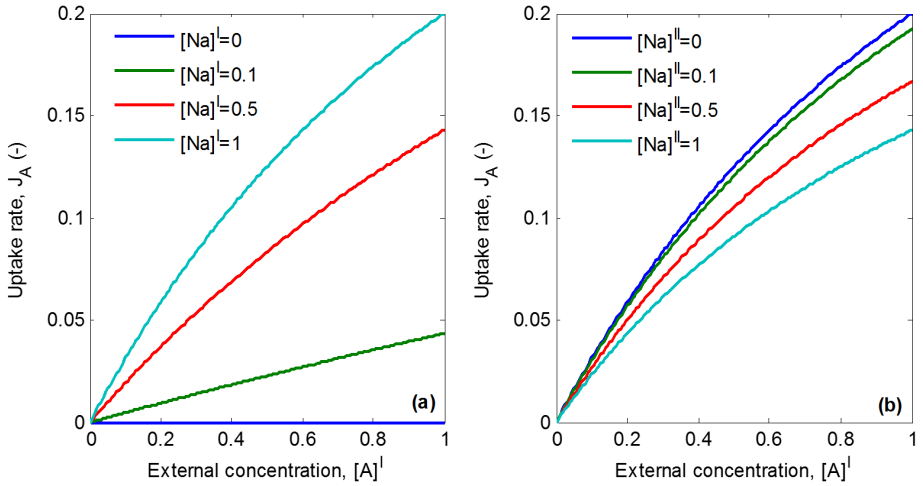


FIGURE 4.3: Simulation of simple cotransport model uptake rates: The plots show uptake rates of solute $A$ at each external concentration for (a) different sodium levels externally with nothing inside (zero-*trans*) and (b) different internal sodium level with external sodium fixed at 1.

Next, time integration was applied to the simple cotransport model to show changes in substrate $A$ concentration over time for various sodium levels. External substrate $A$ was fixed at a value of 1. Figure 4.4 shows the plot of internal substrate $A$ over time, at various external sodium levels, with internal sodium level initially at 1. Again, each transport rate and dissociation constant (of both $A$ and $Na$) were set to 1. The simulation results suggested different equilibrium levels of uptake of $A$ for different sodium levels. It was reaffirmed that the uptake level is dependent on the magnitude of the sodium gradient and no sodium to be co-transported with from the same side would result in no uptake. However, importantly, note that uptake of $A$ still occurs even if the internal and external sodium are initially equal at 1. This is because the gradient of $A$ drives uptake until the substrate and sodium ratios balance according to Equation 4.17.

The effects of transmembrane potential were then explored. It was shown in the model derivation that the driving force due to the electrical-potential difference can be applied to different individual transport rates depending on the assumption for the transporter charge. Therefore, the following results are shown for both transporter charge assumptions in comparison. Note that following constants and parameter values were used in the model simulations: ideal gas constant, $R = 8.314$ VC K$^{-1}$ mol$^{-1}$, room temperature, $T = 298$ K, and Faraday constant, $F = 9.65$ x $10^4$ C mol$^{-1}$.

The effects of transmembrane potential difference were simulated in Figure 4.5 for the transporter charge assumption as negative (a,b) and neutral (c,d). In order to separate

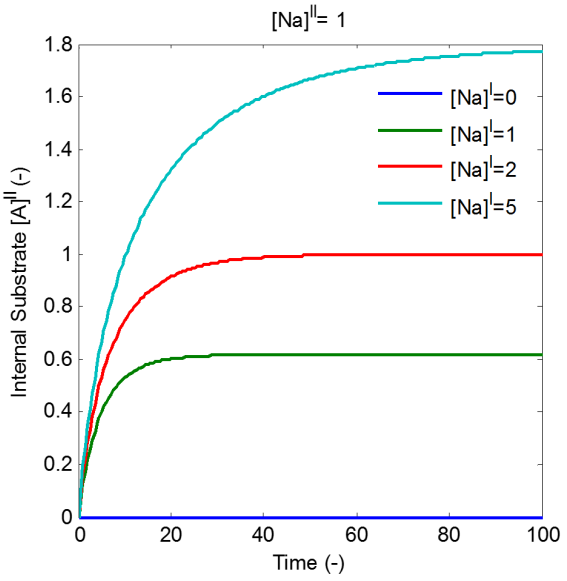


FIGURE 4.4: Simulation of cotransport model uptake level: Uptake levels of substrate $A$ were shown over a time for various external sodium levels, with internal sodium level initially at 1. Note uptake of $A$ still occurs even for initially equal internal and external sodium.

out clearly only the electrical effects, all initial substrate and sodium levels inside were set at 1 to match the fixed external levels, ensuring no chemical gradients. Again, each transport rate and dissociation constants (of both $A$ and $Na$) were set at 1. In Figure 4.5a and Figure 4.5c, it was shown that without electrical potential difference ($\Delta\psi = \psi_2 - \psi_1$), there would be no uptake. Note that the electrical bias term, $\beta$, was set at 0.5 here. Moreover, high potential difference (*i.e.* higher potential outside) was shown to promote the steady state uptake level. In Figure 4.5b and Figure 4.5d, the model simulated various values for the electrical bias term for a fixed transmembrane potential difference of -60 mV. The results suggested that the electrical bias only affected the transient uptake, but did not affect the equilibrium uptake level. Higher $\beta$ values were shown to give slower uptake. In addition, the results showed that equilibrium uptake levels are unaffected by which transporter charge assumption is made.

Next in Figure 4.6, the cotransport model simulated the uptake rates of 20 mmol $l^{-1}$ alanine over a range of sodium levels externally for comparison with the literature data [99]. The internal sodium was set at physiological level of 15 mmol $l^{-1}$. The parameters were chosen as the following: dissociation constant of alanine at 100 $\mu$mol $l^{-1}$, transmembrane potential at -60 mV, and the transport rates at 1 $\mu$mol $l^{-1}$ $s^{-1}$. The results in Figure 4.6 shows the uptake of $A$ with various $\beta$ value, for both negative (a to c) and neutral (d to f). The substrate $A$ uptake rates were shown to follow Michaelis-Menten process across the sodium concentration levels. Higher uptake rates of substrate were observed for lower $\beta$ value, as low $\beta$ value means that the bias on the transport rates in favour of back-transport of substrate is lowered (*i.e.* $k_2$ is lowered in negative transporter charge assumption, or $k_{-1}$ is lowered in neutral transporter

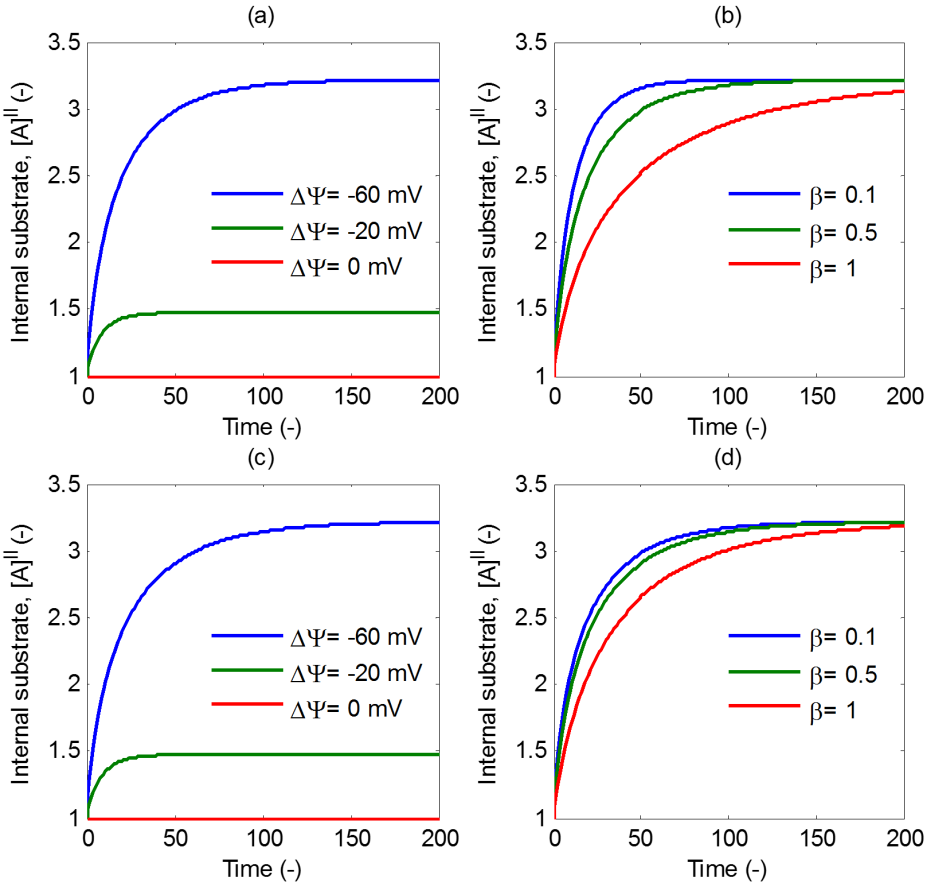


FIGURE 4.5: Effects of *trans*-membrane potential on the cotransport model assuming transporter charge as negative (a, b) or neutral (c, d): Uptake of substrate $A$ is shown for various transmembrane potential differences ($\Delta\psi = \psi_2 - \psi_1$) for fixed electrical bias term $\beta$ at 0.5 (a, c) and for different $\beta$ with fixed $\Delta\psi$ at -60 mV (b, d). Chemical gradients of substrate $A$ and sodium were initially zero with all concentrations equal to 1.

charge assumption case). When compared with the literature data, the prediction curves suggested that the dissociation constant $K_{Na}$ is in the same order as 100 mmol $l^{-1}$ rather than the same order as the substrate $K$ in the 100 $\mu$mol $l^{-1}$ range.

Furthermore, it was shown in the model simulations that the uptake behaviours of substrate $A$ by the cotransport model are in fact Michaelis-Menten processes with respect to substrate and sodium concentration levels, therefore the corresponding apparent $K_m$ parameters were explored in response to the electrical potential. Figure 4.7 shows the $K_m$ parameters for alanine (a, c) and sodium (b, d) as a function of transmembrane potential difference for various $\beta$ parameters under the negative (a, b) and neutral (c, d) transporter charger assumption. The results were generated under zero-*trans* condition with 500 $\mu$mol $l^{-1}$ alanine as substrate and 100 mmol $l^{-1}$ sodium [98] with dissociation constant $K$ of 100 $\mu$mol $l^{-1}$ and $K_{Na}$ of 100 mmol $l^{-1}$. It was shown that the transmembrane potential affected the $K_m$ parameter of both alanine and sodium in all cases except for when $\beta$ is one under the neutral transporter charge assumption (shown in c, d). In general, the $K_m$ parameters increased as the transmembrane potential

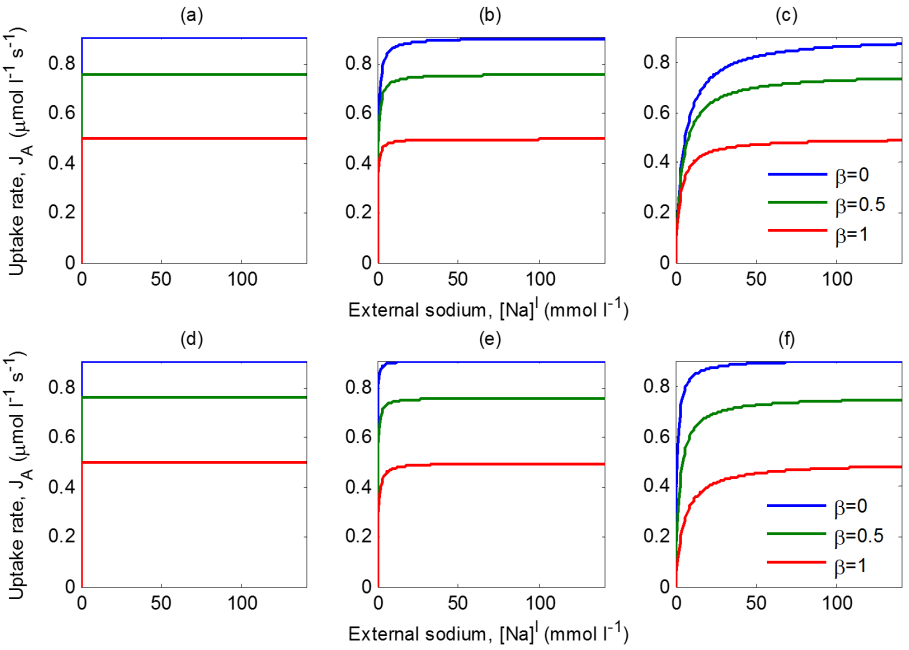


FIGURE 4.6: Uptake rate of alanine (20 mmol $l^{-1}$) over a range of external sodium, as predicted by the cotransport model. Two cases were considered, assuming the transporter charge as either negative (a to c) or neutral (d to f). A fixed dissociation constant $K$ of 100 $\mu$mol $l^{-1}$ for alanine was used, with varying $K_{Na}$ of: 100 $\mu$mol $l^{-1}$ (a, d); 100 mmol $l^{-1}$ (b, e); and 1 mol $l^{-1}$ (c, f).

difference becomes less negative. However, in Figure 4.7a, it was shown that $K_m$ of alanine responded to the transmembrane potential difference differently depending on the value of $\beta$. For a $\beta$ value equal to zero, the $K_m$ of alanine increased as the transmembrane becomes more negative and then appeared to be reaching a constant plateau. In contrast, when $\beta$ is unity the $K_m$ value appeared to be exponentially increasing when the transmembrane potential difference became less negative.

Lastly, the uptake rate of alanine was explored in response to both chemical and electrical potential gradient driving effects. In Figure 4.8 the flux equation from Equation 4.16 was plotted over a range of transmembrane potentials for various electrical bias parameter values ($\beta$ of 0 (a, d), 0.5 (b, e), and 1 (c, d)) and sodium levels (4, 10 and 60 mmol $l^{-1}$) for the negative (a to c) and neutral (d to f) transporter assumption. The cotransport model simulated uptake of 200 $\mu$mol $l^{-1}$ alanine, assuming zero-*trans* conditions with dissociation constants $K$ of 100 $\mu$mol $l^{-1}$ and $K_{Na}$ of 100 mmol $l^{-1}$, and transport rate of 1 $\mu$mol $l^{-1}$ $s^{-1}$. In general, the results showed an increase in the uptake for more negative transmembrane potential differences, with eventual saturation. Moreover, the results showed that saturation at high negative potential difference lagged behind for $\beta$ values closer to 1. This can be seen clearly under the neutral transporter charge assumption (d, e). However, constant low levels of uptake were observed when $\beta$ was 1 in case of the neutral transporter charge assumption, which is similar to Figure 4.7. Higher external sodium translated to higher uptake rates as expected.

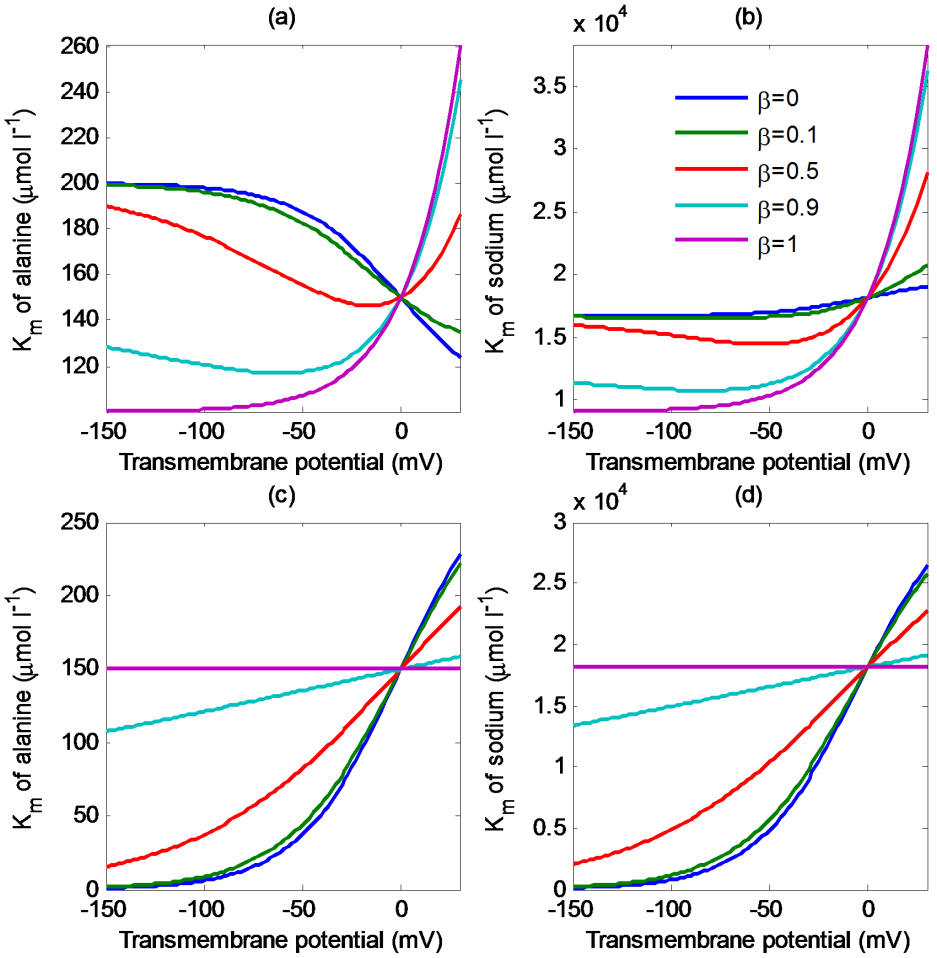


FIGURE 4.7: Simulation of transmembrane potential effects on the apparent Michaelis-Menten half-saturation parameters $K_m$, of alanine (a, c) and sodium (b, d) under the negative (a, b) and neutral (c, d) transporter charge assumption. 500 $\mu$mol l$^{-1}$ of alanine and 100 mmol l$^{-1}$ sodium were used under zero-*trans* conditions [98], and dissociation constants $K$ of 100 $\mu$mol l$^{-1}$ and $K_{Na}$ of 100 mmol l$^{-1}$.

### 4.3.2 Parameter estimation results

In this section, the cotransport model as investigated in the previous section was applied for parameter fitting based on the literature data. The simulations in Figure 4.7 were configured in line with uptake experiments of alanine into *Xenopus* oocytes [98] and now this data was used to fit the dissociation constant parameters $K$ and $K_{Na}$ and the electrical bias term $\beta$. Note that the total transport rate, $kx_T$, was also fitted in the routine, however, its value was not reported since this parameter affects only the relative scaling of the uptake curve. The results were obtained for both the transporter charge assumptions for comparison.

In Figure 4.9, the fitting of the apparent Michaelis-Menten parameters $K_m$ as a function of the transmembrane potential difference was attempted. Both the $K_m$ of alanine and sodium showed an upwards trend as the transmembrane potential difference increased and approached zero. For the negative transporter charge assumption (4.9a, b), this

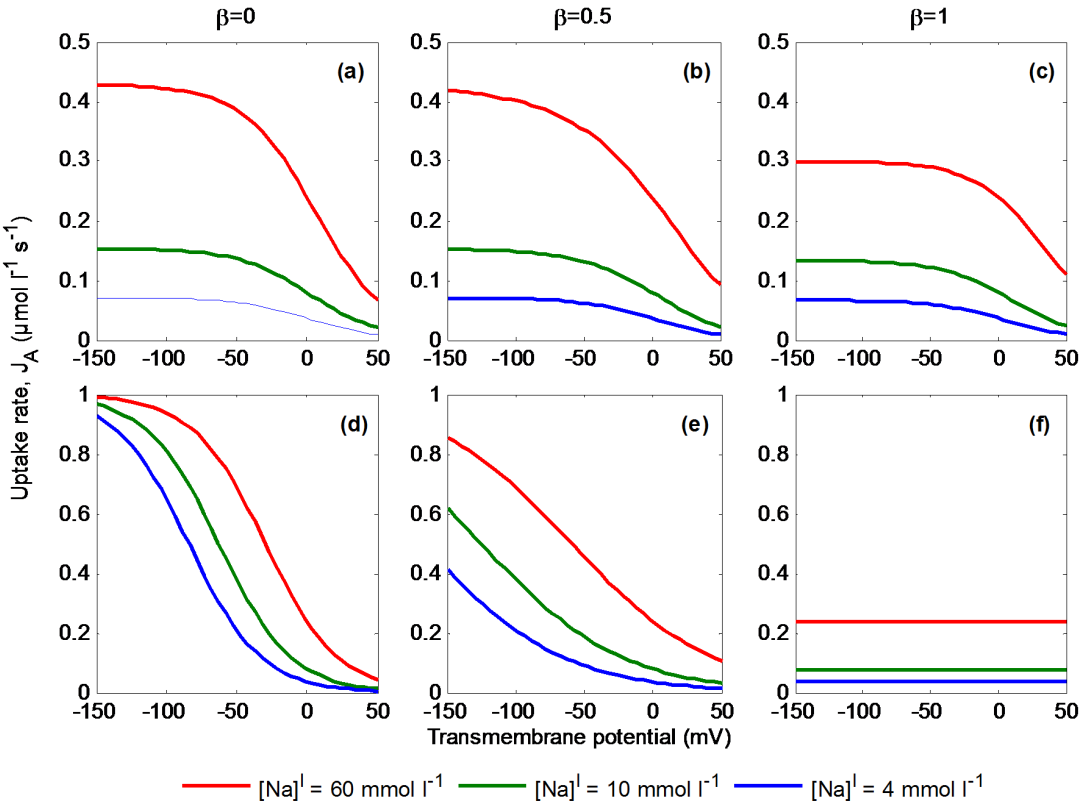


FIGURE 4.8: Cotransport model simulation of transmembrane potential effects on the uptake rate of 200 $\mu$mol $l^{-1}$ alanine for various sodium inputs and electrical bias parameters: $\beta = 0$ (a, d), $\beta = 0.5$ (b, e), and $\beta = 1$ (c, d) under the negative (a to c) and neutral (d to f) transporter charge assumptions.

could only occur at high $\beta$ value (approaching one) as any other value would not give the corresponding trend. This resulted in a bias of one for the back transport rate $k_{-2}$ of the empty transporter and low bias for the forward transport rate $k_2$, which translated to overall promoting transport of the substrate. From the fit results ($R^2 = 0.50$), the $\beta$ value was confirmed to be at the limit of 1. The dissociation constant of alanine and sodium were fitted to be 176 $\mu$mol $l^{-1}$ and 156 mmol $l^{-1}$, respectively, which were impressively close to what was previously suggested by the simulation results in Figure 4.6 (values in the order of 100 $\mu$mol $l^{-1}$ and 100 mmol $l^{-1}$, respectively). However, for the neutral transporter charge assumption (Figure 4.9c, d), a high $\beta$ value approaching 1 would not correspond to the experimental $K_m$ trend, as suggested by the flat line in the model simulation in Figure 4.7c, d. The fitting results ($R^2 = 0.62$) indeed suggested a midrange $\beta$ value of 0.65, while the dissociation constant of alanine and sodium were fitted to be 740 $\mu$mol $l^{-1}$ and 25 mmol $l^{-1}$, respectively. However, the results of the fittings for either transporter charge assumption case did not conclusively suggest one is better than the other, as evidenced by similar reported R-squared values.

Next, the flux equation of the cotransport model was applied to fit the uptake data

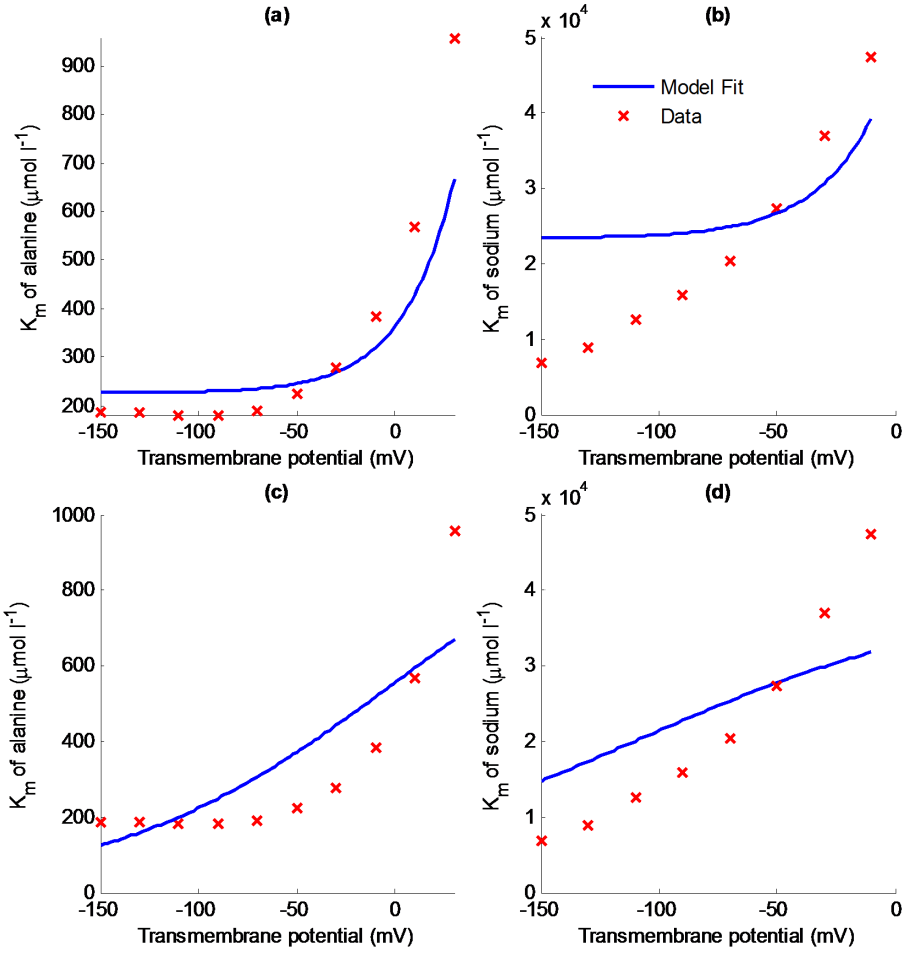


FIGURE 4.9: Model fitting of apparent $K_m$ parameters at different transmembrane potentials for the cotransport model simulation as shown in Figure 4.7 under the negative (a, b; $R^2 = 0.50$) and neutral (c, d; $R^2 = 0.62$) transporter charge assumption.

from literature, which was measured in terms of electrical current proportional to the flux of alanine transported with sodium, in opposite direction. Under the same conditions as the simulation results in Figure 4.8, the flux equation of alanine in the cotransport model was fitted for different sodium levels assuming zero-*trans* conditions (Figure 4.10a and Figure 4.10c). For the model assuming negative transporter charge, the result in Figure 4.10a showed a poor fit in general ($R^2 = 0.18$). The model appeared to be insensitive to different sodium levels, as it produced the same fit for all three sodium concentrations. In addition, the model was also fitted assuming an intracellular sodium level for oocytes set at 10 mmol $l^{-1}$ [100]. The results shown in Figure 4.10b, suggested that changes in the sodium level improved the overall fit to the data to some extent ($R^2 = 0.58$), but the effect of external sodium concentrations still could not be captured. In contrast, when the model for the neutral transporter charge assumption was evaluated, the model fits appeared to be in good agreement with the data ($R^2 = 0.99$). In Figure 4.10c, the model parameters fitted for the zero-*trans* condition were: 0.33 for $\beta$, and 1561 $\mu$mol $l^{-1}$ and 32 mmol $l^{-1}$ for the dissociation constants of alanine and sodium, respectively. For the case of 10 mmol $l^{-1}$ internal sodium (Figure 4.10d), the

model parameter values fitted were: 0.33 for $\beta$, and 2263 $\mu$mol l$^{-1}$ and 25 mmol l$^{-1}$ for the dissociation constants of alanine and sodium, respectively.

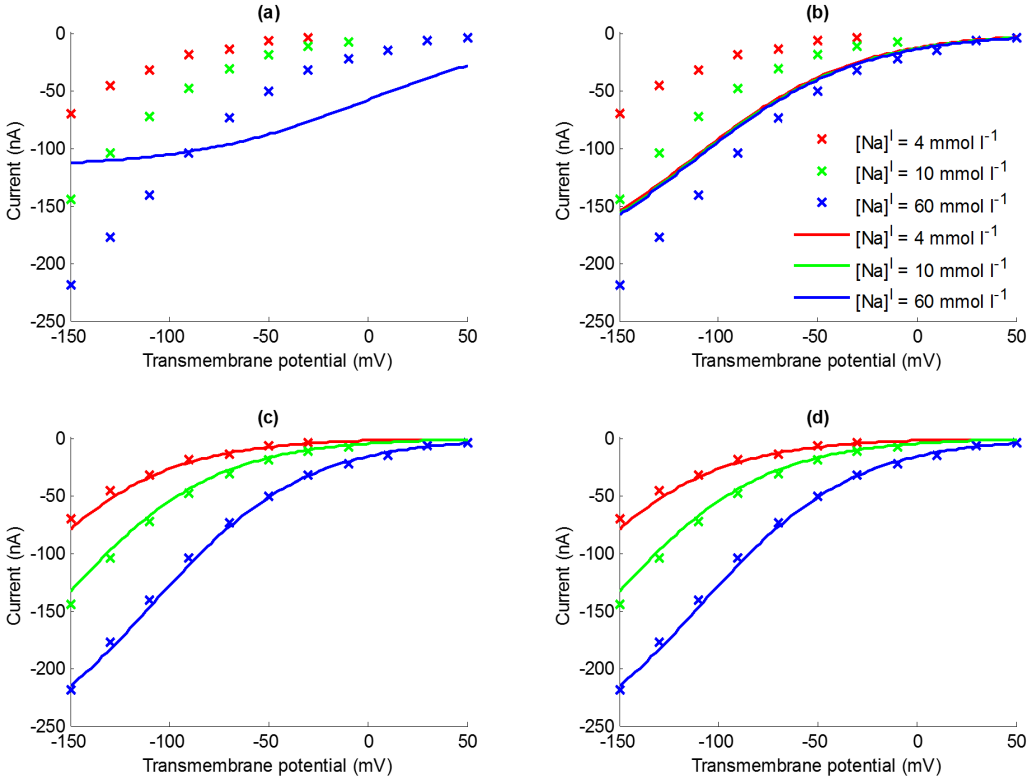


FIGURE 4.10: Cotransport model fits (solid lines) of electrical current data (x), as a measure proportional to the flux of alanine together with sodium in oocytes. Model predictions in response to transmembrane potential and different external sodium concentrations based on the simulations as shown in Figure 4.8 under the negative (a, b) and neutral (c, d) transporter charge assumption with no sodium (a, c) and 10 mmol l$^{-1}$ sodium (b, d) initially present internally. $R^2$ values for each plot are: a) 0.18; b) 0.58; c) 0.99; d) 0.99.

## 4.4 Discussion

Novel cotransport models were developed to represent the accumulative transporter, which is a secondary active transporter that derives its energy indirectly through the sodium gradient and transmembrane potential. Cotransport models based on carrier-mediated transport, were explored in terms of both the chemical and electrical gradient, which provide the underlying physical driving forces. This more mechanistic approach served as an essential improvement compared to a previous study in which the accumulative transporter was simply modelled phenomenologically as a Michaelis-Menten process [16]. The model was also shown to be capable to achieve active amino acid build-up. However, importantly, in contrast to a simple Michaelis-Menten model, it did not suggest perpetual uptake, as equilibrium levels were reached when the

electrochemical potential differences of sodium and substrate were balanced.

The fundamental cotransport model with no electrical driving force was developed similar to other passive transporter classes using carrier-mediated transport theory. The process assumed binding of sodium as the cotransport solute prior to the amino acid substrate in order to be transported across the membrane. It was shown that the sodium gradient directly promoted the transport of the substrate as anticipated. Interestingly, the model simulations showed that sodium is only required to be present on the *cis* side for transport to occur (*i.e.* no sodium present on the *trans* side). Importantly, substrate transport down its gradient occurs even if sodium concentrations are initially equal on both sides of the membrane, which may be unexpected and could have implications for the interpretation of experiments.

In this chapter, for the first time a cotransport model for the accumulative transporter was developed specifically including the effect of electrochemical potential. In order to consider the driving forces due to the electro potential, further model development was undertaken based on the principle of carrier-mediated transport of a charged substrate. The model utilized the biasing effects of electrochemical potential on the transport rates as additional terms to actively drive the transport process. However, it was shown by the model that depending on the transporter charge assumption, different individual transport rates are affected by the electro potential bias. Therefore, simulation results were presented to provide a comparison between the negative and neutral transporter charge assumptions, which suggested variations in the initial uptake rate, but not equilibrium uptake levels. Interestingly, this is consistent with varying the electrical bias parameter $\beta$ which leaves the equilibrium uptake levels unaffected. Hence, it could be inferred that if the interest is solely in the absolute levels of amino acid accumulation at steady state, then the assumptions on the accumulative transporter charge and the degree of the electrical biasing of the individual transport rates would not be important. In addition, the uptake rates and the apparent Michaelis-Menten $K_m$ parameters were shown to be affected by variations in the transmembrane potential; however these would not result in changes of the equilibrium uptake levels either.

### 4.4.1 Cotransport model parameter fitting

Initial model validation was performed by fitting the model using previous literature data, which included the fitting of the Michaelis-Menten $K_m$ parameters and the uptake rates in response to variations in electrical parameters. The results of the fitting of the $K_m$ did not conclusively suggest any transporter charge assumption is better than another as shown by the reported R-squared values. For the negative charge assumption, the results of the fitting suggested a $\beta$ value of one, which meant that the forward transport rate of the empty transporter ($k_2$) had a value less than one, while the backward transport rate ($k_{-2}$) was kept at unity. The results indeed demonstrated

this resulted in promoting the transport of the substrate. However, it appeared that the value of $\beta$ was forced to the limit of one since from the simulation it was clear that under the negative transporter assumption this was the only value that would result in an exponentially increasing trend for increasing transmembrane potential difference, as seen in the data. While the fitting of the data for the Km of alanine was able to replicate the data points well, the fitting of the $K_m$ of sodium was not. This was due to the fitting algorithm that equally weighted all data points from both Km plots to fit one set of parameter values. Note that the fitted value of dissociation constant of alanine 176 $\mu$mol $l^{-1}$ agrees well with the reported half-maximal concentration constant ($K_m$) 200 $\mu$mol $l^{-1}$ in a separate study [95]. Considering the other case of the neutral transporter assumption, it appeared that the fit of both $K_m$ parameters could not to be made to match well to the data points; however, the reported R-squared values were slightly higher than for the negatively charged case. Overall, this indicated that the model equation for the $K_m$ parameters did not correspond well to the data under either assumption. Note that in each case, the fitting algorithm estimated a single set of parameters for both $K_m$ equations for sodium and alanine simultaneously and the results in each graph, therefore, represent a compromise determined by the minimisation of the total error.

In addition, the model parameters were also fitted to the uptake rate curves as a function of transmembrane potential differences. For the negative transporter assumption under zero-*trans* condition, the model was unable to represent the data, as predictions appeared to be identical despite different external sodium concentrations. However, in oocytes experiments an internal sodium level should be initially assumed (at the intracellular level). This meant that the curves appeared to vary slightly for different external sodium. However, despite this assumption, the quality of fits did not considerably improve, suggesting that the negatively charged transporter case could not account for the behaviour observed experimentally. In contrast, for the neutral transporter assumption, the model generated good fits of the data for both zero-*trans* and intracellular sodium cases. The model's dissociation constant for alanine was fitted to be within acceptable ranges of approximation – although one order of magnitude higher than the reported value in a separate study [95]. However, the fit was shown not to be very sensitive to the dissociation constants, as changes of theses parameters did not significantly affect the fit to the data.

As a result, different $K_m$ values we obtained depending on the transporter charge assumption and data set used for fitting, indicating the complexity of the accumulative transporter behaviour. Nonetheless, based on the excellent fits of the latter data set in Figure 4.10, it was suggested that the model hypothesis of the neutral charge transporter assumption was better suited to mechanistically explain the data. However, the choice of either hypothesised mechanism becomes insignificant if the model is observed at equilibrium, since they produce identical steady state responses.

### 4.4.2 Cotransport model and experimental design

Preliminary experiments were carried out to further investigate the accumulative transporter behaviour in comparison to the model, as presented in Appendix B. The vesicle uptakes experiments were designed using the model to systematically consider different levels of driving forces due to either the electrical potential difference or the sodium gradient across the membrane. However, while the model made logical predictions of the behaviour, a more thorough experiment must be carried out in the future as the pilot results ($n = 1$) did not entirely agree with the model predictions and what would be expected based on physical considerations. This indicated the sensitivity of the experimental protocol and complexity of the cotransport system as there are many contributing factors that can affect the uptake results. Hence, a well-defined experimental protocol is needed to improve the model validation.

## 4.5 Conclusion

A model for an accumulative amino acid transporter was developed, to mechanistically integrate the effects of the chemical and electrical potential driving forces related to the cotransport of sodium ions. This cotransport model was investigated in detail, including the effect of different assumptions depending on the charge of the transport proteins. However, it was suggested by the simulation results that the ultimate level of accumulation at steady state is essentially indifferent to the transporter charge assumption, since this is determined by the electrochemical potential differences. This study also acted as a significant improvement on a previous study where the accumulative transporter was modelled as simple Michaelis-Menten type behaviour. Finally, together with the exchanger/facilitative model from the previous chapter, the cotransport model representing the accumulative transporters will be used in the integrated study of the placental amino acid transport system in the next chapter.

# Chapter 5

# Integrated model of placental amino acid transport system

## 5.1 Introduction

The placenta is important for fetal development as it mediates the transfer of all essential nutrients, such as amino acids, required by the fetus. Insufficiency of amino acids during pregnancy as a result of impaired placental transport mechanism is associated with poor fetal growth, which can lead to chronic disease in adult life [2, 4, 35, 72, 101]. While currently there are no treatments for intrauterine growth restriction, a better understanding of the placental transport system could potentially contribute to advancement in treatment strategies for intervention and prevention. The transport of amino acids from the maternal blood through the placenta to the fetal circulation is a complex process and difficult to understand intuitively. This is because amino acids do not simply diffuse through the placental membranes, but instead their transfer is mediated by transport proteins or transporters, which have different passive or active transport mechanisms and substrate specificities. Chapter 2 provides further background on each transporter mechanism. Furthermore, there are over twenty amino acids (nine of which are essential), which can either inhibit or promote each other's transport. Additionally, the transport system is influenced by physiological factors including placental blood flow, metabolism, and placental morphology [5, 102]. Hence, given this inherent complexity a systematic approach using mathematical modelling is necessary to help describe the transport system.

While many studies of amino acid transport across epithelia have focussed on individual transporters, the integrated study of the interactions between multiple transporters is limited [19, 73]. We have previously introduced an integrated model of the placental amino acid transport system, applied to the uptake and exchange of serine and alanine [16]. However, a systematic analysis of the transport system as a whole is required,

including more mechanistic transporter models [5, 103], which have been explored extensively in Chapter 3 and Chapter 4. This chapter will present for the first time such a systematic fully-integrated approach, with the aim of understanding how the composition of amino acids and transporter activity can drive the overall net transfer of all amino acids to the fetus. This modelling framework represents an important novel contribution to the field by describing the placenta as a whole system, allowing us to capture for the first time the fundamental interactions between different transporters and amino acids transferred across the placenta.

Ultimately, this knowledge can lead to treatment that is administered to the mother and designed to stimulate the transport of specific amino acids as required. The treatment can be in a form of an intravenous supply of amino acids to the mother or gene therapy to regulate the placental transporters [104]. Without such mechanistic insights into how placental amino acid transport functions as a system, these treatments are deemed difficult, if not impossible. Moreover, this systematic model can also provide predictive information on transport behaviour in response to certain pathological conditions, which can help clinicians understand disease mechanisms better. Finally, this type of modelling framework could also be applied to other epithelial transport systems, such as in kidney, intestine, and brain

The chapter will start by explaining the placental amino acid transport system and its model implementation. This is followed by the results using simplified model situations to explain step by step the processes of how amino acids are transferred to the fetus across each placental membrane individually. Subsequently, both placental membranes are combined, producing a complete representation of how amino acids get across the placenta to the fetus. Sensitivity analyses of model parameters are presented to understand the transport system as a whole and how this affects different classes of amino acids. Lastly, an example of the impact of a certain genetic condition with elevated phenylalanine levels on the amino acid transport system is explored by the model.

### 5.1.1 The placental amino acid transport system

The placenta serves as an interface between the maternal and fetal blood circulations. The maternal blood perfused in the intervillous space becomes in contact with the fetal villi at the syncytiotrophoblast, which is the barrier layer that prevents the mixing of the two circulations. At the syncytiotrophoblast, the microvillous membrane (MVM) acts as the first barrier for amino acids to cross from the maternal side. Secondly, once inside the syncytiotrophoblast amino acids then need to get across the basal membrane (BM) to reach the fetal side. Amino acids, as with other nutrients, do not simply diffuse through these membranes; instead, their transfer is mediated via specific transport proteins [5]. The schematic in Figure 5.1 shows the different transporter classes localised at each

placental membrane, as included in our model. These different transporters operate using distinct mechanism, and all of these types of transporters need to work together to get all the required amino acids to the fetus, as it is not possible for one to do so without the others. Accumulative transporters (Ac) actively pump amino acids into the placental syncytiotrophoblast against their concentration gradient, using secondary active transport driven by the sodium electrochemical potential gradient. This serves as an important driving force for the transport system as a whole since the fetal amino acid levels are higher than the maternal levels in general [6, 74]. Another significant class of transporter are the exchangers (antiporters), which take an amino acid from one side of the membrane and swap it for another from the other side, resulting in changes in the amino acid composition but not the overall net amount. This exchange process allows amino acids that are not substrates of the accumulative transporter to be transported the other side. In combination, both accumulative and exchange transporters account for the amino acid transports across the MVM [5, 6, 73]. Meanwhile, a facilitative transporter has recently been identified at the BM, in addition to the exchangers, for producing net transport to the fetus, via facilitative diffusion dictated by the amino acid gradients [6, 18, 73]. Similarly, the exchangers at the BM assist the transport of amino acids that are not substrates of the facilitative transporter across to fetus. Note that the accumulative transporters are not being considered at the BM because their role is thought to be insignificant, since the only known amino acid that is being transported actively from the fetus into the placental syncytiotrophoblast is non-essential glutamate [73]. Within these three general classes of transporter, different individual transporters can be distinguished, each of which is specific to certain overlapping subsets of amino acids, and all of these transporters work together as a system to transport all the amino acids required by the fetus.

## 5.2 Methods

### 5.2.1 Compartmental model

For an integrated representation of the placental amino acid transport system, a compartmental model was implemented based on our previous study [16]. The schematic of the compartmental model, as shown in Figure 5.1, described the transport system as consisting of three volume compartments: maternal, syncytiotrophoblast, and fetal. The compartments were assumed to be well mixed and do not include any geometric features to reduce complexity, as the focus here is on the transporter interactions. The transfers of amino acids between the compartmental volumes were modelled as fluxes mediated by various transporters as previously defined [73]. The transporter localisation at the microvillous membrane (MVM) was given by the accumulative-exchange configuration, and at basal membrane (BM) the facilitative-exchange configuration. Changes in

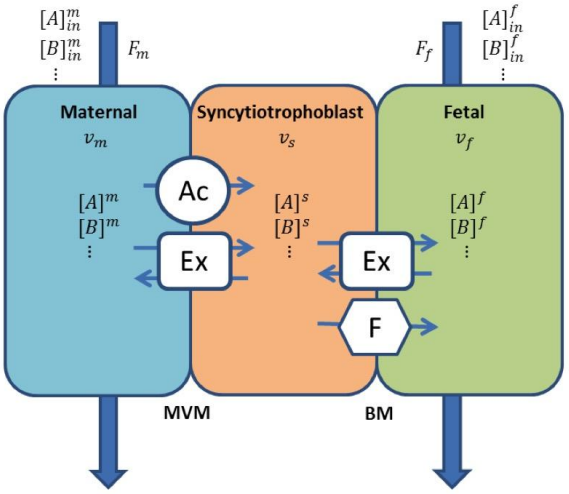


FIGURE 5.1: Compartmental model of the placental amino acid transport system. The schematic shows three compartments representing the maternal intervillous space, placental syncytiotrophoblast, and fetal capillaries. The fluxes between compartments, which produce changes in the concentration of amino acids, are assumed to be via transporter-mediated routes only. Amino acid transporters included at the maternal-facing microvillous membrane (MVM) are active accumulative transporters (Ac) and exchangers (Ex), and those at the fetal-facing basal membrane (BM) are facilitative transporters (F) and exchangers. Flow inputs and outputs are modelled for the maternal and fetal compartments. $[Y]^i$ and $[Y]^i_{in}$ denote concentration and inlet concentration of substrate $Y$ in compartment $i$, respectively (only substrate $A$ and $B$ shown in figure). $F_i$ and $v_i$ represents constant flow rate and volume of compartment $i$, respectively.

concentration of amino acid levels in each compartment are observed in response to different amino acid compositions, blood flow inputs/outputs, and transporter activities. Note that placental metabolism is not considered in the model, therefore mass is conserved and there is no net loss of amino acids. Another aspect not included in the model is transport via paracellular route that can be represented by simple diffusion which bypasses the placental tissue – which is poorly understood anatomically [105]; since, the main focus is on the transport and flow relationship. Note that paracellular diffusion will reduce the efficiency of the system because of high fetal amino acid levels causing net diffusion in the fetal to maternal direction. As a result, changes in the concentration of a certain amino acid $A$ within each compartment are given by:

$$\frac{d[A]^m}{dt} = \frac{1}{v_m}\left(J^m_{A,flow} - J^{m\to s}_{A,ac} - J^{m\to s}_{A,ex}\right) \tag{5.1}$$

$$\frac{d[A]^s}{dt} = \frac{1}{v_s}\left(J^{m\to s}_{A,ac} + J^{m\to s}_{A,ex} - J^{s\to f}_{A,ex} - J^{s\to f}_{A,fa}\right) \tag{5.2}$$

$$\frac{d[A]^f}{dt} = \frac{1}{v_f}\left(J^f_{A,flow} + J^{s\to f}_{A,ex} + J^{s\to f}_{A,fa}\right) \tag{5.3}$$

where $[A]^i$ denotes concentration (in mol $l^{-1}$) of substrate $A$ in compartment $i$, $v_i$ represents volume of compartment $i$ (in l), $J^i_{A,flow}$ denotes net molecular flux of substrate $A$ due to flow in compartment $i$, $J^{i\rightarrow j}_{A,x}$ represents the net molecular flux of substrate $A$ from compartment $i$ to $j$ mediated by transporter $x$. $i$ and $j$ can either be $m$, $s$, or $f$, which represent the maternal, syncytiotrophoblast, or fetal, compartments, respectively. $x$ can either be $ac$, $ex$, or $fa$ for accumulative, exchange, and facilitative transporters, respectively.

### 5.2.2 Representative amino acids concentrations

For the purpose of the model the amino acids transported across the placenta were categorised according to their transporter specificity into four generic groups. As shown in Table 5.1, these representative amino acid groups were AcEx – substrate of the accumulative and exchange transporters, Ex – exchange-only substrate, ExF – substrate of exchange and facilitative transporters, and, finally, AcExF – substrate of all transporter classes. The inclusion of these four amino acid groups for the integrated model represents a novel contribution of this chapter and a significant step up in complexity compared to previous work [16], in which the exchange between only two amino acids was considered. Measurements for each amino acid concentration from the placental tissues [74] and fetal circulation [106] at normal physiological levels were listed for each compartment, and the amino acid levels were summed per representative group. These values were used for the initial conditions for the time integration of the transporter models for each amino acid in each compartment.

### 5.2.3 Transporter models

Transporter models were developed based on carrier mediated transport as described previously [63, 103]. These mechanistic transporter models describing the amino acids fluxes due to the various transporter mechanisms represented significant improvements over previous simple phenomenological models. Briefly, parameters describing the transporter's kinetic properties were kept to the minimum required to represent the function of each transporter class. Therefore, in first instance, transporter translocation rates were assumed symmetric and binding affinities equal on both sides of the membrane. In addition, all substrates of a certain transporter were assumed to have identical kinetic and binding properties. To allow interactions between different amino acids and specific transporters as required in the compartmental model, the transporter models were configured to account for multiple amino acid substrates. For passive transporters (*i.e.* facilitative and exchange), the flux equations representing the transporter models are expressed only in terms of substrates concentrations and kinetic parameters, of which the model derivation can be found in published work [103] and in Chapter 3. However, for the accumulative transporters, the model has to consider

TABLE 5.1: Amino acid concentration measurements as categorised by transporter specificity.

| Amino Acid Group (Transporter specificity) | Name | Maternal concentration ($\mu$mol l$^{-1}$)* | Syncytio-trophoblast concentration ($\mu$mol l$^{-1}$)^ | Umbilical artery ($\mu$mol l$^{-1}$)* | Umbilical vien ($\mu$mol l$^{-1}$)* |
|---|---|---|---|---|---|
| AcEx (Accumulative and Exchange) | Arginine | 51 | 320 | 101 | 108 |
| | Glutamine | 368 | 1135 | 428 | 494 |
| | Glycine | 107 | 1655 | 217 | 218 |
| | Histidine | 85 | 74 | 108 | 119 |
| | Lysine | 131 | 508 | 317 | 343 |
| | Serine | 84 | 721 | 144 | 142 |
| | **sum** | **826** | **4413** | **1369** | **1424** |
| Ex (Exchange) | Threonine | **170** | **786** | **258** | **270** |
| ExF (Exchange and Facilitative) | Isoleucine | 43 | 105 | 56 | 63 |
| | Leucine | 81 | 305 | 105 | 120 |
| | Phenylalanine | 39 | 173 | 63 | 65 |
| | Tyrosine | 34 | 220 | 59 | 59 |
| | Valine | 141 | 342 | 200 | 216 |
| | **sum** | **338** | **1145** | **483** | **523** |
| AcExF (Accumulative Exchange and Facilitative) | Alanine | **215** | **1987** | **238** | **282** |

^ denotes measurements from Philipps *et al.*, 1978 [74]
* denotes measurements from Cetin *et al.*, 2005 [106]

additional parameters for the effects of the electrochemical potential as specified below, which as shown in Chapter 4 led to the development of a much more sophisticated mechanistic model than the phenomenological Michaelis-Menten type equations used previously [16]. The flux equations for each transporter model are given as follows:

**Exchanger model**

For the multiple-substrate exchanger model, the net flux of substrate $A$ from compartment $I$ to $II$ (unit of mol min$^{-1}$) is expressed by:

$$J_{A,ex}^{I \to II} = V_{ex} \frac{[A]^I [R]^{II} - [A]^{II} [R]^I}{K_{ex}([Tot]^I + [Tot]^{II})/2 + [Tot]^I [Tot]^{II}} \tag{5.4}$$

where $[A]^i$ denotes the concentration of substrate $A$ in compartment $i$, $[Tot]^i$ denotes the sum of all exchanger substrates in compartment $i$, while $[R]^i$ denotes the sum of all exchanger substrates, but excluding substrate $A$ in compartment $i$. Note that all concentration terms have unit of mol l$^{-1}$. $K_{ex}$ is the dissociation constant for all substrates of the exchanger (unit of mol l$^{-1}$), and $V_{ex}$ is the maximum transport rate (in mol min$^{-1}$).

**Facilitative transporter model**

For the multiple-substrate facilitative transporter model, the net flux of substrate $A$ from compartment $I$ to $II$ (unit of mol min$^{-1}$) is expressed by:

$$J_{A,fa}^{I \rightarrow II} = V_{fa} \left( \frac{[A]^I}{K_{fa} + [Tot]^I} - \frac{[A]^{II}}{K_{fa} + [Tot]^{II}} \right) \tag{5.5}$$

where $[A]^i$ denotes concentration of substrate $A$ in compartment $i$, $[Tot]^i$ denotes the sum of the concentrations of all substrates of the facilitative transporter in compartment $i$. Note that all concentration terms have unit of mol l$^{-1}$. $K_{fa}$ is the dissociation constant for all substrates of the facilitative transporter (unit of mol l$^{-1}$), and $V_{fa}$ is the maximum transport rate (in mol min$^{-1}$).

**Accumulative transporter model**

To represent sodium-driven secondary active transport by accumulative transporters (system A), a cotransport model was adopted in which sodium ion was assumed to bind to the transporter first, followed by the amino acid [17]. For the model distinguishing two different amino acid substrates, the net flux of substrate $A$ from compartment $I$ to $II$ (unit of mol min$^{-1}$) is expressed by:

$$J_{A,ac}^{I \rightarrow II} = \frac{V_{ac}}{D/2} \left\{ \varepsilon \varepsilon^{'} [Na]^I [Na]^{II} ([A]^I [B]^{II} - [A]^{II} [B]^I) + K_{ac} K_{Na} (\varepsilon^{'} [A]^I [Na]^I - \varepsilon [A]^{II} [Na]^{II}) \right\}$$

where,

$$\begin{aligned} D = {} & [Na]^I [Na]^{II} (\varepsilon^{'} [Tot]^I ([Tot]^{II} + K_{ac}) + \varepsilon [Tot]^{II} ([Tot]^I + K_{ac})) \\ & + K_{ac} K_{Na} \left\{ (\varepsilon^{'} + 1)[Tot]^I [Na]^I + (\varepsilon + 1)[Tot]^{II} [Na]^{II} \right\} \\ & + K_{ac}^2 K_{Na} ([Na]^I + [Na]^{II}) + 2(K_{ac} K_{Na})^2, \end{aligned}$$

and,

$$\varepsilon = e^{(\frac{\beta z F}{RT} \Delta \psi)}, \text{and } \varepsilon^{'} = e^{(\frac{(\beta - 1) z F}{RT} \Delta \psi)}, \tag{5.6}$$

where $[A]^i$ and $[B]^i$ denote concentration of substrate $A$ and $B$ in compartment $i$, respectively, $[Tot]^i$ denotes the sum of substrates $A$ and $B$ in compartment $i$. Note that all concentration terms have unit of mol l$^{-1}$. $K_{ac}$ and $K_{Na}$ represent the dissociation constants of the amino acid substrates of the accumulative transporter and sodium, respectively (unit of mol l$^{-1}$), and $V_{ac}$ is the transport rate (in mol min$^{-1}$).

Note that this model assumed that the transporter was neutrally charged, binding to the sodium ion and then the neutral amino acid to form an overall positively charged complex. Hence, it was assumed that only the translocation of the carrier-sodium-substrate complex was electrogenic. As described in the previous chapter, the electrical-

potential induced bias in the cotransport model was given by $\varepsilon^{'}$ and $\varepsilon$ for the forward and backward transport rate, respectively [97]. $\beta$ represents the degree of such electrical bias, $z$ represents the charge of sodium, $F$ is the Faraday constant, $R$ is the gas constant, $T$ is temperature and $\Delta\psi$ is the membrane potential difference between side $I$ and $II$.

### 5.2.4 Flow modelling

Blood flows are being modelled as constant in and outputs of the maternal and fetal compartments. For the flow characteristics inside the compartments, it was assumed that the compartments were well mixed for simplicity. For this study, this was deemed justifiable since observations were only based on steady state values. In the compartmental model, flows result in a net molecular flux of amino acid in compartment $i$ (in mol $\text{min}^{-1}$) as follows:

$$J^i_{A,flow} = F_i([A]^i_{in} - [A]^i) \tag{5.7}$$

where $[A]^i$ and $[A]^i_{in}$ denote concentration and inlet concentration (in mol $\text{l}^{-1}$) of substrate $A$ in compartment $i$, respectively, $F_i$ represents the constant flow rate in and out of compartment $i$ (unit of l $\text{min}^{-1}$). Note that the flow rate and the inlet concentrations were kept constant implying no change in the either maternal or fetal input.

### 5.2.5 Compartmental and transporter model parameters

Baseline model parameters are reported in Table 5.2, which includes the parameters for the compartmental and transporter models along with corresponding references. In general, the parameters were chosen for normal physiological conditions. A single functional unit of the placenta (cotyledon) was modelled with a weight of 30 grams, which can be scaled easily for the placenta as a whole since cotyledons operate in parallel. The placental cotyledon was partitioned into three compartments by volume with the largest being the maternal compartment (34%), followed by the syncytiotrophoblast (15%), and then the fetal compartment (7.5%), as described previously [16, 107]. Blood flow rates were set at physiological levels in the maternal and fetal compartments to 2 and 0.2 ml $\text{min}^{-1}$ $\text{g}^{-1}$, respectively [108, 109]. For the transporter models, the transport rates $V$, were initially taken equal at a value of 0.005 mmol $\text{l}^{-1}$ $\text{min}^{-1}$ for each class of transporter to clearly evaluate their influence on the system [16]. The dissociation constant of the exchanger substrate, $K_{ex}$, was chosen at 200 $\mu$mol $\text{l}^{-1}$ in the same order of the reported half-saturation constants ($K_m$) [67, 89], while a higher value was chosen for the facilitative transporter ($K_{fa} = 1000$ $\mu$mol $\text{l}^{-1}$) [73]. For the accumulative model, the dissociation constants of the substrate and sodium and electrical bias constants were

fitted from experimental data [98], as explored in the previous chapter ($K_{ac} = 2.26$ mmol $l^{-1}$, $K_{Na} = 25.07$ mmol $l^{-1}$, $\beta = 0.33$).

TABLE 5.2: Reference parameter values for the compartmental and transporter models.

| Parameter | Value | Unit | Reference |
|---|---|---|---|
| **Compartmental Model:** | | | |
| Total placental cotyledon volume | 30 | ml | [16, 18] |
| %maternal compartment (intervillous space) | 34% | - | [16, 107] |
| %syncytiotrophoblast compartment | 15% | - | [16, 107] |
| %fetal compartment (fetal capillaries) | 7.5% | - | [16, 107] |
| Maternal blood flow rate | 2 | ml $min^{-1}g^{-1}$ | [108] |
| Fetal blood flow rate | 0.2 | ml $min^{-1}g^{-1}$ | [109] |
| **Transporter Model:** | | | |
| **Accumulative** | | | |
| Effective transport rate, $V_{ac}$ | 0.005 | mmol $min^{-1}$ | [16] |
| Charge of sodium ion, $z$ | 1 | - | - |
| Faraday constant, $F$ | 9.65 x $10^4$ | C $mol^{-1}$ | - |
| Gas constant, $R$ | 8.314 | VC $K^{-1}mol^{-1}$ | - |
| Body temperature, $T$ | 310 | K | - |
| Transmembrane (MVM) potential difference, $\Delta\psi$ | -21 | mV | [110] |
| Maternal sodium level | 134 | mmol $l^{-1}$ | [111][a] |
| Syncytiotrophoblast sodium value | 15 | mmol $l^{-1}$ | [112][b] |
| Individual transport rate's electrical bias constant, $\beta$ | 0.33 | - | [98][c] |
| Substrate dissociation constant, $K_{ac}$ | 2.26 | mmol $l^{-1}$ | [98][c] |
| Sodium dissociation constant, $K_{Na}$ | 25.07 | mmol $l^{-1}$ | [98][c] |
| **MVM Exchanger** | | | |
| Effective (maximum) transport rate, $V_{ex,mvm}$ | 0.005 | mmol $min^{-1}$ | [16] |
| Substrate dissociation constant, $K_{ex}$ | 200 | $\mu$mol $l^{-1}$ | [67, 89][d] |
| **BM Exchanger** | | | |
| Effective (maximum) transport rate, $V_{ex,bm}$ | 0.005 | mmol $min^{-1}$ | [16] |
| Substrate dissociation constant, $K_{ex}$ | 200 | $\mu$mol $l^{-1}$ | [67, 89][d] |
| **Facilitative** | | | |
| Effective (maximum) transport rate, $V_{fa}$ | 0.005 | mmol $min^{-1}$ | [16] |
| Substrate dissociation constant, $K_{fa}$ | 1000 | $\mu$mol $l^{-1}$ | [13][d] |

[a] Mean of lower and upper later pregnancy values. [b] Intracellular value for different cell type as no specific information available. [c] Fitted based on data Yao *et al.*, Fig.5f.
[d] Representative value based on weighted average dissociation constants.

### 5.2.6 Numerical implementation

The compartmental model and transporter models were implemented in Matlab (R2013a). To predict the concentrations of amino acids in each compartment, time integration of the flux equations, which were non-linear ordinary differential equations, was performed using the 'ode45' function (Runge-Kutta (4th, 5th) method), which used a variable time step with relative and absolute tolerances of $10^{-4}$ and $10^{-6}$, respectively. Note that time integration was performed with the initial conditions for each amino acid group in each compartment as reported in Table 5.1 for the physiological case. In addition, to clearly illustrate the fundamental transporter

behaviour, various hypothetical conditions were evaluated as stated in the tables above each plot. Sensitivity analysis of the model parameters was carried out to determine the impact of the model parameters, which included the transporter activities, flow rates, and initial as well as arterial inlet amino acid concentrations. The analysis was done by plotting the net fetal transfer (umbilical venous-arterial difference) of each amino acid group in response to variation in the parameter values. Note that the range for each parameter was selected to cover an adequate interval to show clear trends or saturation in the transfer response.

### 5.2.7 Parameter estimation

An automated parameter estimation algorithm was applied to find the best-fitting combination of the model's transport rates for each transporter. The effective transport rate parameters for each transporter class ($V_{ac}$, $V_{ex,mvm}$, $V_{ex,bm}$, and $V_{fa}$) were fitted based on the relative (normalised) error between the model's net fetal transfer and the fetal venous-arterial difference levels from literature, using a least square criterion with all amino acid groups weighted equally. The fitting procedure was implemented using the 'fminsearch' function in Matlab (Nelder-Mead method) with the cost function defined as the residual sum of squares based on the errors between model simulations and experimental measurements as described below:

$$RSS = \sum_{i=1}^{n} \left( \frac{[A]_i^{Fetal,Model} - [A]_i^{Fetal,Literature}}{[A]_i^{Fetal,Literature}} \right)^2 \tag{5.8}$$

To account for the variation in absolute values between experimental conditions, for each data point the difference between model prediction and literature was normalised first by the literature value, squared and then summed over all points to yield the overall error criterion. Note that the initial guess values for the fitted parameters that were used by the 'fminsearch' minimisation function were chosen within the same order of magnitude of physically feasible and/or experimentally reported values. Multiple initial guess values were attempted to confirm that the fitting algorithm converged to a unique solution.

## 5.3 Results

### 5.3.1 Fetal delivery of amino acids: Transport interactions across the basal membrane

The exchange and facilitative transporters localised at the basal membrane are responsible for the final delivery of the amino acids to the fetus. While the exchangers

are important in regulating the composition of the amino acids delivered to the fetus, the facilitative transporter is crucial in getting the overall net amount of amino acids from the syncytiotrophoblast to the fetus. The interactions of these transporters were explored and shown in Figure 5.2. The compartmental model implemented to study the BM distinguished only two types of amino acids: BMEx, which was the exchanger-only substrate and BMExF, which was the substrate for both transporters. The initial concentration in the fetal compartment was set to the same as for the fetal inflow. Since both transporters are passive, both amino acid levels in the syncytiotrophoblast compartment were set to be 10 times the inlet concentrations of the fetal compartment, to ensure net transport to the fetus. The syncytiotrophoblast concentrations were held constant throughout the simulation, to provide a clear overview of BM transport alone. Note that the relative fractions of both amino acid groups were the same (50%) in both compartments. The summary of the inputs is shown in Table 5.3. Intuitively, when only the facilitative transporters were active, only BMExF was transported to the fetal compartment along its concentration gradient. Conversely, when only the exchangers were considered, both amino acids levels in the fetal compartment showed no net changes since the amino acid compositions were already at equilibrium. Hence, for either case where only one type of transporter was localised at the basal membrane, the system was unable to transport both types of amino acids across to the fetus. However, when both the facilitative and exchange transporters were present, BMEx was successfully transported to the fetus along with BMExF (Figure 5.2). This is because the efflux of BMExF via the facilitative transporter, altered the relative amino acid composition on the fetal side, and the resulting lower fraction of BMEx in the fetal compartment then in turn enabled the exchanger activity to produce net transport of BMEx into the fetal compartment.

Furthermore, the effect of the relative transport activity was explored using the model. As shown in Figure 5.3, changing each transporter's relative activity can influence the steady state uptake levels in the fetal compartment for both amino acid species. In Figure 5.3a, the model implemented various exchange rates relative to a constant facilitative rate. The results suggested that fast exchange activity would result in equalising the ratio of both amino acids in the compartments. In addition, Figure 5.3b shows the results generated by the model assuming various facilitative activities with respect to the exchange activity, which suggested that having fast facilitative activity could indirectly drive transport of the exchanger substrate BMEx.

As passive transporters, both exchangers and facilitative transporters are dependent on the substrate concentration gradients to drive transfer across the membrane. The effects of varying the relative amino acid concentration levels were examined (according to inputs in Table 5.4) and shown in Figure 5.4. As mentioned previously, it is the difference in the relative compositions of amino acids in each compartment that determines transfer via the exchangers, rather than the absolute concentrations on each

side of the membrane. As can be observed in Figure 5.4a for an exchanger alone, varying the syncytiotrophoblast concentration as a fraction of the total for a certain species to be higher than the fetal ratio would lead to net transfer into the fetal circulation. If the ratio is lower, reverse transport occurs. When the ratios on both sides were equal, no change occurred on the fetal side. However, when both facilitative and exchange transporters were considered (Figure 5.4b), a positive uptakes into the fetal circulation was observed in all cases for BMExF, which was due to the facilitative transport pathway. For BMEx, however, the fetal net transfer was shown to be positive when the ratio of BMEx was equal or higher, while the lower ratio of BMEx would result in negative transfer. Net transport of BMEx occurred even for equal initial fractions of BmEx, since the facilitated transport of BmExF reduces the fraction of BmEx in the fetal compartment, leading to a favourable ratio for transport of BMEx by exchange at steady state.

TABLE 5.3: Amino acid concentration inputs for each group at the BM: Fetal values represent both the initial and inlet concentrations, while the syncytiotrophoblast concentrations were kept constant throughout the simulation.

| Amino acid group | Syncytiotrophoblast compartment | Fetal compartment |
|---|---|---|
| **BMEx** | **100** $\mu$mol $l^{-1}$ | **10** $\mu$mol $l^{-1}$ |
| (ratio of total) | (0.5) | (0.5) |
| **BMExF** | **100** $\mu$mol $l^{-1}$ | **10** $\mu$mol $l^{-1}$ |
| (ratio of total) | (0.5) | (0.5) |

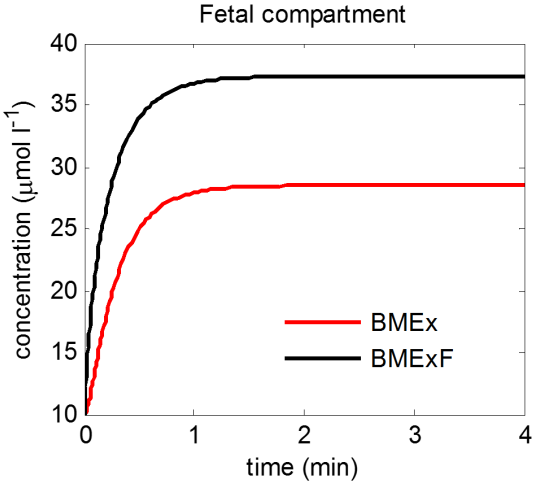


FIGURE 5.2: Fetal amino acid concentrations from simplified model simulations across the BM for the conditions described in Table 5.3: The concentrations of amino acid group BMEx and BMExF in the fetal vein were simulated using the compartmental model as shown in Figure 5.1.

Next, the model considered physiological amino acid levels from Table 5.1, which were grouped according to their transporter specificity at the BM (as summarised in Table 5.5). BMEx was then considered to consist of AcEx and Ex, while BMExF

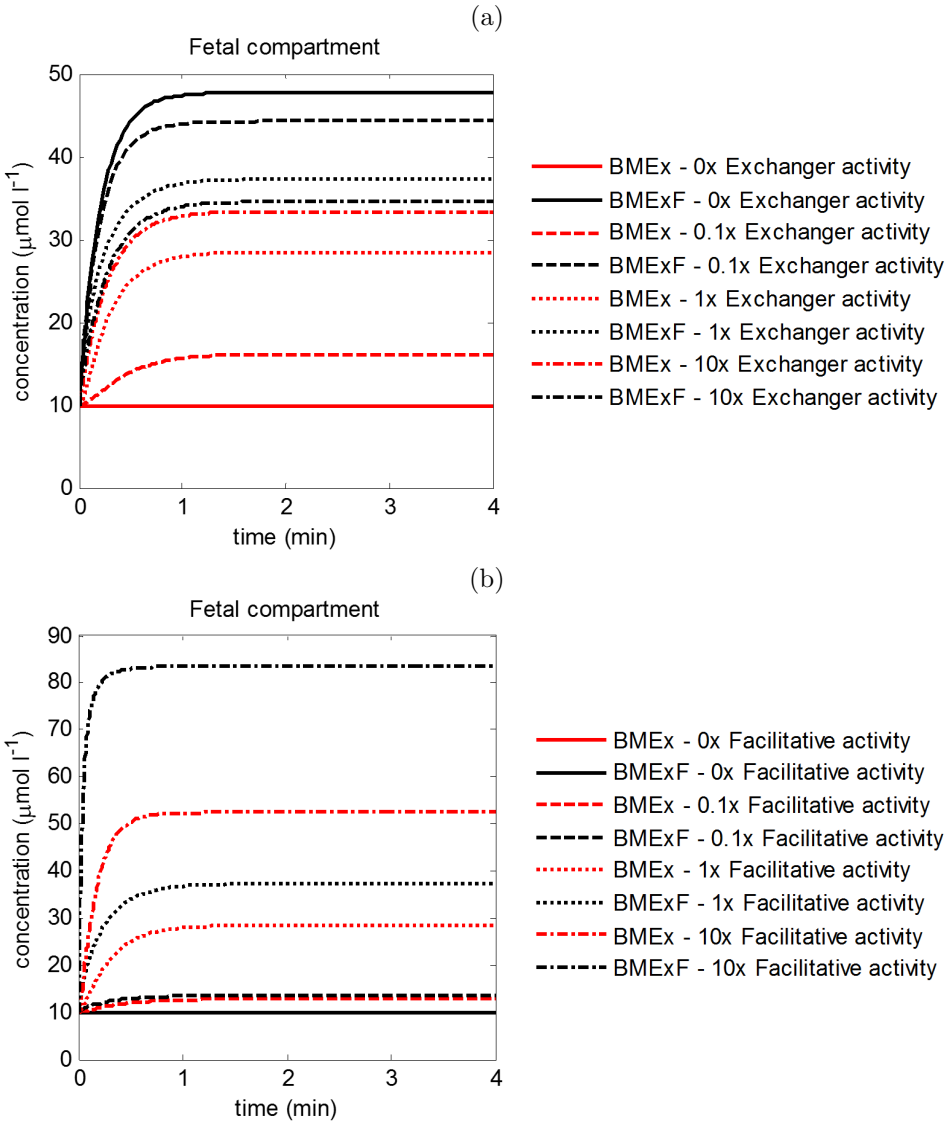


FIGURE 5.3: Model simulations of the effects of variation in transporter activity at the BM. Each amino acid concentration in the fetal compartment was modelled to show the transport interactions across the BM, with conditions given in Table 5.3, over a range of relative exchange (a), or facilitative (b) transport activities.

included ExF and AcExF. Figure 5.5 illustrates an increase in fetal uptake for BMExF only, however with a slight decrease of the fetal concentration of BMEx, which would imply reverse transport into the syncytiotrophoblast. As shown before, this was due to the higher input ratio of BMEx in the fetal compartment and the baseline facilitative transporter activity was inadequate to offset this effect. Hence, as previously explored, increasing the facilitative activity (*e.g.* by 10 fold, as shown in the figure) can indirectly boost the fetal BMEx uptake to obtain positive transport. However, this resulted in a substantial increase in the fetal BMExF level that is much higher than the physiological level in the umbilical vein.

TABLE 5.4: Amino acid concentration inputs for each group at the BM with variation in the composition: Fetal values represent both the initial and inlet concentrations, while the syncytiotrophoblast concentrations were kept constant throughout the simulation.

| Amino acid group | Syncytiotrophoblast compartment | Fetal compartment |
|---|---|---|
| **BMEx** | **[10,100,200]** $\mu$mol l$^{-1}$ | **10** $\mu$mol l$^{-1}$ |
| (ratio of total) | (0.09,0.5,0.67) | (0.5) |
| **BMExF** | **100** $\mu$mol l$^{-1}$ | **10** $\mu$mol l$^{-1}$ |
| (ratio of total) | (0.91,0.5,0.33) | (0.5) |

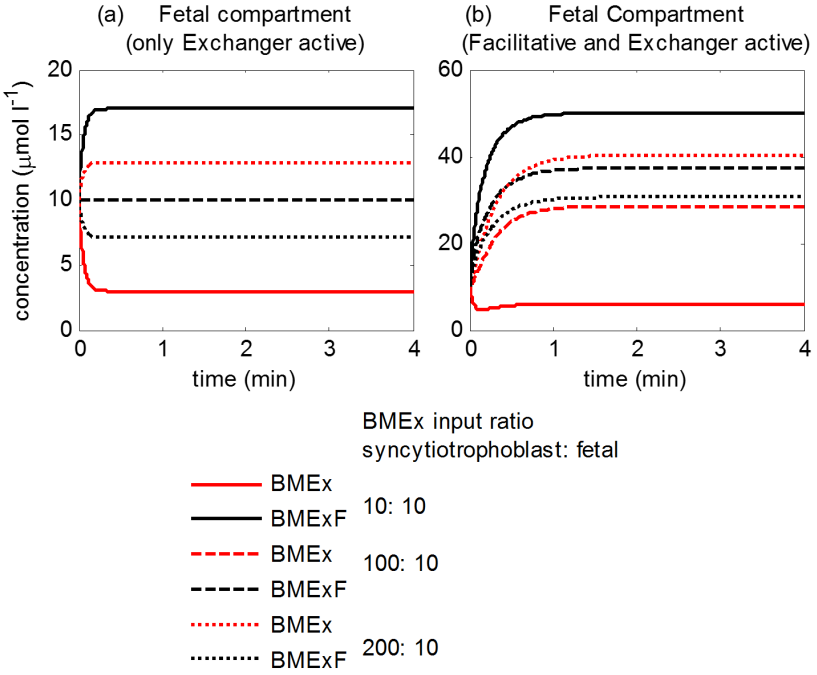


FIGURE 5.4: Model simulations showing the effects of various amino acid levels on transport interactions across the BM: The compartmental model simulated fetal concentrations with various input conditions as in Table 5.4 for the case when (a) only the exchangers were active and (b) when both facilitative and exchange transporters were active.

### 5.3.2 Uptake of amino acids into the placenta: Transport interactions across the microvillous membrane

After having demonstrated the mechanisms underlying the transfer of amino acids from the syncytiotrophoblast to the fetal compartment, the next step was to explore how syncytiotrophoblast concentrations are established as a result of uptake of amino acids from the maternal circulation. As shown in Figure 5.1, the transport of amino acids across the MVM is mediated by the accumulative transporter and the exchanger. While the accumulative transporters actively pump the amino acids into the syncytiotrophoblast, the exchangers are responsible for equalising the composition of the

TABLE 5.5: Physiological amino acid concentrations for each group at the BM: Fetal values represent both the initial and inlet concentrations, while the syncytiotrophoblast concentrations were kept constant throughout the simulation. From Table 5.2, amino acid group BMEx comprises of AcEx and Ex, while BMExF comprises of Ex and AcEx.

| Amino acid group | Syncytiotrophoblast compartment | Fetal compartment |
|---|---|---|
| **BMEx** (ratio of total) | **5199** $\mu$mol l$^{-1}$ (0.62) | **1627** $\mu$mol l$^{-1}$ (0.69) |
| **BMExF** (ratio of total) | **3132** $\mu$mol l$^{-1}$ (0.38) | **721** $\mu$mol l$^{-1}$ (0.31) |

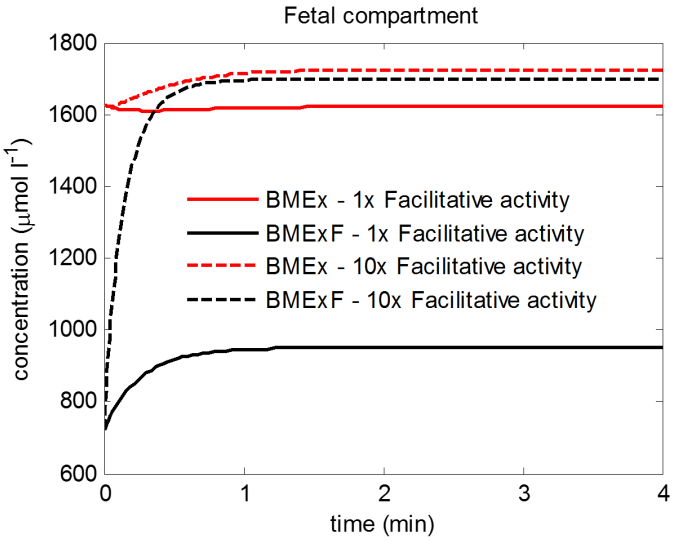


FIGURE 5.5: Physiological model simulations of transport interactions across the BM for equal exchanger and facilitative transporter activity (solid), and results for 10x increased facilitative transport activity (dashed line) using compartmental model with inputs from Table 5.5.

amino acids. Amino acid substrates were categorised for the model into two groups as: 1) accumulative and exchange transporter substrate, MVMAcEx, and 2) exchanger-only substrate, MVMEx. The compartmental model was then implemented to explore the uptake interactions across the MVM, assuming a constant inlet concentration of amino acids into the maternal compartment with values shown in Table 5.6. Furthermore, transport across the BM was disabled to clearly demonstrate the potential for uptake across the MVM. As shown in Figure 5.6, the model simulated uptake in to the initially empty syncytiotrophoblast compartment (*i.e.* zero-*trans*), which showed the high accumulation of both amino acids in the syncytiotrophoblast compartment over time. The accumulative transporters and exchangers configuration allowed uptake of both amino acid MVMEx and MVMAcEx, while the exchanger only substrate would not have been transferred if only the accumulative transporters were considered. Note that the initial dip in concentrations on the maternal side was the result of placental uptake,

which goes to zero as steady state is approached. The uptake profile of MVMEx slightly lagged behind, which was due to initial absence of exchangeable MVMEx in the placental compartment. Once MVMAcEx was pumped in to the placenta, then the exchangers start to operate in conjunction with the accumulative transporters. Steady states were reached when the difference in accumulative transporter substrate and sodium electrochemical potential were equilibrated and the fraction of exchanger substrates equalised in both compartments.

TABLE 5.6: Amino acid concentration inputs for each group at the MVM: The maternal values represent inlet and initial concentrations, while in the syncytiotrophoblast compartment is zero.

| Amino acid group | Maternal compartment | Syncytiotrophoblast compartment |
|---|---|---|
| **MVMAcEx** (ratio of total) | **100** $\mu$mol l$^{-1}$ (0.5) | **0** $\mu$mol l$^{-1}$ |
| **MVMEx** (ratio of total) | **100** $\mu$mol l$^{-1}$ (0.5) | **0** $\mu$mol l$^{-1}$ |

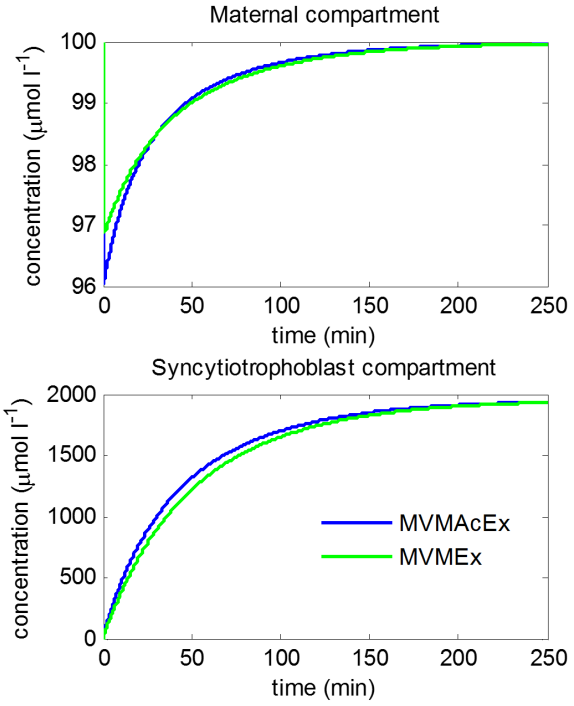


FIGURE 5.6: Syncytiotrophoblast amino acid concentrations for the simplified model simulations of transport across the MVM with conditions from Table 5.6. The concentrations of amino acid group MVMAcEx and MVMEx in the maternal vein and placental syncytiotrophoblast layer were simulated using the compartmental model in Figure 5.1.

The model simulated the effects of varying the transporter activity, which is shown in Figure 5.7. The results suggested that changes in the activities did not affect the steady levels, but only the uptake rate and thus the speed at which the equilibrium was

reached. In similar manner as in the previous section, high relative exchanger activity resulted in bringing amino acids profiles together (shown in Figure 5.7a). However, a small lag in the transfer of MVMEx was still present. For low relative exchange activity, the transfer of MVMEx into syncytiotrophoblast compartment occurred at a slower rate. Also, it reduced the amount of MVMAcEx exchanged back to the maternal side, which resulted in the faster accumulation of MVMAcEx in the syncytiotrophoblast compartment. Moreover, the model showed that with increased relative accumulative activity (Figure 5.7b), the uptake rate of MVMEx also increased along with MVMAcEx. Note that, the effects of MVMEx uptake rate lagging behind MVMAcEx was also amplified when relative accumulative activity increased.

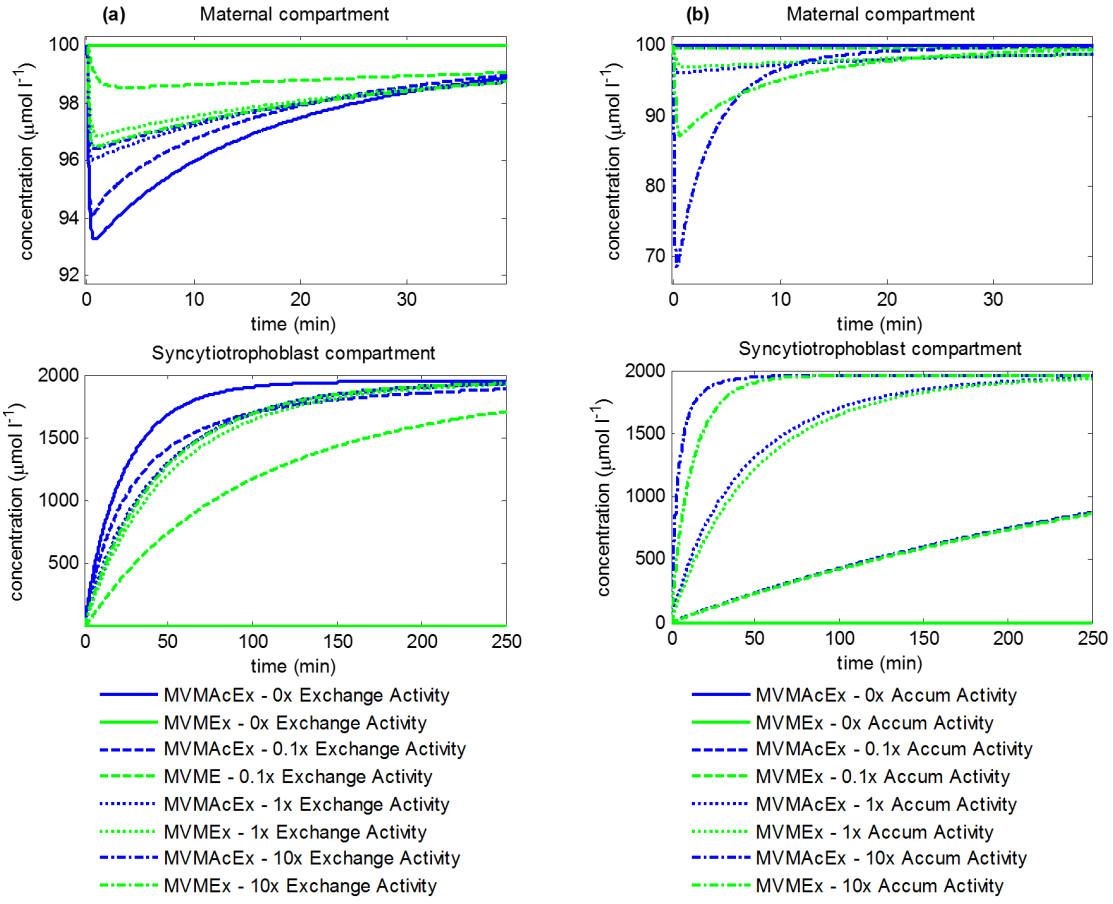


FIGURE 5.7: Model simulation of the effects of variation in transporter activity at the MVM. The model shows each amino acid concentrations in the maternal and syncytiotrophoblast compartment for the interactions across the MVM with input conditions given in Table 5.6 over a range of relative (a) exchange or (b) accumulative transport activities.

In addition, different maternal amino acid input levels (as shown in Table 5.7) in the maternal compartment were modelled, which is shown in Figure 5.8. By keeping the MVMAcEx level constant, the model suggested that an increase in MVMEx results in an increase in its concentration in the syncytiotrophoblast compartment and the uptake

of MVMAcEx reaches steady state slower. In particular when the maternal level of exchange-only MVMEx was higher (than MVMAcEx), it was shown that the uptake in the syncytiotrophoblast compartment of MVMEx could surpass that of the accumulative substrate, MVMAcEx. This was due to the continuation of exchange over time until syncytiotrophoblast concentration ratios matched those of the maternal inlet. Note that in all cases, the uptake levels in the syncytiotrophoblast compartment of both species were higher than the maternal levels.

TABLE 5.7: Amino acid concentrations for each group at the MVM to investigate variations in the composition: The maternal values represent inlet and initial concentrations, while the initial concentration in the syncytiotrophoblast compartment is zero.

| Amino acid group | Maternal compartment | Syncytiotrophoblast compartment |
|---|---|---|
| **MVMAcEx** (ratio of total) | **100** $\mu$mol l$^{-1}$ (0.91,0.5,0.33) | **0** $\mu$mol l$^{-1}$ |
| **MVMEx** (ratio of total) | **[10,100,200]** $\mu$mol l$^{-1}$ (0.09,0.5,0.67) | **0** $\mu$mol l$^{-1}$ |

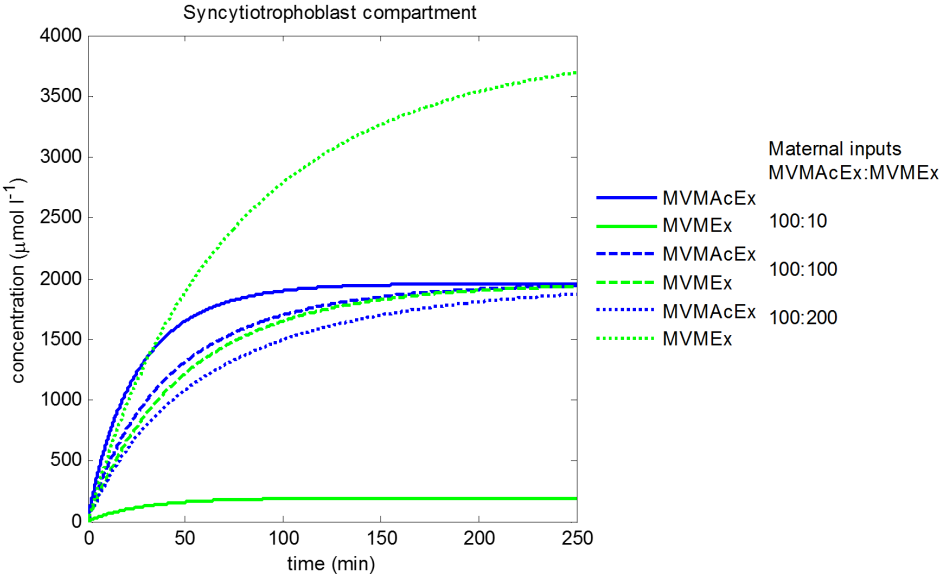


FIGURE 5.8: Model simulations showing the effects of various amino acid concentration levels on transport interactions across the MVM: The compartmental model simulated syncytiotrophoblast concentrations with various input conditions as given in Table 5.7.

For the physiological levels of the amino acid groups as prescribed in Table 5.1, the amino acids concentrations can be further grouped according to their transporter specificity at the MVM. MVMAcEx was then considered to consist of AcEx and AcExF, while MVMEx included Ex and ExF. With these values as inputs (summarised in Table 5.8), the model simulated the physiological uptake for these amino acid groups in to the syncytiotrophoblast, which suggested high uptake levels for both MVMAcEx

and MVMEx (shown in Figure 5.9). The uptake profile in the syncytiotrophoblast compartment of MVMEx and MVMAcEx showed monotonic increase. Although it was difficult to see, a slow increase of MVMAcEx initially was observed, which can be explained by the exchanger working against the accumulative transporter since the initial concentration ratio of MVMAcEX was higher in the syncytiotrophoblast. The model showed that the syncytiotrophoblast concentrations of both species continued to rise well above physiological values, however it is important to note that the model here only considered the MVM and did not include the efflux transport across the BM, which would lead to a lower equilibrium.

TABLE 5.8: Physiological amino acid concentrations for each group at the MVM: The maternal values represent inlet and initial concentrations, while the syncytiotrophoblast values represent the initial concentration. From Table 5.2, amino acid group MVMAcEx comprises of AcEx and AcExF, while MVMEx comprises of Ex and ExF.

| Amino acid group | Maternal compartment | Syncytiotrophoblast compartment |
|---|---|---|
| **MVMAcEx** (ratio of total) | **1041** $\mu$mol l$^{-1}$ (0.67) | **6400** $\mu$mol l$^{-1}$ (0.77) |
| **MVMEx** (ratio of total) | **508** $\mu$mol l$^{-1}$ (0.33) | **1931** $\mu$mol l$^{-1}$ (0.23) |

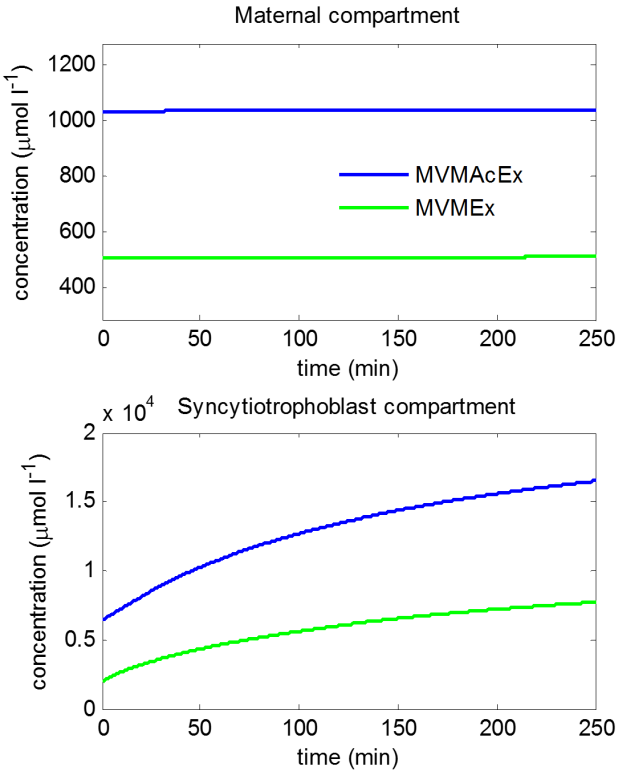


FIGURE 5.9: Physiological model simulations of transport interactions across the MVM: The amino acid concentrations in the maternal vein and placental syncytiotrophoblast layer were simulated using the compartmental model with input conditions in Table 5.8.

### 5.3.3 Transport across the placenta to the fetus

As we have now separately established the mechanisms of transport at the microvillous membrane (separating the maternal and syncytiotrophoblast compartments) and basal membrane (in between the syncytiotrophoblast and fetal compartments), the next step was to simultaneously consider all transporters at both membranes. All three placental compartments were considered (Figure 5.1) and the model simulations of the four classes of amino acids were generated using the maternal and fetal arterial physiological input levels from Table 5.1. Similarly, initial conditions were set at the physiologically maternal, syncytiotrophoblast and umbilical artery values. Choices of parameters for the model were made corresponding to the values in Table 5.2, which included the assumption that all transport rates were equal (*i.e.* same transport activity for all three transporters). The results of the model simulation are shown in Figure 5.10 and Table 5.9, which suggested that all four amino acids were successfully transferred to the fetal compartment as evident from a net increase in their concentrations. For the physiological input values used, the model also indicated to be operating near steady state, especially in the maternal compartment. All amino acids showed reductions from the initial levels in the syncytiotrophoblast compartment, inferring that they were net-transported to either maternal or fetal compartments. From the simulations, net concentrations delivered to the fetus of each amino acid were computed from steady state levels in the fetal compartment, which are shown in Table 5.10 in comparison with the umbilical venous-arterial difference from literature. The overall simulated and the experimental results appeared to correspond reasonably well, without any tuning of the model parameters. More specially, two amino acid groups under-predicted the literature's net transfer values: AcEx by 9 $\mu$mol $l^{-1}$ and Ex by 9.3 $\mu$mol $l^{-1}$. AcExF was over-predicted by 25.5 $\mu$mol $l^{-1}$ and ExF by 3.6 $\mu$mol $l^{-1}$.

TABLE 5.9: Initial physiological input levels and model simulated concentrations at steady state for each amino acid group including the ratios per as a fraction of total amino acid in each compartment.

| | **Maternal** | | **Syncytiotrophoblast** | | **Fetal** | |
|---|---|---|---|---|---|---|
| $\mu$mol $l^{-1}$ (ratio of total) | Initial and inlet | Steady state | Initial | Steady state | Initial and inlet | Steady state |
| **AcEx** | **826** (0.53) | **821** (0.54) | **4413** (0.53) | **4209** (0.62) | **1369** (0.58) | **1415** (0.56) |
| **Ex** | **170** (0.11) | **170** (0.11) | **786** (0.09) | **725** (0.11) | **258** (0.11) | **261** (0.10) |
| **ExF** | **338** (0.22) | **334** (0.22) | **1145** (0.14) | **1090** (0.16) | **483** (0.21) | **527** (0.21) |
| **AcExF** | **215** (0.14) | **208** (0.14) | **1987** (0.24) | **735** (0.11) | **238** (0.10) | **305** (0.10) |

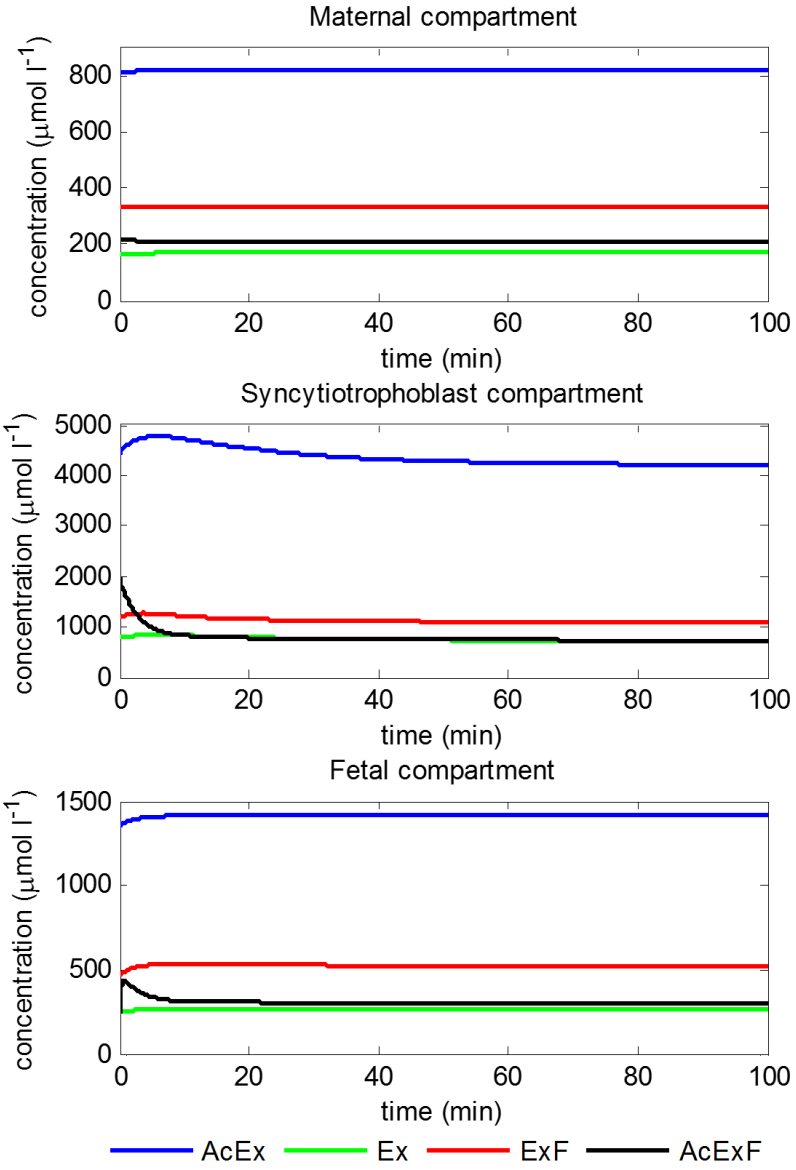


FIGURE 5.10: Compartmental model simulations of physiological amino acid levels in each compartment with steady state levels reported in Table 5.9.

TABLE 5.10: Comparison of net fetal transfer levels at steady state of each amino acid group for baseline simulated results, umbilical venous-artery difference as reported by the literature, and generated by model fitting of transporter activities.

| Amino acid group | Baseline simulation ($\mu$mol l$^{-1}$) | Literature value ($\mu$mol l$^{-1}$) | Fitting* ($\mu$mol l$^{-1}$) |
|---|---|---|---|
| **AcEx** | **46** | **55** | **53** |
| **Ex** | **2.7** | **12** | **9.3** |
| **ExF** | **43.6** | **40** | **32.5** |
| **AcExF** | **67.4** | **44** | **70** |

*Note that model fitting suggested the following transporter activities with respect to the baseline values: 2.8x exchange at MVM, 59x Exchange at BM, 1.3x facilitative, and 0.75x accumulative activity

### 5.3.4 Sensitivity analysis of transporter activities

The effect of variation in relative transporter activity on the net fetal transfer of each amino acid group was analysed. The impact of variations in transport activity parameters for each transporter class ($V_{ac}$, $V_{ex,mvm}$, $V_{ex,bm}$, and $V_{fa}$) was explored and shown in Figure 5.11 for the accumulative, MVM exchange, BM exchange, and facilitative transporter separately. Reference transport activity parameters, as mentioned in Table 5.2 were varied using a multiplier factor to explore the response across a wide range of each transporter's activities. The results showed the net fetal transfer of the different amino acid classes plotted as a function of the transport activity multipliers. The results in Figure 5.11a, d suggested that the activities of accumulative and facilitative transporters promote the fetal transfer for all amino acids. In addition, saturation levels in the fetal transfer were achieved when the transporter's activities were high. The results also suggested that an increase in the activity of particular transporters can promote transfer of certain substrates at the price of decreasing the transfer of others. Specifically, as shown in Figure 5.11c, increasing BM exchanger activity would result in a decrease in fetal transfer of amino acids that are transportable by facilitative transporters (*i.e.* ExF, AcExF). This could be explained by equalisation of the composition of the amino acids in the syncytiotrophoblast and fetal compartments as a result of high BM exchanger activity (as was previously demonstrated), which subsequently reduces the net fetal transfer of these substrates by promoting back exchange into the syncytiotrophoblast compartment. Similarly, in Figure 5.11b, increasing MVM exchange activity would result in equalising the composition of amino acids in maternal and syncytiotrophoblast compartments. As expected, increased MVM exchange activity promoted uptake of those amino acids that are transported by exchange only at the MVM (Ex and ExF), resulting in increased fetal delivery. This comes at the price of the reduction in fetal transfer of AcEx demonstrated, since increasing exchange activity across the MVM promoted back transfer of the substrate into the maternal compartment. However, surprisingly an increase in fetal transfer was observed for AcExF, which has the same transporter specificity at the MVM. This is because the syncytiotrophoblast ratio of AcExF, which was high initially, dropped to a ratio lower than on the maternal side at steady state (Table 5.9), for the baseline simulations. Increasing MVM exchange activity would then promote AcExF uptake in the syncytiotrophoblast compartment and in turn increase transfer to the fetal compartment via facilitated transport. Thus MVM exchangers affected BM transfer indirectly, and in opposite manners depending on how the overall transport system shifted the concentration ratios of each amino acid in the three compartments. Lastly, it can be noted from Figure 5.11a–d that the fetal transfer of amino acid Ex (transported by exchanger only) could be driven by increasing any transporter activity, but only to a small degree. Negative net fetal transfer, which translated to amino acids transport out of the fetal compartment, can occur for AcEx at very low facilitated (Figure 5.11d) or accumulative (Figure 5.11a) activity.

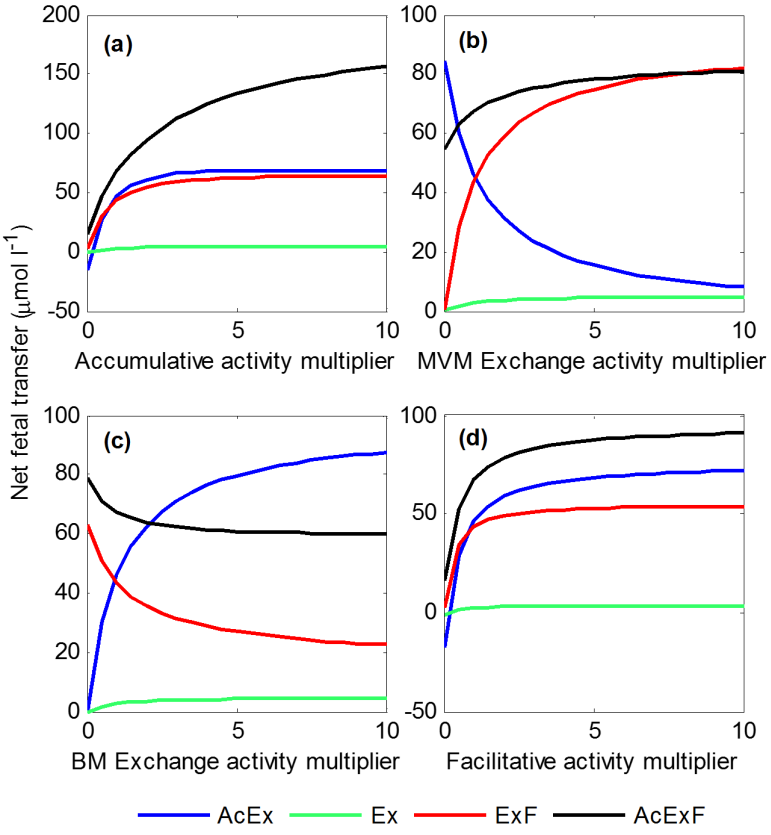


FIGURE 5.11: Transporter activity sensitivity analysis: Net fetal transfer values for each amino acid were simulated in response to a range of variations in individual transporter activity.

In addition, dual transport activity sensitivity tests were performed in which two activity parameters were varied simultaneously. As previous, net fetal transfer of each amino acid was observed in response to various transport activity multipliers. At first, the overall impact of exchanger activity was explored. Net transfer of each amino acid was simulated, varying both exchanger activities at the MVM and BM simultaneously (shown in Figure 5.12). The 3D plot suggested that for amino acid AcEx, increasing exchange activity at the BM while reducing exchange activity at the MVM would result in optimal fetal delivery. This was the result of promoting exchange across to the fetal compartment while reducing back exchange to the maternal compartment. In contrast, for ExF and AcExF, both of which are facilitative substrates, increasing BM exchange activity would lead to reuptake in to the syncytiotrophoblast compartment. However, for AcExF, the BM exchanger activity has opposite effects on net transfer depending on whether the MVM exchanger activity is high or low. Interestingly, it was shown that in addition of having both exchanger activities high, additional high AcExF transfer could be maintained when both activities were low. (Note that a separate maximum peak in transfer of AcExF could even occur under certain conditions, as can be seen in the results in Figure C.7 in Appendix C for the case in which the accumulative transporter charge was assumed to be negative). This scenario could be explained because for effectively low

exchange activities the accumulative and facilitative transporters would dominate the transfer, and back exchange into the maternal and syncytiotrophoblast compartments is essentially limited. Also, the transfer of AcExF, regardless of the exchange activities at both membranes, would always result in positive net transport. For substrate Ex, it was shown that higher fetal uptake can be achieved by increasing both exchange activities, however, the relative change is small. These results were consistent when compared to previous individual sensitivity analyses (in Figure 5.11b and c).

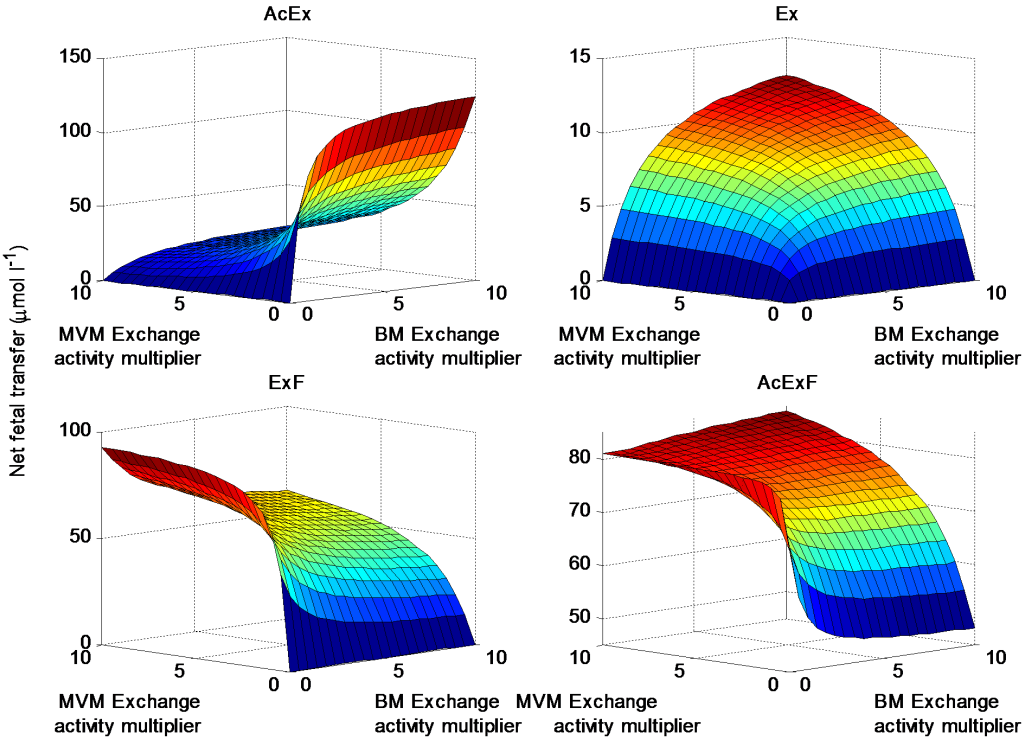


FIGURE 5.12: Dual transport activity sensitivity analysis: MVM *vs* BM exchange activity. Net fetal transfer values for each amino acid were simulated in response to varying the exchange activities at the MVM and BM simultaneously.

Next the case for how transport is affected by the transporters on the MVM was explored. The simulation, as shown in Figure 5.13, modelled net fetal transfer in response to simultaneous variation of the accumulative and exchange activities in the MVM. The results suggested that maximal fetal transfer of amino acid AcEx or AcExF occurs when the accumulative activity is high, which promotes uptake in to the syncytiotrophoblast, and the exchange activity is low, which limits back-exchange. For amino acids Ex and ExF, the maximum delivery in the fetal compartment was achieved when both transporter's activities at the MVM were high. This is because both transporters promote uptake via exchange into syncytiotrophoblast for these substrates, either directly or indirectly by increasing the intracellular levels of the driving substrates. Note that negative net fetal transfer (transport out of the fetal compartment) could occur under certain conditions; for instance, when the accumulative activity is significantly low in amino acid AcEx. This occurred because of the substrate AcEx was swapped out of

the fetus by the exchanger due to higher ratio of AcEx in the fetal compartment in combination with inadequate inputs by the accumulative transporter from the maternal side to offset the ratio in the syncytiotrophoblast in favour of the net positive fetal transfer direction.

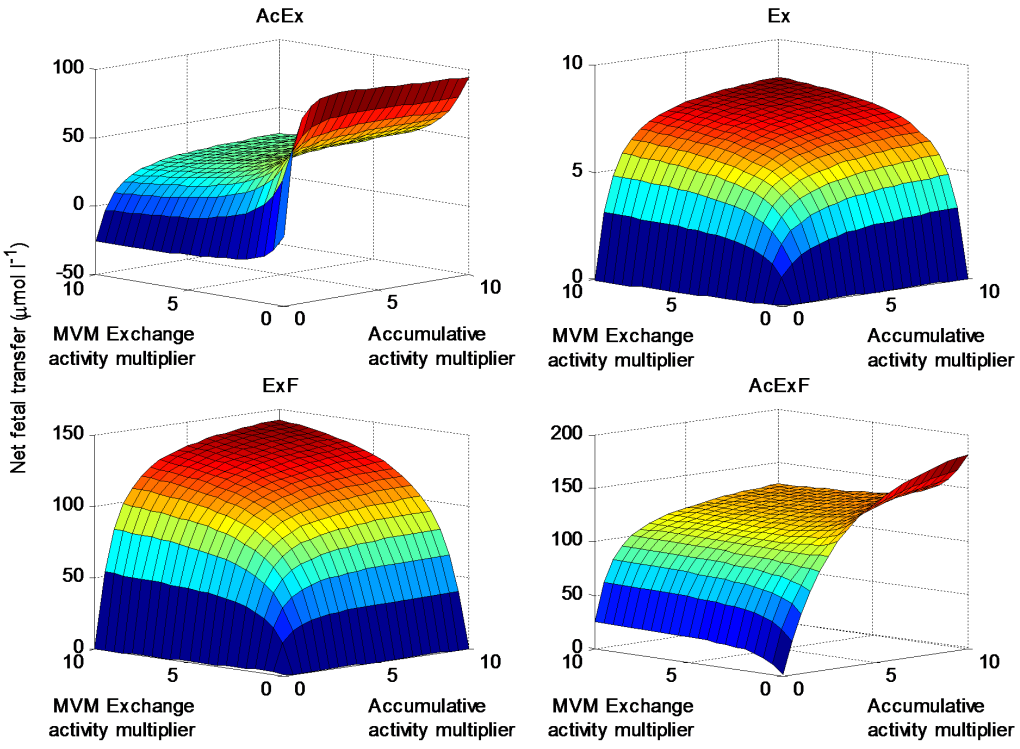


FIGURE 5.13: Dual transport activity sensitivity analysis at the MVM. Net fetal transfer values for each amino acid were simulated in response to varying the MVM exchange and accumulative transport activities simultaneously.

Finally, in the same manner, the impact of the transporter activities on the BM was simulated. As shown in Figure 5.14, the simultaneous variation in transport activities of the exchangers and the facilitative transporter were examined. The model suggested that for ExF and AcExF, the fetal uptake was optimal when the facilitative activity was high and the exchange activity at BM was low. This combination appeared to promote fetal transfer while, at the same time, limiting reuptake. Additionally, it was shown that for AcEx and Ex, which are not substrates of the facilitative transporter, the fetal transfer was increased when all of transport activities were high at the BM. These substrates must be exchanged to transport across the BM, therefore promoting exchange will directly increase the fetal transfer. Also, increasing the facilitative rate will indirectly increase the fetal transfer, since it leads to a more favourable concentration ratio for exchange.

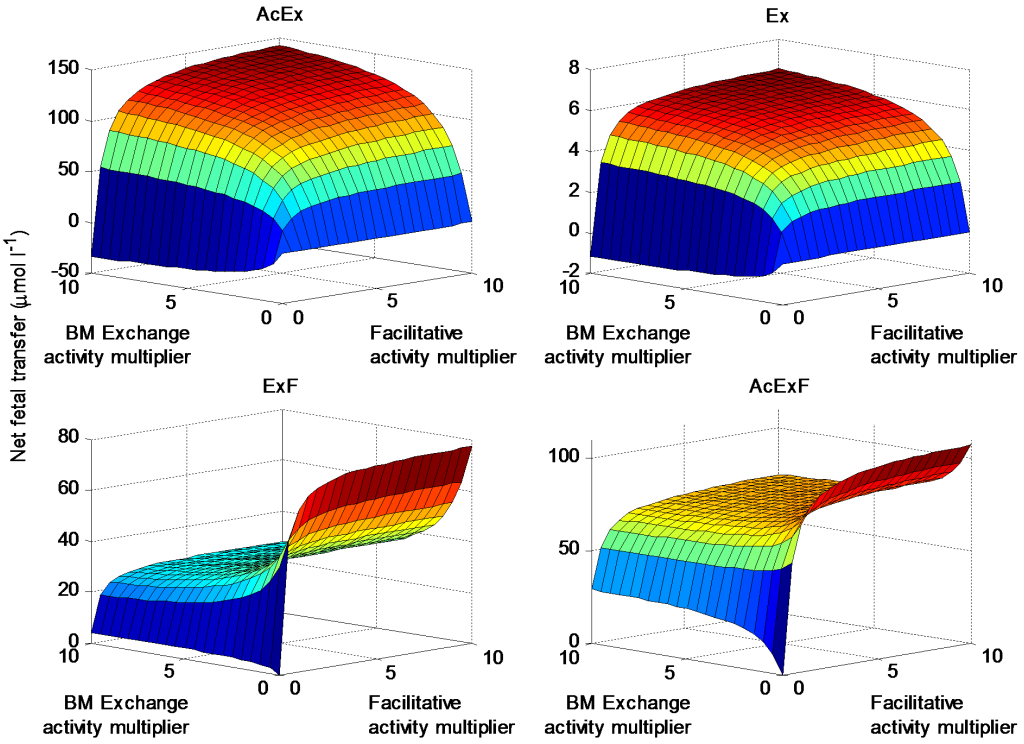


FIGURE 5.14: Dual transport activity sensitivity analysis at the BM. Net fetal transfer values for each amino acid were simulated in response to varying the BM exchange and facilitative transport activities simultaneously.

### 5.3.5 Flow Sensitivity

The compartmental model implements constant flow inputs in the maternal and fetal compartment. The flow can potentially affect the transfer of the amino acids, hence, the flow sensitivity was analysed in response to variations in maternal and fetal flow. From Table 5.2, the current baseline values for maternal and fetal flow rates were 6 x $10^{-5}$ $m^3$/min and 6 x $10^{-6}$ $m^3$/min, respectively. A flow multiplier ranging from zero to two was used to model the fetal transfer for each amino acid. As shown in Figure 5.15, the system appeared to be more sensitive to the changes in the fetal flow due to the small volume proportion. While in the larger-volume maternal compartment, the flow rate did not appear to be affecting the fetal delivery (unit of mol $min^{-1}$) as much. The model suggested that a slow fetal flow rate translated to high fetal delivery for amino acid group AcEx and Ex (not facilitative substrate), while faster fetal flow rate would stimulate fetal delivery of amino acid ExF and AcExF (facilitative substrate). This is because for the facilitative substrate, high fetal flow maintains the BM concentration gradients driving facilitated transport. While for amino acids that cannot be transported by facilitative transporters, high fetal flow would maintain the less favourable inlet concentration ratios, which determine transport via the exchangers.

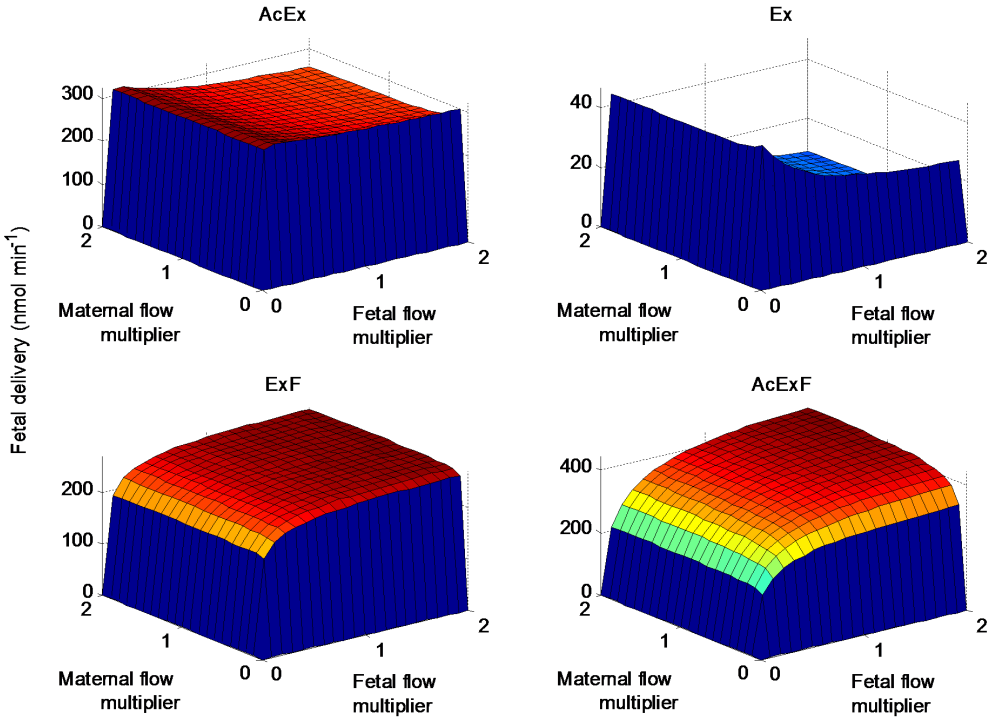


FIGURE 5.15: Flow sensitivity analysis: Net fetal delivery values for each amino acid were simulated in response to varying the maternal and fetal flow inputs simultaneously.

### 5.3.6 Model sensitivity to amino acid input concentrations

Lastly, the analysis of the model sensitivity was implemented to investigate the effect on fetal transfer due to changes in the overall amino acid inputs in the maternal and fetal compartments. The test performed variation in the initial amino acid levels and inputs by using a single multiplier for all four amino acid groups with respect to the baseline levels as prescribed in Table 5.1. The results, as shown in Figure 5.16, suggested that low fetal amino acid levels and high maternal amino acid levels would generally promote fetal transport. In addition, the maternal amino acids became limiting at low levels. The results also suggested that negative net transfer could occur when maternal levels are extremely low and fetal levels are high.

### 5.3.7 Coordinated regulation of transporter activity

The fitting algorithm was performed to find which combination of all the transporter activities would provide the best overall fit when compared to the fetal venous-arterial difference from literature. The simulated and model fitting results, along with the comparison to the literature values, are shown in terms of the net fetal transfer in steady state for each amino acid group (Table 5.10). The baseline simulated results showed reasonably good overall correspondence when compared to the literature's values.

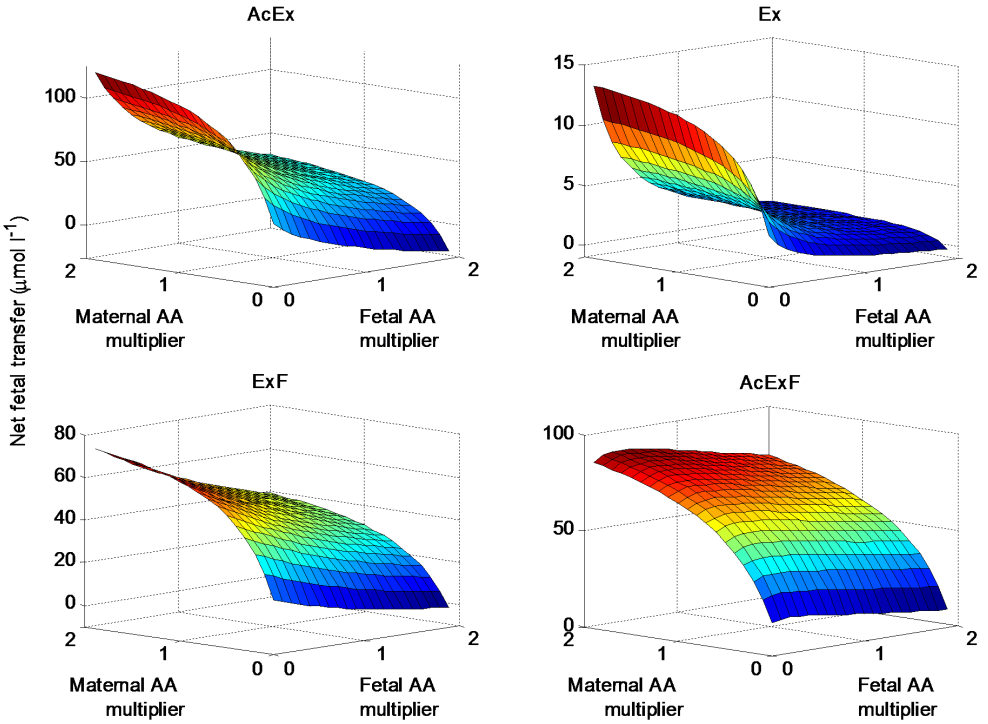


FIGURE 5.16: Amino acid level sensitivity analysis: Net fetal transfer values for each amino acid were simulated in response to varying the overall maternal and fetal amino acid concentration levels simultaneously.

Specifically, amino acid group ExF showed an insignificant discrepancy. The baseline model slightly under-predicted AcEx and Ex, while over-predicting AcExF. The model fitting results showed some improvements when compared to the baseline simulation, especially for the substrates that were initially under-predicted. Impressively, the fit was able to almost match amino acid AcEx to the literature values (within 3.7%). Also, the fit made significant improvement in bringing up the low-level amino acid Ex. However, for AcExF the values remained nearly unaffected, while ExF deviated more than the original baseline results. The model fitted the following adjustments to the baseline transporter activities parameters: 0.75 times the accumulative, 2.8 times exchange at MVM and 59 times exchange at the BM, and 1.3 times the facilitative activity.

### 5.3.8 Elevated maternal phenylalanine level

The compartmental model was also implemented to explore the effects of a specific clinical condition on the amino acid transport system. For instance, the model simulated the genetic condition of maternal phenylketonuria – where lack of a specific enzyme causes an excess level of phenylalanine that can affect fetal development and function [113]. As shown in Figure 5.17, net transfer of each amino acid group was modelled over a range of multiple levels of maternal ExF relative to the baseline value, since this is the

amino acid group phenylalanine belongs to. The results suggested that the elevated level of ExF in the maternal compartment reduces the net transfer level of all other amino acid groups as anticipated by the condition. Moreover, the model predicted negative net transfer levels of other amino acids at high maternal level of ExF (*e.g.* at 5x the baseline value), which inferred that the amino acids were transported out of the fetus.

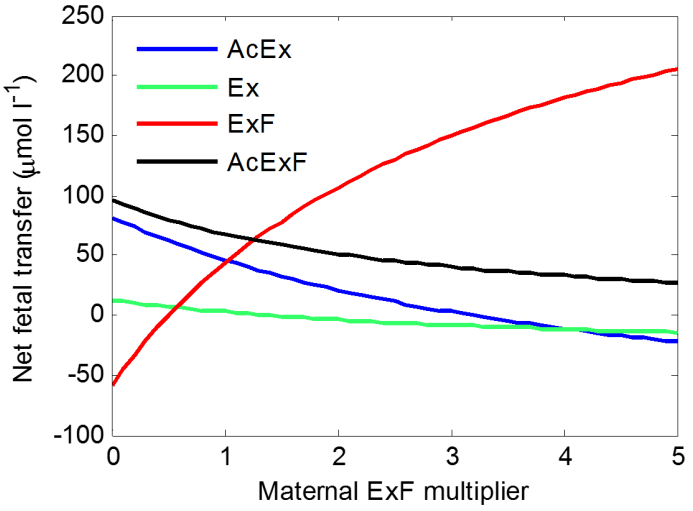


FIGURE 5.17: Effects of elevated maternal amino acid ExF level (Phenylalanine) on the fetal transfer of each amino acid.

## 5.4 Discussion

This study served as novel integrated approach for modelling the amino acid transport system in the placenta. The compartmental model incorporated carrier models for three different classes of amino acid transporters to represent the placental transport system. The model for the transport system consisted of three compartments, separated by two placental membranes where transporters are located to mediate amino acid transport. The results demonstrated the application of this modelling framework to address the complexity of the interactions arising when multiple amino acids were considered, which proved to be difficult to fully comprehend without the model.

The study successfully demonstrated the fundamental interactions at each of the placental membranes to explore the transport behaviour of how amino acids are transferred to the fetus (across the BM) or accumulated in the placental syncytiotrophoblast (across the MVM). While the model suggested that the facilitative-exchange transporter configuration at the BM was sufficient in transferring amino acids to the fetus, the arterial composition of the amino acid levels proved to be important in determining the transport efficiency. In addition, indirect stimulation of amino acids that were not a substrate of the facilitative transporter was shown to be possible by increasing the facilitated transport activity. Moreover, the accumulative-exchange transporter

configuration at the MVM proved to be effective in mediating transport of different types of amino acids into the syncytiotrophoblast. It was shown that high accumulations in the syncytiotrophoblast were achievable; however, eventually the syncytiotrophoblast amino acid levels were shown to be approaching steady state. This suggested that the transport across the MVM, even with active accumulative transporter, should not be generally thought of as perpetual uptake. The syncytiotrophoblast uptake levels of both accumulative and exchange amino acid species were higher than the maternal levels. This accumulation against the gradient is enabled by the energy required to maintain the constant sodium gradient whose electrochemical potential provides the driving force for the system. Indirect stimulation of amino acids that were not a substrate of the accumulative transporter across the MVM was also shown possible via exchange. However, in contrast to the fetal transport across the BM, the compositions of amino acids did not solely dictate the direction of transport of all amino acids across the MVM. Amino acids that were substrates of the accumulative transporter were ensured active transport in to the syncytiotrophoblast, even with unfavourable concentration ratios and gradients.

Overall, the MVM's accumulative-exchange transporter configuration allows a large accumulation of amino acids into the placenta, while the facilitative-exchange configuration at the BM permits the transfer to the fetus governed by the syncytiotrophoblast concentration levels. When the overall transport across the placenta was considered under physiological conditions, the integrated model showed a favourable net transfer of all amino acid groups to the fetus. This indicated a perhaps surprising level of robustness, considering that the amino acid transport rates and kinetic parameters were assumed equal and highly simplified per amino acid group. In addition, the predicted uptake and delivery profiles appeared to be near steady state, which was encouraging given that the amino acid concentration inputs were from normal pregnancy levels, which should be maintained stable. However, it was evident that there were discrepancies in the net fetal transfer levels and the literature's umbilical venous-arterial difference levels for each amino acid. Hence, a fitting algorithm was then applied, which suggested that by changing transport activities for each transporter these discrepancies could be improved. Though, it appeared difficult to adjust levels of certain amino acid groups without affecting the others. In particular, improving the prediction for the exchange only substrate required a disproportional increase in BM exchanger activity (Table 5.10).

As we have explored the possibility of adjusting the transporter activities to achieve improved overall results across all amino acids. It was also important to consider the several factors and simplifying assumptions made in the current compartmental model that could contribute to the discrepancies in the results. For instance, these would include the simplified transporter representation, where generic values were used instead of different transport affinities for each substrate at each interface. Also, the grouping

of amino acids, approximations and experimental variation in amino acids levels from literature, and absence of amino acid metabolism, could all contribute to the relatively limited discrepancy in the simulated results. In particular, as was previously shown, the composition of the input concentrations plays an important role in fetal transfer. Despite these limited discrepancies, our current model has shown to be robust in representing the key features of transport and a valuable first approach in the study of the placental amino acid transport as an integrated multivariable system.

### 5.4.1 Model assumptions to reduce number of parameters

In this study, certain simplifying assumptions were made for the model application to help generalise parameters together. This included the transporter translocation rates, which were assumed symmetric and binding affinities, which were chosen to be equal on both sides of the membrane and the same for all substrates of each transporter. Although, these parameters could be otherwise separately explored in the model, the simulations could only result in minor changes in the transient uptake responses. Since for current study where steady state uptake values were examined, it was reasonable to make generalised assumption on these parameters as other option was thought unnecessary.

### 5.4.2 Sensitivity of the model variables and parameters

Sensitivity analyses of the compartmental model's parameters were examined in order to observe the changes in the transfer level in response to each parameter. Initially, the parameter for each transporter activity was observed individually. The results in Figure 5.11 clearly showed how increasing the activities of each transporter would affect the transfer; however, the effect on transfer would eventually be limited by other factors. It was also logical to see how the accumulative and facilitative activities were directly promoting the transfer of all amino acids; since the first transporter is responsible for the uptake of substrate into the placental syncytiotrophoblast while the latter is for delivering substrate to fetus. However, it was interesting to see how the exchange activities at each membrane affected the transfer differently for each amino acid substrate, which was clearly simulated by the model. This highlights the importance of our model for investigating the transport interactions. Moreover, this point was again emphasized when simultaneous dual parameter variation studies were performed. One of the benefits of the computational model was that it allowed multiple factors to be analysed concurrently, which would otherwise be hard to intuitively visualise. Also, the dual sensitivity analysis pointed out that multiple optimal transfer configurations can occur (as shown in Figure 5.12 for AcExF), which might be overlooked had it not been demonstrated using the model. The model's sensitivity analyses also suggested that the amino acid groups displayed different transport behaviour at the different membranes.

For instance, those amino acids that were substrate of the accumulative transporter behaved in the same way when considered at the MVM, in clear contrast with to those that were not an accumulative transporter substrate (as shown in Figure 5.13). Similarly, the amino acids that can be taken up by the facilitative transporter displayed the same response when observed at the BM, showing a distinctly different response compared with those that were not taken up by the facilitative transporter (Figure 5.14). In addition, a sensitivity analysis was performed on the flow inputs of the maternal and fetal compartment. The results implied that the flow rate can significantly affect the fetal transfer of the amino acids, and it is important to consider that this is in relation to the volume of the compartment (more sensitive to flow for a smaller volume). Additionally, the flow rates were shown to be rate limiting when both maternal and fetal flow rate approach zero. Interestingly, the flow rates were affecting the various amino acid groups differently. It appear that, with the current amino acid concentration inputs, the transfer of the amino acids that were substrates of the facilitative transporter show a direct relationship to the flow rates, whereas the other group showed an opposite relationship. This novel finding suggested the potential effects of lower than normal physiological flow rates (*e.g.* in placental disorders) affecting the amino acid transfer and this should be addressed in future experiments. For instance, further investigation with the current compartmental model can consider various heterogeneous flow patterns as in previous models [55, 56] that took the geometry and structural organisation of the placenta into account (as described in Section 2.5.1). Lastly, in regards to the amino acid levels, a sensitivity analysis was performed with varying overall maternal and fetal amino acid levels. As shown by the results, it was inferred that the transfer of amino acids is promoted when the mother has a high level of amino acids while the fetus has low amino acid levels, which was deemed logical. However, as was shown, at a certain point the amino acid transfer appeared to be reaching saturation. This could potentially be thought of as a preventive mechanism to protect the fetus from excessive transfer of amino acids despite high levels in the maternal circulation. In conclusion, the sensitivity analyses of the model are important in understanding the transport behaviour of the amino acids in the placenta, especially when considering multiple parameters simultaneously. Dual parameters analyses implemented in this study effectively provide a fundamental understanding of the transport behaviour. However, additional parameters or variables can be added to the analyses to further investigate the multi-variability of parameters on the transport system. Nonetheless, at the current stage, the model was shown to be able to capture the main features of the placental transport system based on the principal underlying transport mechanisms.

### 5.4.3 Coordinated regulation of transporter activity

As shown by the model, the system using baseline parameters already appeared to be in reasonable agreement with the literature. This implied that our compartmental model

realisation, despite many simplifying assumptions, was able to represent robustly the placental amino acid transport system. Moreover, with our knowledge of the model sensitivity and kinetic behaviour, possible refinements to the model can be made. The model's transporter activities were fitted in an attempt to match the literature data. However, the transport model appeared to be restricted as the change in transfer of some amino acids was limited by and indirectly dependent on one another. For instance, for the low level amino acids (Ex), the fit was able to increase the fetal transfer, however, at the expense of decreasing the fit quality of others (*i.e.* ExF). However, this shouldn't be discouraging considering the inherent experimental variation in amino acid concentrations used for comparison and the approximations made in deriving the model such as the grouping together of individual amino acids with different transport affinities. In addition, the model fitting results suggested that the rates of transport by the exchanger should be high. Specifically, the model inferred much higher exchange activity at the BM from the fit. This also suggested that the system is not sensitive to the transport rate of the BM exchanger for the given inputs. It is worth noting that our simulations were performed with given constant inputs which could contribute to the system's response being restricted. While in reality, varying levels in the inputs could occur which the fetus will determine what recirculates back.

### 5.4.4 Elevated maternal phenylalanine level

The robustness of the model was again assured in the ability to address certain circumstances that are thought to affect the amino acid transport system. This was exemplified in the case of elevated maternal phenylalanine in phenylketonuria. The model was able to confirm the effects of the condition as a result of restricted fetal delivery of all other amino acids that are essential for fetal development and function. This serves as the motivation for future applications where the model can be used for disease screenings by clinicians, or predictive medicine design in the pharmaceutical industry.

## 5.5 Conclusion

Our integrated modelling framework served as novel approach for simulating the amino acid transport system in the placenta. The implementation of the compartmental model that combines carrier models for various classes of amino acid transporters was shown to be robust in representing the transport system as a whole. At the present stage, the model was shown to be able to capture successfully the principal features of the transport system in spite of simplifying assumptions that were made. Further improvements to the model could distinguish individual transporters, their kinetics and substrate specificity in greater detail as informed by experimental data available, which would ultimately

contribute to a better understanding of placental transport as a whole and hopefully lead to the development of new clinical applications.

# Chapter 6

# Discussion

Placental transport of amino acids is highly complex as it incorporates many interdependent mechanisms and factors, including numerous amino acid transport proteins and a wide variety of different substrates. In this thesis, a new computational modelling approach has been developed and proven to be valuable in the gaining a better understanding of the transport system as a whole. This serves as an important development in the effort to create a 'virtual' placenta. A systematic understanding of the placental transport systems could provide insightful contributions to the design of intervention or treatment for pathological conditions, such as IUGR. In addition, the placental transport models can also be applied in a similar manner to other epithelial tissues, such as transfer of pharmaceuticals across the blood-brain barrier.

## 6.1 Model contributions

The transfer of amino acids across the placenta is mediated by transport proteins in the membranes of the syncytiotrophoblast layer. As described (in Section 2.2.1), this carrier-mediated process fundamentally requires binding of the substrate to the transport protein to allow translocation between the two sides of membrane. These transport proteins were categorised according to their transport mechanisms and modelled as: 1) exchanger, 2) facilitative transporter, and 3) accumulative transporter. As reviewed (in Section 2.5.3), previous studies have mainly investigated the transport of nutrients using uptake experiments described as a Michaelis-Menten process. The commonly-used Michaelis-Menten kinetic representation was then shown not to provide a full mechanistic representation of transporter behaviour, as it does not account for intracellular concentrations and thus cannot meaningfully describe experimental scenarios other than initial uptake in zero-trans experiments (Chapter 3).

**The exchange-facilitative transporter model derived was able to address experimental variations**: A more mechanistic carrier-mediated transport model was

developed to represent both the exchanger and facilitative transporter, with only a single parameter controlling the relative contribution of these two transporter mechanisms (Section 3.2.2). It was shown for the first time how this model could give rise to different apparent Michaelis Menten constants as a function of internal concentration, which may help explain variation in experimental literature.

**The model suggested a non-obligatory exchange mechanism for the LAT2 transport protein**: Subsequently, the exchange-facilitative transport model was implemented to design experiments and comprehensively test the behaviour of the transport protein LAT2 over a wide range of conditions. LAT2 has been widely reported to have a 1:1 obligatory exchange mechanism. However, the model fitted to the vesicle experiments clearly suggested a slow non-obligatory component. Although it is not possible to distinguish for certain whether the transporter itself has a non-obligatory pathway or if there is a presently unknown facilitative transporter working in parallel. In addition, an extensive investigation of the model was carried out that included a sensitivity analysis of the model parameter estimation (Section 3.3.6) and an exploration of the impact of asymmetric kinetic parameters (Section 3.3.8). Given the data available, this supported the application of the model using only a minimum number of parameters (with symmetric kinetic parameters) to successfully represent overall transporter behaviour for a wide range of experimental conditions.

**A cotransport model was successfully developed to address the electrochemical potential effects of sodium**: For the accumulative transporter, a new carrier-mediated cotransport model was developed (Chapter 4) that incorporated the effects of the driving forces due to the sodium chemical and electrical potential. The model was able to demonstrate active transport behaviour, as evident from its ability to transport against the gradient. The cotransport model was investigated extensively based on various model assumptions, such as the transporter charge, since the effect of this on transport is currently unknown. The cotransport model also served as significant improvement compared to a previous study [16], which simply modelled the accumulative transport process as Michaelis-Menten kinetics and could not account for the thermodynamics limitations to substrate accumulation.

**The integrated compartmental modelling framework demonstrated the fundamental amino acid interactions and key factors regulating placental transfer**: Finally, an integrated model of the placental amino acid transport system was developed and examined in detail (Chapter 5). The model incorporated all the transporter models derived in the previous chapters into a three-compartment model of the placenta with four amino acid subgroups and flow inputs in the maternal and fetal compartments. The compartmental model behaviour was investigated in detail, starting from simple cases with transport across the BM and MVM separately, followed by the complete physiological configuration. The results confirmed that the model design and transporter configuration were adequately capable of fetal transfer of all

amino acids subgroups under physiological conditions. In addition, sensitivity analyses of the compartmental model parameters and conditions were performed (Section 5.3.4–5.3.6), which included transporter activities, blood flow rates, and amino acid levels. Importantly, this revealed that it is difficult to adjust levels of certain amino acid groups without affecting the transfer of others. This has clear implications for designing clinical intervention strategies to prevent unwanted side effects.

## 6.2 Recommendations for future work

Although the current integrated model framework was sufficient in representing the overall transport behaviour, it was implemented based on several simplifying assumptions. In particular, the amino acids were grouped together by their specificity for the various transporter types and each transporter type was modelled as a single representative transporter. For future studies, the model can be extended by including many individual transporters that can be distinguished for each transporter type, each of which is specific to certain overlapping subsets of amino acids, with different affinities [19]. Moreover, the transporter model parameters (*e.g.* asymmetry of translocation and binding parameters in the exchanger/facultative model) were configured to be relatively simple to reduce the number of parameters but still capture the fundamental transport mechanisms. However, as determined by our studies, to lift this restriction may not dramatically change the overall model behaviour, although this can be done readily in the future if model refinement is found necessary in the light of experimental data. For the accumulative model, future experiments to investigate specific transport protein should be carried out systematically to validate the cotransport model, as suggested in Appendix B. In addition, placental metabolism should be included in future models, which could potentially change the amount of amino acids and their composition. However, placental metabolism is still not well characterised and therefore this study was focused on transport alone in first instance. Another aspect that can be included further in the model was paracellular transport, which is poorly understood anatomically [105]. Paracellular diffusion will reduce the efficiency of the system because of high fetal amino acid levels, causing net diffusion in the fetal to maternal direction. Finally, the current compartmental model was for the placenta alone and did not include influences by the fetus. Hence, refinement of the model by considering variation in amino acid concentration inputs due to fetal metabolism could improve the response of the system.

## 6.3 Further model applications and prospects

The transport models developed for each type of transporters were applied to the transfer of amino acids across the placenta, but these carrier based models can also

be readily adapted to other substances in various epithelia. For instance, nutrient transport across brush border membranes in the intestine could be modelled as carrier based transport process [47, 48]. In another example, a recent study has suggested the use of carrier-mediated models to investigate the oral uptake of pharmaceuticals [114]. However, only simple Michaelis-Menten kinetics were used. The work stressed the importance of the model but requires further improvements in the kinetic parameter determination. It could be suggested that our transporter modelling approach can be applied instead, to potentially give a more comprehensive representation of transport phenomena, without necessarily needing more parameters. Furthermore, the integrated modelling framework – addressing the complex interactions between multiple species of amino acids and various transporters – will prove to be instrumental in determining the contribution of specific transporters to epithelial transport in the placenta and other systems. If successful, this can potentially lead to the design of targeted interventions in epithelial transport disorders. For example, strategies to target placenta to deliver pharmacological or genetic therapies are being explored [104]. The modelling approach could also be used to suggest clinical considerations in relation to epithelila transport. For instance, the model can test whether simply increasing certain maternal amino acid levels can improve fetal transfer, or determine rate-limiting factors in drug transport that are essential for pharmaceutical development process. To exemplify the potential applications of the model for representing pathological scenarios, the case of phenylketonuria was modelled, which demonstrated how elevated maternal phenylalanine restricted fetal delivery of all other amino acids (Section 5.3.8). Lastly, the detail of any newly discovered individual transporters, their kinetics and substrate specificity, can be readily included in the model framework in the future to study their role in the transport process as a whole.

## 6.4 Conclusion

In conclusion, the current body of work, which utilized computational modelling approaches to investigate the placental amino acid transport system, serves as an important effort towards a better understanding of complex placental functions. The systematic modelling approach adopted has proven to be highly valuable in both exploring fundamental transporter behaviours and designing and interpreting experiments to reveal inherent characteristics of specific transporter mechanisms. This is equally applicable to different transport systems in various epithelia, including kidney, liver and gut. In moving forward, this thesis reaffirms the importance of computational methods for designing experiments in biology to get optimal results. Finally, this work is ultimately hoped to be useful in facilitating clinical assessment, or the development of treatments or preventive measures for nutrition related fetal pathologies.

# Appendix A

# Effects of vesicle size distribution in amino acid uptake experiments

In a vesicle experiment, when considering a vesicle solution consisting of vesicles of all the same size, the mean effect of uptake must be the same as the uptake level in a single vesicle of the same size. However, this is not the case when considering a vesicle solution that is inconsistent in vesicle size. The weighted average of the substrate uptake can be computed according to the volume of the vesicles and their solute content could be computed as follows:

$$[A]_{AVG} = \frac{\sum_{j=1}^{n} vol_j \cdot [A]_j}{\sum_{j=1}^{n} vol_j} \tag{A.1}$$

where, $vol_j = \frac{4}{3}\pi \cdot r_j^3$. $[A]_{AVG}$ has unit of mol $l^{-1}$. $vol_j$ represents the spherical volume of the vesicle with radius $r_j$.

The weighted average for the concentration takes the ratio of the sum of the product of the each vesicle volume and its corresponding uptake concentration $[A]_j^{II}$, over the sum of the vesicle volumes. For each vesicle of radius $r$, the uptake concentration can be expressed in terms of surface area over volume and the flux per unit of area. The uptake concentration is directly proportional to the surface area of the vesicle, whereas for the volume it is inversely proportional.

For the uptake concentration in the facilitated diffusion model, the individual uptake of a single vesicle of size $r$ was given, for example, by the following:

$$[A]_j^{II} = \frac{area_j}{vol_j} \cdot \int \frac{Dx_T}{2} \left( \frac{[A]^I}{K + [A]^I} - \frac{[A]^{II}}{K + [A]^{II}} \right) dt \tag{A.2}$$

where, $vol_j = \frac{4}{3}\pi \cdot r_j^3$, $area_j = 4\pi \cdot r_j^2$.

An example simulation of the effects of weighted average in uptake concentration with inconsistent vesicle sizes is shown in Figure A.1. The figure shows the individual uptake curves for single vesicles of various sizes in solid and the weighted average of the uptake concentration in the dashed curve. Various radii for the vesicle size were evaluated, ranging from 1 to 5 in arbitrary units. A sample distribution of the number of vesicles for each radius was chosen as 100 for the case of $r = 1$, 10 for $r = 5$, and 1 for each of the rest. Parameters and the concentration of solute $A$ at side $I$ were kept constant at $[A]^I = 15$ and $K = 10$.

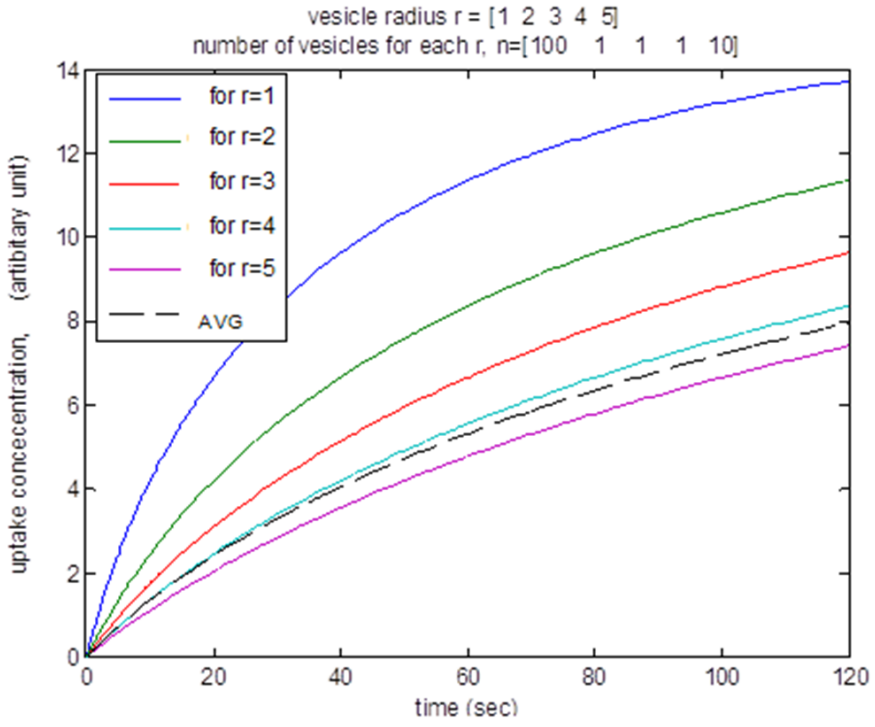


FIGURE A.1: Simulated uptake concentration curves with the effects of vesicle size variation.

Notice the average uptake curve was located between the uptake of the vesicles of radius sizes of 4 and 5, despite the much larger number of vesicles that had a radius of 1 ($n = 100$), compared to those with a radius of 5 ($n = 10$). Consequently, from the result it could be concluded that the larger-sized vesicles contribute to the weighted average uptake more significantly than smaller-sized vesicles, which yield a lesser effect. Additionally, the result showed that the smaller the vesicle size, the faster it was to react (*i.e.* faster uptake), as observable by the curves representing the uptake for each individual vesicle of the various sizes.

# Appendix B

# Accumulative transporter experiment; design and preliminary results

In this appendix, a validation of the accumulative transporter model by experimental procedures is presented. The design of the experimental procedures was aimed to observe the uptake of the substrate by the accumulative transporter over various electrical conditions and levels of sodium which is the co-solute in the coupled transport mechanism. Experiment procedures are planned to systemically investigate the isolated effects of the two driving forces of accumulative transporter; which are sodium concentration and potential difference created by the ions. In order observe the uptake response at various electro-potential difference levels, the 'voltage clamping' technique is employed to chemically set the membrane potential to the desired values [50]. The principle behind this was to use the ionophore valinomycin to increase the permeability of potassium ions, which in turn would dominate the membrane potential. Hence, the membrane potential is simply dependent only on the potassium ions, instead of all of the ions present.

Placental membrane vesicles are prepared with specific conditions so that the internal and external levels can represent two electro potential levels (one at physiological level, another at lower level) and two sodium gradient levels (at zero net gradient and at high net gradient). Additionally, the specifications of the experimental protocol are shown in Table B.1, listing the specific amounts of the ionic solutions in the buffers for the vesicle uptake. Note that the cell's osmolality in buffer solutions was carefully considered in protocol. In the experiments, various amount of potassium sulphate solution was added to achieve physiological (-17.6 mV) and lower (-2.7 mV) membrane potentials. For the zero net gradient cases, 10 mmol $l^{-1}$ sodium sulphate is added in both inside and outside of the vesicles netting in zero gradient in EXP 1 and 3, and 40 mmol $l^{-1}$ more was added

to the outside for the net sodium gradient of 80 mmol $l^{-1}$ in EXP 2 and 4.

In Figure B.1, the model predictions (a) and pilot experiment results (b) are presented for the uptake of substrate MeAIB (methylaminoisobutyric acid), which is a unique substrate for System A transport. The model prediction was based on the cotransport model from Table 4.1 under the negatively charged transporter assumption in Chapter 4. Note that following constants and parameter values were used in the model simulations: ideal gas constant, $R = 8.314$ VC $K^{-1}$ $mol^{-1}$, room temperature, $T = 298$ K, Faraday's constant, $F = 9.65$ x $10^4$ C $mol^{-1}$, electrical bias term, $\beta = 0.5$, and dissociation constants of substrate and sodium of 100 $\mu$mol $l^{-1}$ and 10 mmol $l^{-1}$, respectively, with total transport rates of 10 (arbitrary unit). For the experimental pilot results ($n = 1$) in Figure B.1b, 165 $\mu$mol $l^{-1}$ $C^{14}$-labelled MeAIB was used to observe the uptake into the vesicles over time. The model simulated logical predictions showing distinct uptake levels for each of the experimental conditions. For the control, the model showed no uptake as sodium is required for cotransport. However, low uptake was shown in the experiment suggesting leakage. For zero net gradient (equal sodium internally and externally), the model predicted uptake at physiological transmembrane potential (EXP 1) to be higher than for the low transmembrane potential (EXP 3), which corresponded to the experimental results, although the difference was very small. However, when the chemical driving force by sodium gradient was high, the model logically predicted higher uptake in the case of physiological transmembrane potential (EXP 2a) than the case of low transmembrane potential (EXP 4), which is opposite to the experimental results. These counterintuitive experimental results may be caused by experimental error or leakage. Lastly, a higher uptake level was observed for the case when the external substrate level was increased three-fold higher (EXP 2b) than normal (EXP 2a), which is correctly predicted by the model.

In conclusion, while this study served as a functional preliminary experimental approach in the investigating of the accumulative transport mechanism, further experimental procedures must be carefully carried out in future studies, since there are many factors that can contribute to error in the uptake results. It was shown that the cotransport model can provide a quantitative understanding of the accumulative transport mechanism.

TABLE B.1: Proposed experimental protocol for investigating sodium-dependent accumulative transporter.

| $Na^+$=0 | | | Zero net $Na^+$ gradient | | | High $Na^+$ gradient | | |
|---|---|---|---|---|---|---|---|---|
| **Physiological transmembrane potential** | | | | | | | | |
| **Control** | **Transmembrane potential (mV)** | **-17.6** | **EXP 1** | **Transmembrane potential (mV)** | **-17.6** | **EXP 2a, 2b*** | **Transmembrane potential (mV)** | **-17.6** |
| | **Net $Na^+$ gradient (mmol $l^{-1}$)** | **0** | | **Net $Na^+$ gradient (mmol $l^{-1}$)** | **0** | | **Net $Na^+$ gradient (mmol $l^{-1}$)** | **80** |
| **EVB** | $K_2SO_4$ (mmol $l^{-1}$) | 25 | **EVB** | $K_2SO_4$ (mmol $l^{-1}$) | 25 | **EVB** | $K_2SO_4$ (mmol $l^{-1}$) | 25 |
| | $Na_2SO_4$ (mmol $l^{-1}$) | 0 | | $Na_2SO_4$ (mmol $l^{-1}$) | 10 | | $Na_2SO_4$ (mmol $l^{-1}$) | 50 |
| | Sucrose (mmol $l^{-1}$) | 215 | | Sucrose (mmol $l^{-1}$) | 185 | | Sucrose (mmol $l^{-1}$) | 65 |
| **IVB** | $K_2SO_4$ (mmol $l^{-1}$) | 50 | **IVB** | $K_2SO_4$ (mmol $l^{-1}$) | 50 | **IVB** | $K_2SO_4$ (mmol $l^{-1}$) | 50 |
| | $Na_2SO_4$ (mmol $l^{-1}$) | 0 | | $Na_2SO_4$ (mmol $l^{-1}$) | 10 | | $Na_2SO_4$ (mmol $l^{-1}$) | 10 |
| | Sucrose (mmol $l^{-1}$) | 140 | | Sucrose (mmol $l^{-1}$) | 110 | | Sucrose (mmol $l^{-1}$) | 110 |
| **Low transmembrane potential** | | | | | | | | |
| | | | **EXP 3** | **Transmembrane potential (mV)** | **-2.7** | **EXP 4** | **Transmembrane potential (mV)** | **-2.7** |
| | | | | **Net $Na^+$ gradient (mmol $l^{-1}$)** | **0** | | **Net $Na^+$ gradient (mmol $l^{-1}$)** | **80** |
| | | | **EVB** | $K_2SO_4$ (mmol $l^{-1}$) | 45 | **EVB** | $K_2SO_4$ (mmol $l^{-1}$) | 45 |
| | | | | $Na_2SO_4$ (mmol $l^{-1}$) | 10 | | $Na_2SO_4$ (mmol $l^{-1}$) | 50 |
| | | | | Sucrose (mmol $l^{-1}$) | 125 | | Sucrose (mmol $l^{-1}$) | 5 |
| | | | **IVB** | $K_2SO_4$ (mmol $l^{-1}$) | 50 | **IVB** | $K_2SO_4$(mmol $l^{-1}$) | 50 |
| | | | | $Na_2SO_4$ (mmol $l^{-1}$) | 10 | | $Na_2SO_4$ (mmol $l^{-1}$) | 10 |
| | | | | Sucrose (mmol $l^{-1}$) | 110 | | Sucrose (mmol $l^{-1}$) | 110 |

*2a, 2b have the same $Na^+$ and electrical conditions but 2b has a 3 fold higher substrate tracer level
EVB – extra-vesicular buffer, IVB – intra-vesicular buffer
Note that 10 mmol $l^{-1}$ of Hepes and Tris are added in all cases and 4 $\mu$mol $l^{-1}$ valinomycin in preincubated in the vesicle suspension.

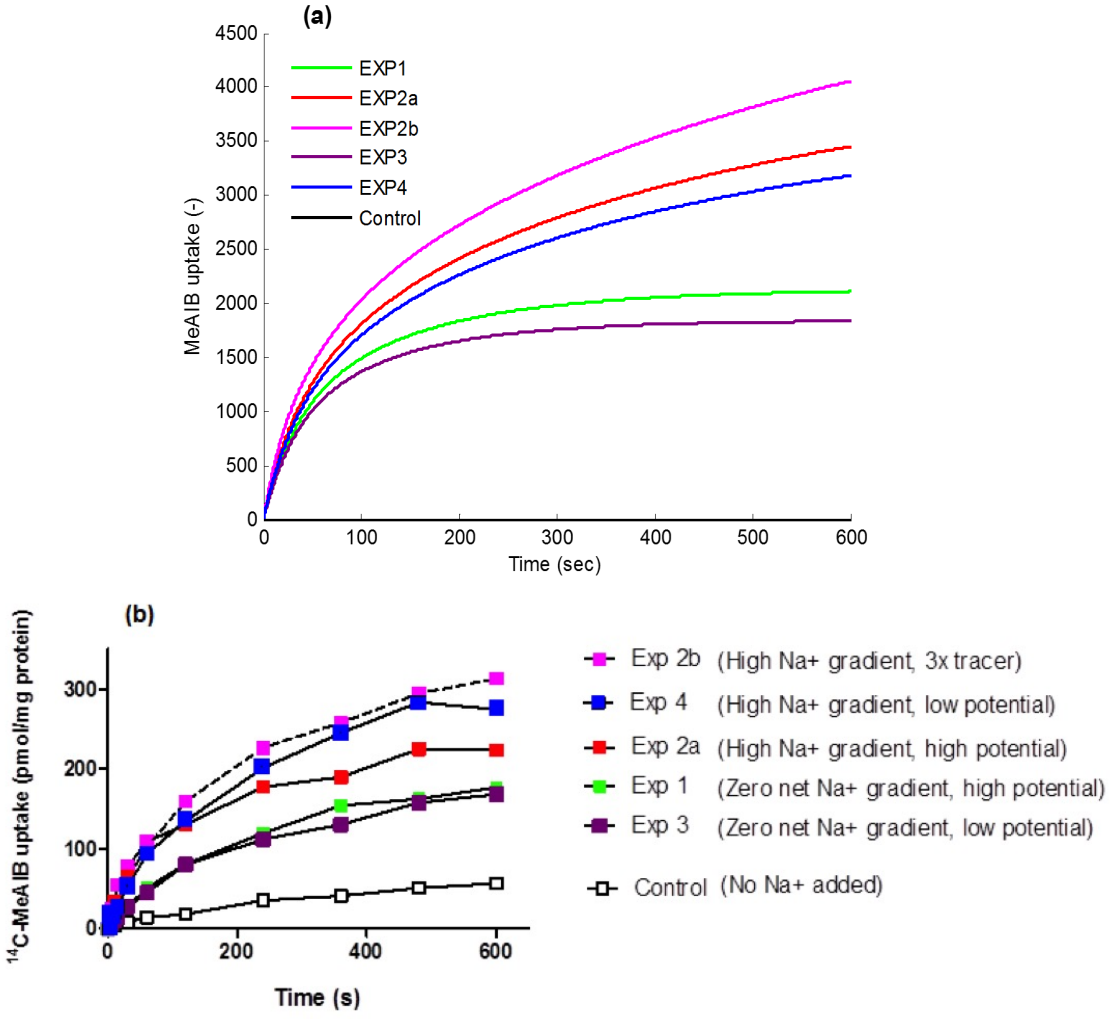


FIGURE B.1: Cotransport model predictions (a) and pilot vesicle experimental results (b) for the uptake of substrate MeAIB by the accumulative transport mechanism. Vesicle experiments were carried out by Dr. Kate Widdows at Institute of Human Development, University of Manchester.

# Appendix C

# Integrated model simulation of placental amino acid transport system: Alternate accumulative transporter model results

In this appendix, additional compartmental model simulations are presented. The compartmental model implemented accumulative transporter model, which assumed the transporter to be negatively charged. The results are shown in the same manner as explored in Chapter 5, which assumed the accumulative transporter to be neutrally charged. Overall, only minor transient variations are observed, especially when complete integrated model were concerned. The compartmental model appeared to be reaching the steady state value faster than the results in Chapter 5. In general, the compartmental model simulated the same characteristic behaviour as the other assumption.

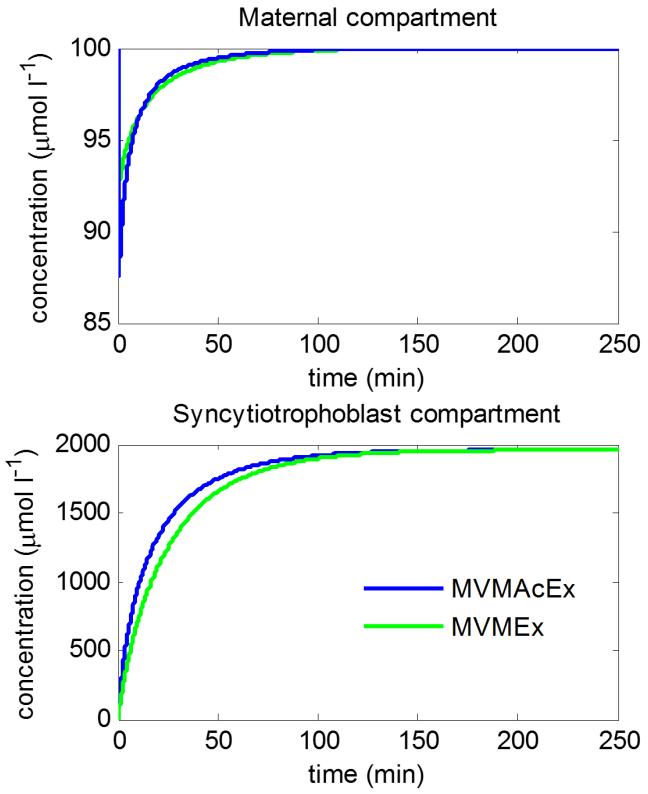


FIGURE C.1: Syncytiotrophoblast amino acid concentrations for the simplified model simulations of transport across the MVM with conditions from Table 5.6. The concentrations of amino acid group MVMAcEx and MVMEx in the maternal vein and placental syncytiotrophoblast layer were simulated using the compartmental model in Figure 5.1. (Accumulative transporter assumed negatively charged).

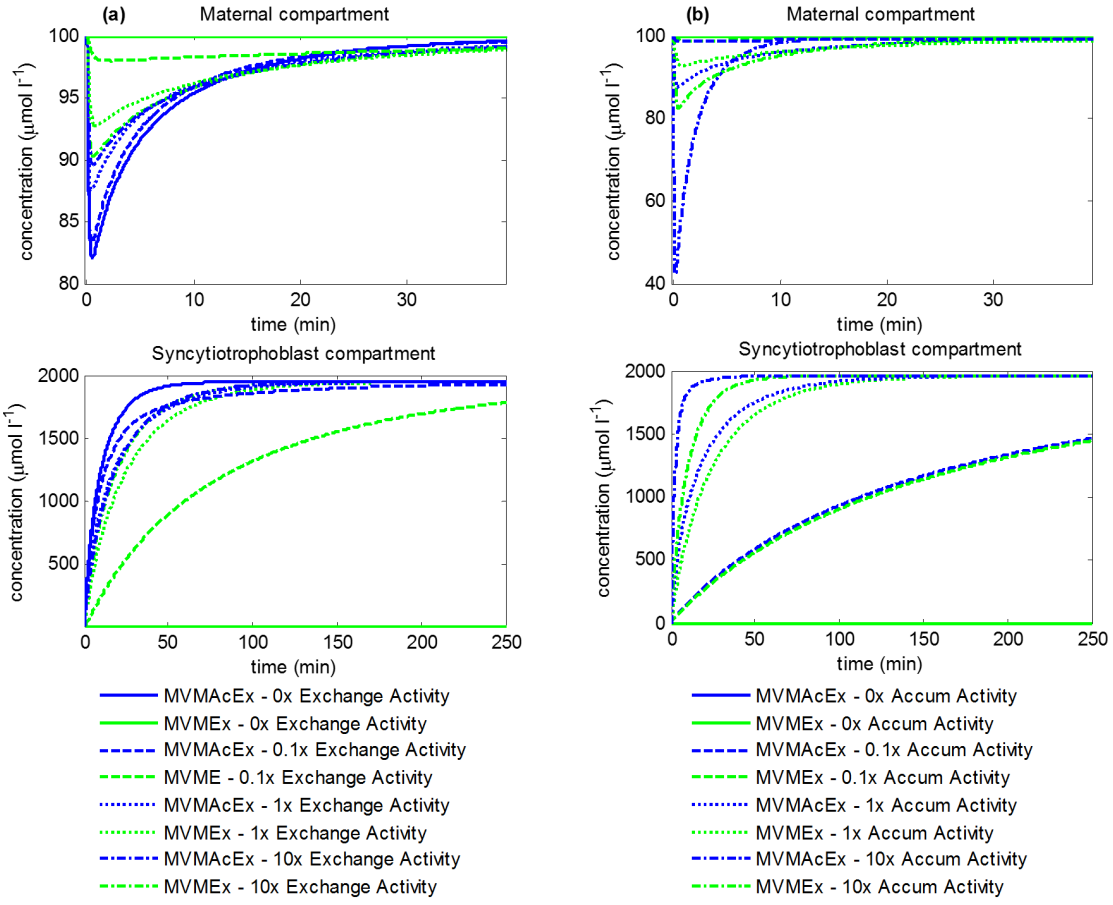


FIGURE C.2: Model simulation of the effects of variation in transporter activity. The model shows each amino acid concentrations in the maternal and syncytiotrophoblast compartment for the interactions across the MVM with input conditions given in Table 5.6 over a range of relative (a) exchange or (b) accumulative transport activities. (Accumulative transporter assumed negatively charged).

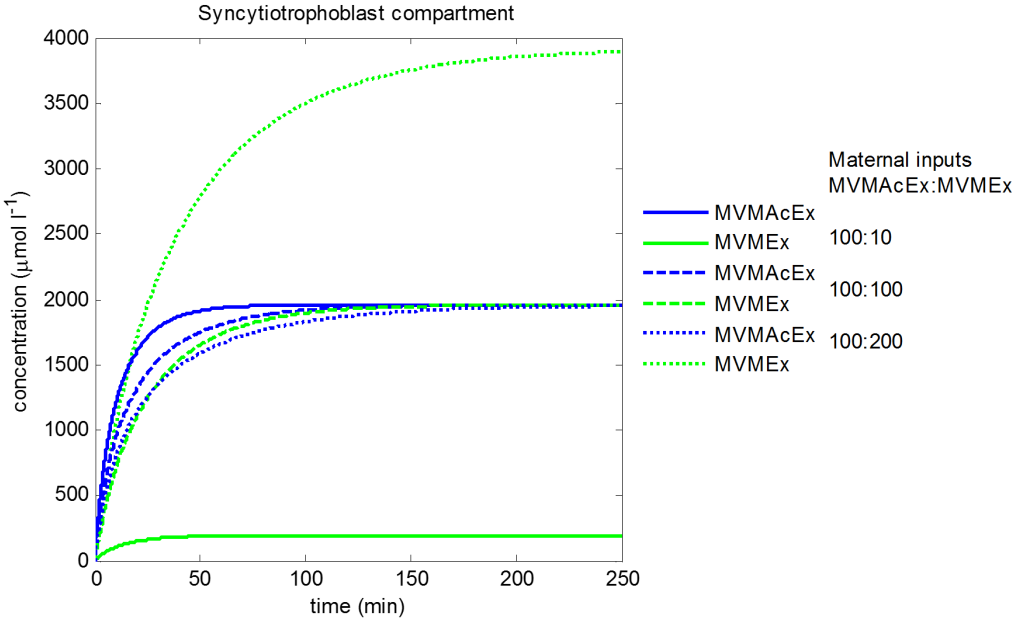


FIGURE C.3: Model simulations showing the effects of various amino acid concentration levels on transport interactions across the MVM: The compartmental model simulated syncytiotrophoblast concentrations with various input conditions as given in Table 5.7. (Accumulative transporter assumed negatively charged).

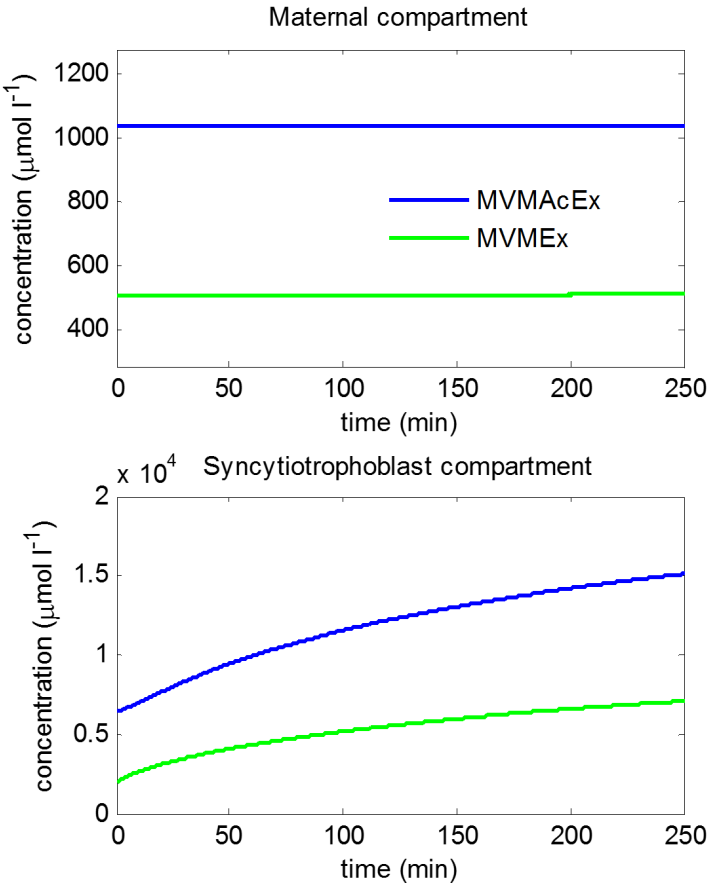


FIGURE C.4: Physiological model simulations of transport interactions across the MVM: The amino acid concentrations in the maternal vein and placental syncytiotrophoblast layer were simulated using the compartmental model with input conditions given in Table 5.8. (Accumulative transporter assumed negatively charged).

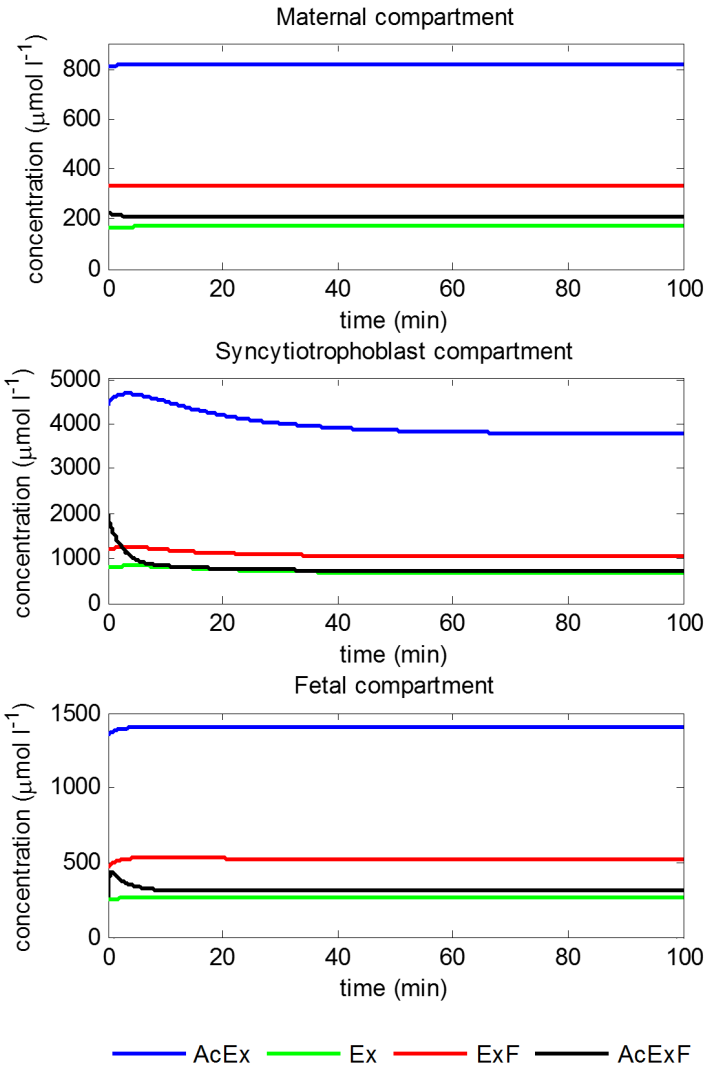


FIGURE C.5: Compartmental model simulations of physiological amino acid levels in each compartment with steady state levels reported in Table 5.10. (Accumulative transporter assumed negatively charged).

TABLE C.1: Model simulated amino acid concentrations at steady state for each group including the ratios as a fraction of total amino acid in each compartment. (Accumulative transporter assumed negatively charged).

| Concentration, $\mu$mol $l^{-1}$ (ratio of total) | Maternal | Syncytiotrophoblast | Fetal |
|---|---|---|---|
| **AcEx** | **822** | **3790** | **1408** |
| | (0.54) | (0.61) | (0.56) |
| **Ex** | **170** | **665** | **261** |
| | (0.11) | (0.11) | (0.10) |
| **ExF** | **334** | **1026** | **523** |
| | (0.22) | (0.17) | (0.21) |
| **AcExF** | **208** | **710** | **308** |
| | (0.14) | (0.11) | (0.12) |

TABLE C.2: Comparison of net fetal transfer levels at steady state of each amino acid group for baseline simulated results, umbilical venous-artery difference as reported by the literature, and generated by model fitting of transporter activities. (Accumulative transporter assumed negatively charged).

| Amino acid group | Baseline simulation ($\mu$mol $l^{-1}$) | Literature value ($\mu$mol $l^{-1}$) | Fitting* ($\mu$mol $l^{-1}$) |
|---|---|---|---|
| **AcEx** | **39** | **55** | **50** |
| **Ex** | **2.5** | **12** | **8.5** |
| **ExF** | **40** | **40** | **33** |
| **AcExF** | **69.5** | **44** | **69** |

*Note that model fitting suggested the following transporter activities with respect to the baseline values: 3x exchange at MVM, 43x Exchange at BM, 1.6x facilitative, and 0.7x accumulative activity

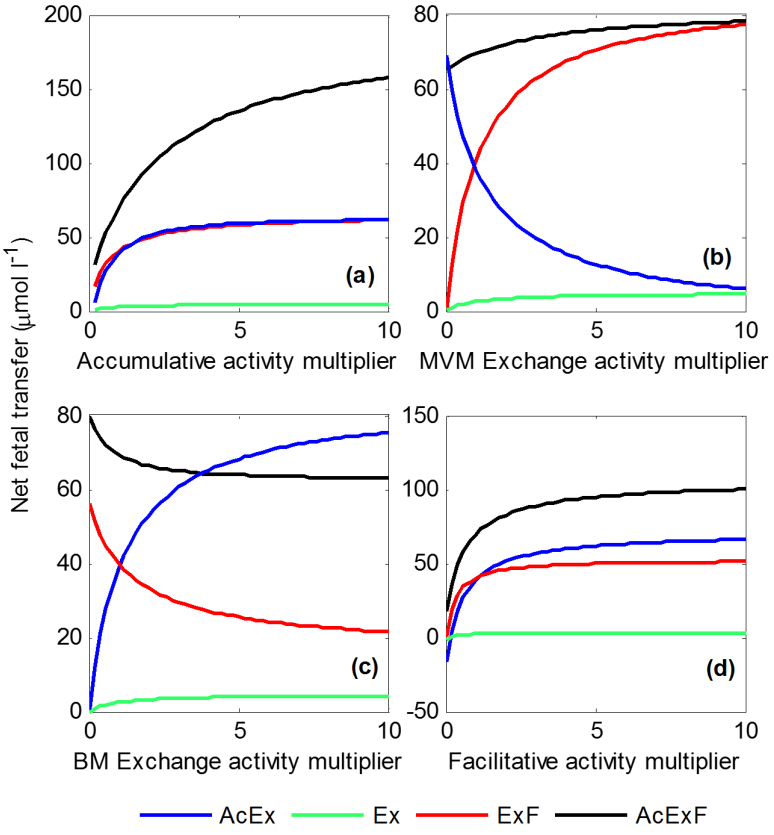


FIGURE C.6: Transporter activity sensitivity analysis: Net fetal transfer values for each amino acid were simulated in response to a range of variations in individual transporter activity. (Accumulative transporter assumed negatively charged).

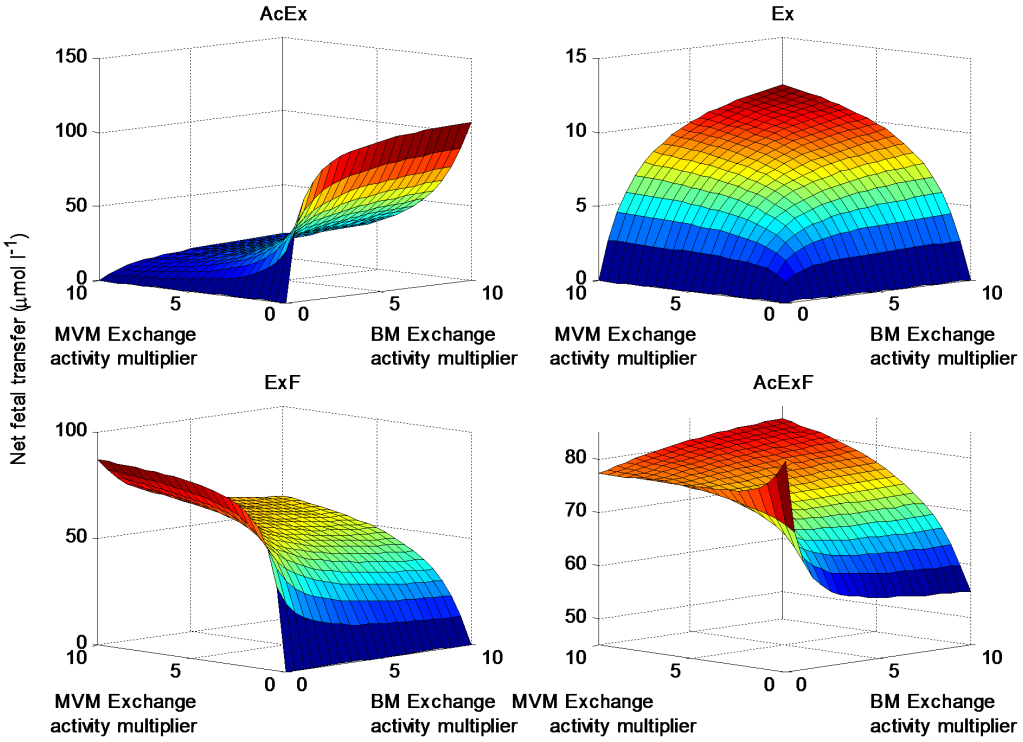


FIGURE C.7: Dual transport activity sensitivity analysis: MVM *vs* BM exchange activity. Net fetal transfer values for each amino acid were simulated in response to varying the exchange activities at the MVM and BM simultaneously. (Accumulative transporter assumed negatively charged).

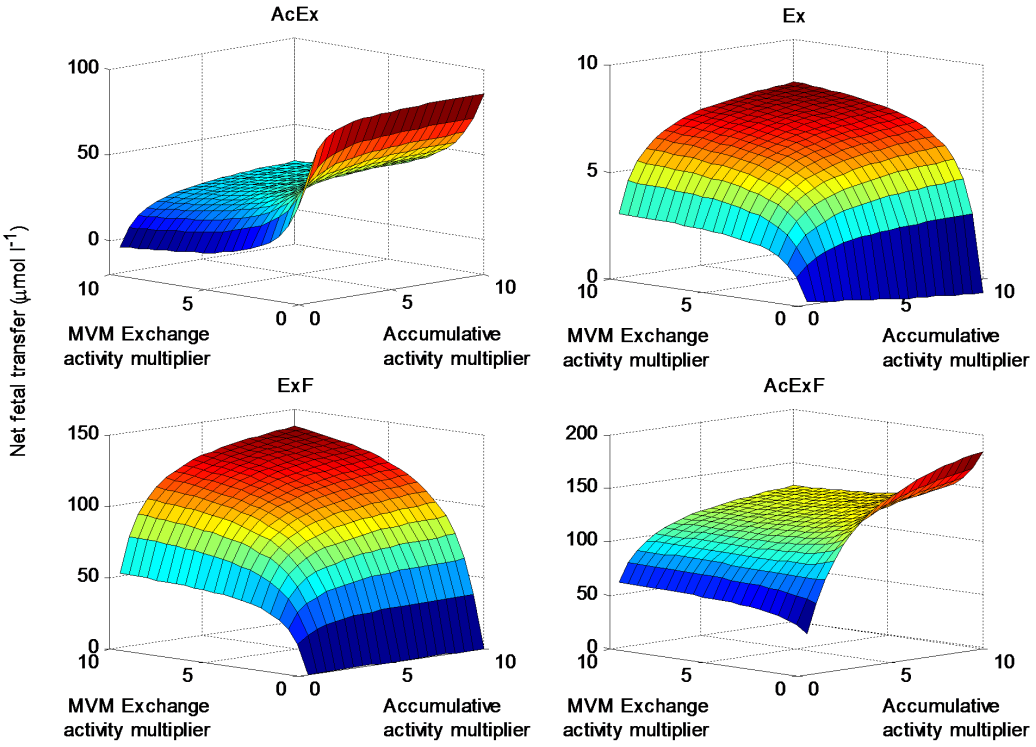


FIGURE C.8: Dual transport activity sensitivity analysis at the MVM. Net fetal transfer values for each amino acid were simulated in response to varying the MVM exchange and accumulative transport activities simultaneously. (Accumulative transporter assumed negatively charged).

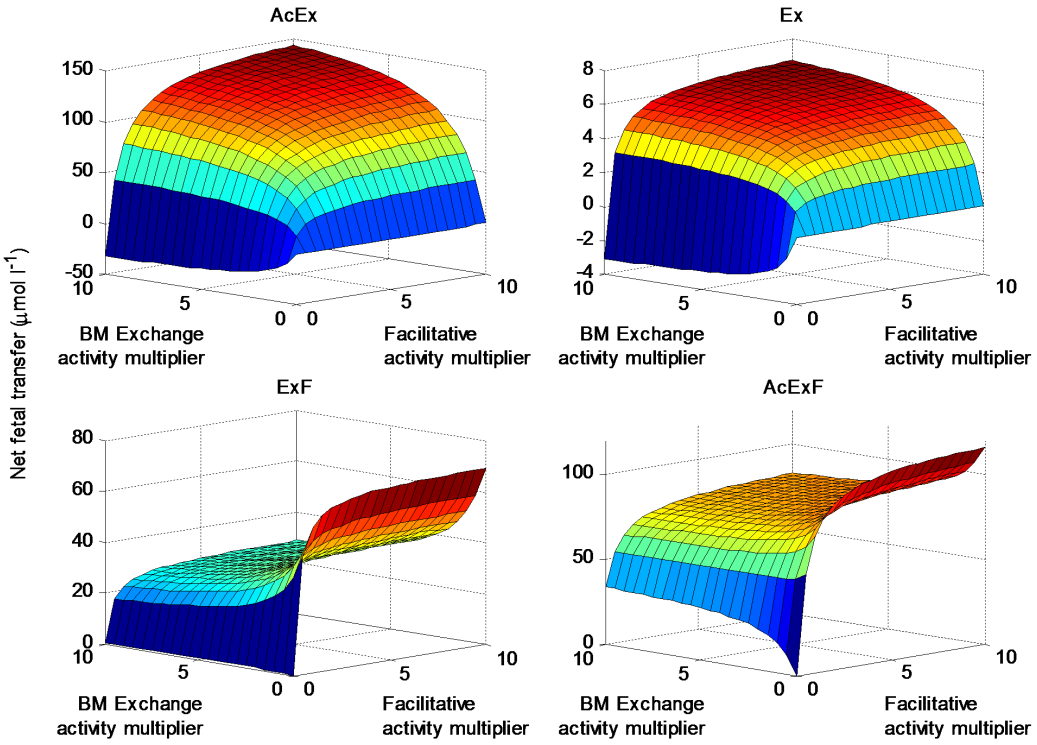


FIGURE C.9: Dual transport activity sensitivity analysis at the BM. Net fetal transfer values for each amino acid were simulated in response to varying the BM exchange and facilitative transport activities simultaneously. (Accumulative transporter assumed negatively charged).

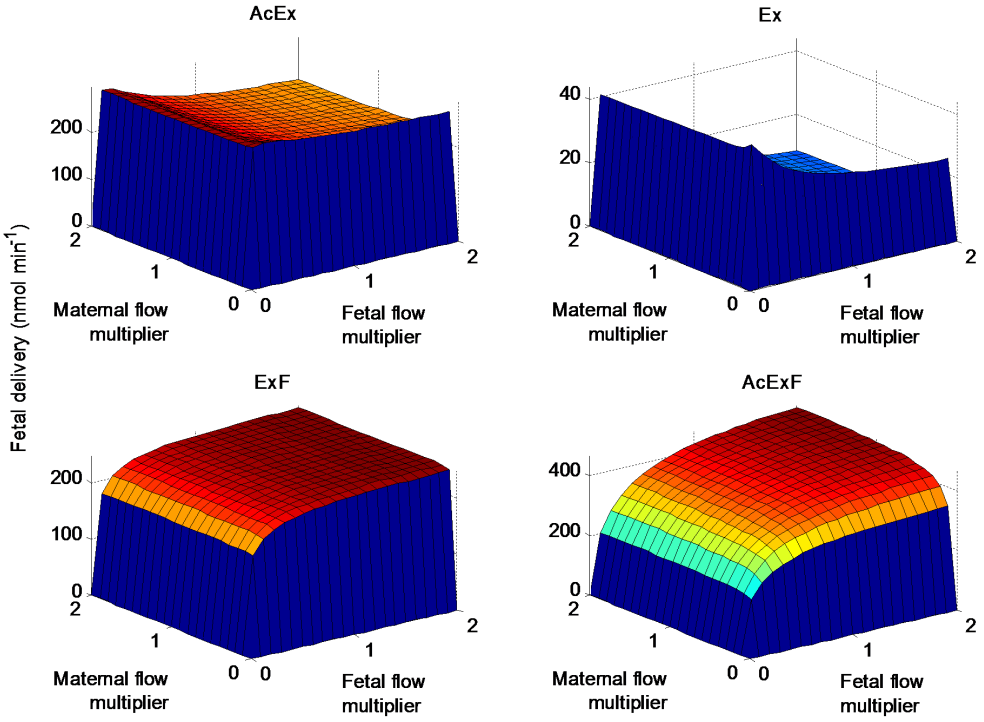


FIGURE C.10: Flow sensitivity analysis: Net fetal transfer values for each amino acid were simulated in response to varying the maternal and fetal flow inputs simultaneously. (Accumulative transporter assumed negatively charged).

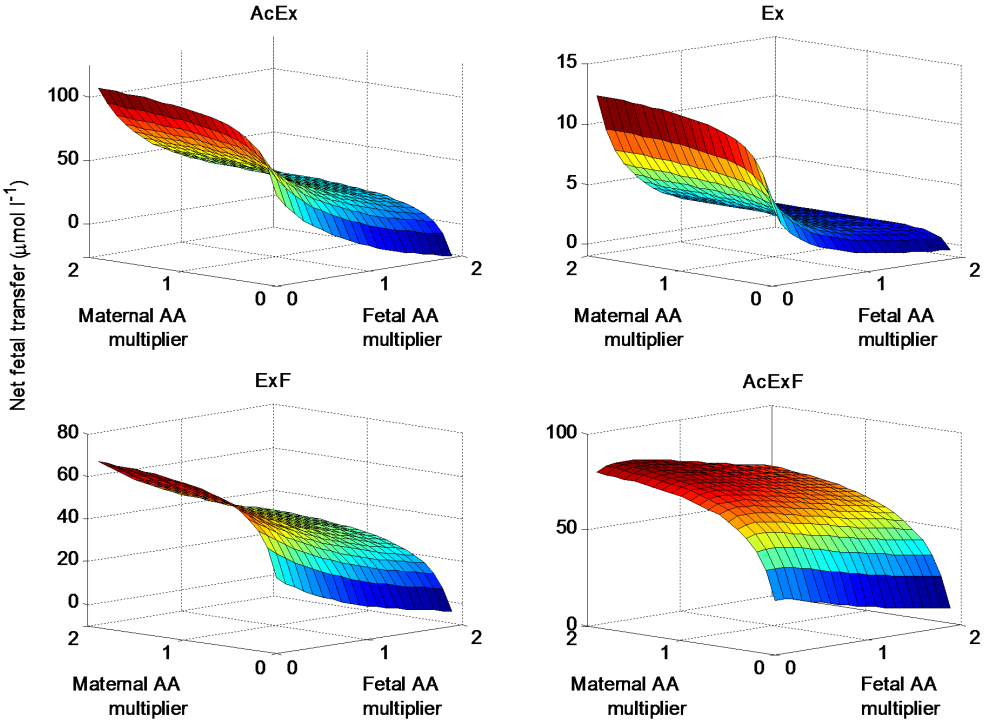


FIGURE C.11: Amino acid level sensitivity analysis: Net fetal transfer values for each amino acid were simulated in response to varying the overall maternal and fetal amino acid concentration levels simultaneously. (Accumulative transporter assumed negatively charged).

# Bibliography


[1] Sibley CP, Turner MA, Cetin I, Ayuk P, Boyd CAR, and D′Souza SW. Placental phenotypes of intrauterine growth. *Pediatric Research*, 58:827–832, 2005.

[2] Sibley C, Glazier J, and D′Souza S. Placental transporter activity and expression in relation to fetal growth. *Experimental Physiology*, 82:389–402, 1997.

[3] Johansson M, Karlsson L, Wennergren M, Jansson T, and Powell TL. Activity and protein expression of $Na^+/K^+$ ATPase are reduced in microvillous syncytiotrophoblast plasma membranes isolated from pregnancies complicated by intrauterine growth restriction. *Journal of Clinical Endocrinology and Metabolism*, 88:2831–2837, 2003.

[4] Jansson T and Powell TL. Role of the placenta in fetal programming: Underlying mechanisms and potential interventional approaches. *Clinical Science*, 113:1–13, 2007.

[5] Lewis RM, Brooks S, Crocker IP, Glazier J, Hanson MA, Johnstone ED, Panitchob N, Please CP, Sibley CP, Widdows KL, and Sengers BG. Review: Modelling placental amino acid transfer – From transporters to placental function. *Placenta*, 34:S46–S51, 2013.

[6] Cleal JK and Lewis RM. The mechanisms and regulation of placental amino acid transport to the human foetus. *Journal of Neuroendocrinology*, 20:419–426, 2008.

[7] Benirschke K, Kaufmann P, and Baergen RN. *Pathology of the Human Placenta, 5th edition.* Springer, 2006.

[8] Leiser R and Kaufmann P. Placental structure: in a comparative aspect. *Experimental and Clinical Endocrinology*, 102:122–134, 1994.

[9] Gray H and Lewis WH. *Anatomy of the Human Body.* Lea & Febiger, Philadelphia PA, USA, 1918.

[10] Brownbill P, Mahendran D, Owen D, Swanson P, Thornburg KL, Nelson DM, and Sibley CP. Denudations as paracellular routes for alphafetoprotein and creatinine across the human syncytiotrophoblast. *American Journal of Physiology. Regulatory Integrative and Comparative Physiology*, 278:R677–R683, 2000.

[11] Edwards D, Jones CJP, Sibley CP, and Nelson DM. Paracellular permeability pathways in the human placenta: A quantitative and morphological study of maternal-fetal transfer of horseradish peroxidase. *Placenta*, 14:63–73, 1993.

[12] Bröer S. Adaptation of plasma membrane amino acid transport mechanisms to physiological demands. *Pflügers Archiv – European Journal of Physiology*, 444: 457–466, 2002.

[13] Babu E, Kanai Y, Chairoungdua A, Kim DK, Iribe Y, Tangtrongsup S, Jutabha P, Li Y, Ahmed N, Sakamoto S, Anzai N, Nagamori S, and Endou H. Identification of a novel system L amino acid transporter structurally distinct from heterodimeric amino acid transporters. *Journal of Biological Chemistry*, 278:43838–43845, 2003.

[14] Bodoy S, Martín L, Zorzano A, Palacín M, Estévez R, and Bertran J. Identification of LAT4, a novel amino acid transporter with system L activity. *Journal of Biological Chemistry*, 280:12002–12011, 2005.

[15] Rosell A, Meury M, Álvarez-Marimon E, Costa M, Pérez-Cano L, Zorzano A, Fernández-Recio J, Palacín M, and Fotiadis D. Structural bases for the interaction and stabilization of the human amino acid transporter LAT2 with its ancillary protein 4F2hc. *Proceedings of the National Academy of Sciences*, 111:2966–2971, 2014.

[16] Sengers BG, Please CP, and Lewis RM. Computational modelling of amino acid transfer interactions in the placenta. *Experimental Physiology*, 95:829–840, 2010.

[17] Souba WW and Pacitti AJ. Review: How amino acids get into cells: Mechanisms, models, menus, and mediators. *Journal of Parenteral and Enteral Nutrition*, 16: 569–578, 1992.

[18] Cleal JK, Brownbill P, Godfrey KM, Jackson JM, Jackson AA, Sibley CP, Hanson MA, and Lewis RM. Modification of fetal plasma amino acid composition by placental amino acid exchangers *in vitro*. *The Journal of Physiology*, 582:871–882, 2007.

[19] Bröer S. Amino acid transport across mammalian intestinal and renal epithelia. *Physiological Reviews*, 88:249–286, 2008.

[20] Ringler GE and Strauss JF III. *In vitro* systems for the study of human placental endocrine function. *Endocrine Reviews*, 11:105–123, 1990.

[21] Patterson BK, Behbahani H, Kabat WJ, O′Gorman MR Sullivan Y, Landay A, Flener Z, Khan N, Yogev R, and Andersson J. Leukemia inhibitory factor inhibits HIV-1 replication and is upregulated in placentae from nontransmitting women. *The Journal of Clinical Investigation*, 107:287–294, 2001.

[22] Barut F, Barut A, Gun BD, Kandemir NO, Harma MI, Harma M, Aktunc E, and Ozdamar SO. Intrauterine growth restriction and placental angiogenesis. *Diagnostic Pathology*, 5:24, 2010.

[23] Almasry SM and Elfayomy AK. Morphometric analysis of terminal villi and gross morphological changes in the placentae of term idiopathic intrauterine growth restriction. *Tissue and Cell*, 44:214–219, 2012.

[24] Mayhew TM, Ohadike C, Baker PN, Crocker IP, Mitchell C, and Ong SS. Stereological investigation of placental morphology in pregnancies complicated by pre-eclampsia with and without intrauterine growth restriction. *Placenta*, 24:219–226, 2003.

[25] Mayhew TM, Charnock-Jones DS, and Kaufmann P. Aspects of human fetoplacental vasculogenesis and angiogenesis. III. Changes in complicated pregnancies. *Placenta*, 25:127–139, 2004.

[26] Nelson SM, Coan PM, Burton GJ, and Lindsay RS. Placental structure in type 1 diabetes: Relation to fetal insulin, leptin, and IGF-I. *Diabetes*, 58:2634–2641, 2009.

[27] Mayhew TM and Burton GJ. Stereology and its impact on our understanding of human placental functional morphology. *Microscopy Research and Technique*, 38: 195–205, 1997.

[28] Bermúdez C, Becerra CH, Bornick PW, Allen MH, Arroyo J, and Quintero RA. Placental types and twin-twin transfusion syndrome. *American Journal of Obstetrics and Gynecology*, 187:489–494, 2002.

[29] Viscardi RM, Tyahla ER, and Sun C-CJ. The relationship of placental pathology to IUGR. *Pediatric Research*, 39:251–251, 1996.

[30] Jauniaux E and Burton GJ. Villous histomorphometry and placental bed biopsy investigation in type I diabetic pregnancies. *Placenta*, 27:468–474, 2006.

[31] Resta L, Capobianco C, Marzullo A, Piscitelli D, Sanguedolce F, Schena FP, and Gesualdo L. Confocal laser scanning microscope study of terminal villi vessels in normal term and pre-eclamptic placentas. *Placenta*, 27:735–739, 2006.

[32] Bajoria R, Wigglesworth J, and Fisk NM. Angioarchitecture of monochorionic placentas in relation to the twin-twin transfusion syndrome. *American Journal of Obstetrics and Gynecology*, 172:856–863, 1995.

[33] Jansson T, Scholtbach V, and Powell TL. Placental transport of leucine and lysine is reduced in intrauterine growth restriction. *Pediatric Research*, 44:532–537, 1998.

[34] Jansson T, Ylven K, Wennergren M, and Powell TL. Glucose transport and system A activity in syncytiotrophoblast microvillous and basal plasma membranes in intrauterine growth restriction. *Placenta*, 23:392–399, 2002.

[35] Glazier JD, Cetin I, Perugino G, Ronzoni S, Grey AM, Mahendran D, Marconi AM, Pardi G, and Sibley CP. Association between the activity of the system a amino acid transporter in the microvillous plasma membrane of the human placenta and severity of fetal compromise in intrauterine growth restriction. *Pediatric Research*, 42:514–519, 1997.

[36] Jansson T, Wennergren M, and Powell TL. Placental glucose transport and GLUT 1 expression in insulin-dependent diabetes. *American Journal of Obstetrics and Gynecology*, 180:163–168, 1999.

[37] Jansson T, Ekstrand Y, Björn C, Wennergren M, and Powell TL. Alterations in the activity of placental amino acid transporters in pregnancies complicated by diabetes. *Diabetes*, 51:2214–2219, 2002.

[38] Hutson JR, Garcia-Bournissen F, Davis A, and Koren G. The human placental perfusion model: A systematic review and development of a model to predict *In vivo* transfer of therapeutic drugs. *Clinical Pharmacology and Therapeutics*, 90: 67–76, 2011.

[39] Lewis RM, Glazier J, Greenwood SL, Bennett EJ, Godfrey KM, Jackson AA, Sibley CP, Cameron IT, and Hanson MA. L-serine uptake by human placental microvillous membrane vesicles. *Placenta*, 28:445–452, 2007.

[40] Brand AP, Greenwood SL, Glazier JD, Bennett EJ, Godfrey KM, Sibley CP, Hanson MA, and Lewis RM. Comparison of L-serine uptake by human placental microvillous membrane vesicles and placental villous fragments. *Placenta*, 31:456–459, 2010.

[41] Glazier JD and Sibley CP. *In vitro* methods for studying human placental amino acid transport: Placental plasma membrane vesicles. *Methods in Molecular Medicine*, 122:241–252, 2006.

[42] Chernyavsky IL, Jensen OE, and Leach L. A mathematical model of intervillous blood flow in the human placentone. *Placenta*, 31:44–52, 2010.

[43] Hennemann G, Docter R, Friesema EC, de Jong M, Krenning EP, and Visser TJ. Plasma membrane transport of thyroid hormones and its role in thyroid hormone metabolism and bioavailability. *Endocrine Reviews*, 22:451–476, 2001.

[44] Mitchell AM, Manley SW, Rowan KA, and Mortimer RH. Uptake of reverse T3 in the human choriocarcinoma cell line, JAr. *Placenta*, 20:65–70, 1999.

[45] Higgins CF and Linton KJ. The ATP switch model for ABC transporters. *Nature Structural and Molecular Biology*, 11:918–926, 2004.

[46] Staud F, Vackova Z, Pospechova K, Pavek P, Ceckova M, Libra A, Cygalova L, Nachtigal P, and Fendrich Z. Expression and transport activity of breast cancer resistance protein (BCRP/ABCG2) in dually perfused rat placenta and HRP-1 cell line. *Journal of Pharmacology and Experimental Therapeutics*, 319:53–62, 2006.

[47] Babcock AK, Garvey TQ, and Berman M. A mathematical model for membrane transport of amino acid and $Na^+$ in vesicles. *Journal of Membrane Biology*, 49: 157–169, 1979.

[48] Weiss SD, McNamara PD, and Segal S. Uptake of proline by renal brushborder vesicles: A mathematical analysis. *Journal of Theoretical Biology*, 93:597–608, 1981.

[49] Devés R and Krupka RM. A general kinetic analysis of transport tests of the carrier model based on predicted relations among experimental parameters. *Biochimica et Biophysica Acta (BBA) – Biomembranes*, 556:533–547, 1979.

[50] Turner RJ. Quantitative studies of cotransport system: Models and vesicles. *Journal of Membrane Biology*, 76:1–15, 1983.

[51] Kolber AR and LeFevre PG. Evidence for carrier-mediated transport of monosaccharides in the Ehrlich ascites tumor cell. *Journal of General Physiology*, 50:1907–1928, 1967.

[52] Burton GJ. The fine structure of the human placental villus as revealed by scanning electron microscopy. *Scanning Microscopy*, 1:1811–1828, 1987.

[53] Gong SP, Zhao YT, and Yu YH. Vascular network modeling reveals significant differences in vascular morphology in growth-restricted placentas. *Reviews in Obstetrics and Gynecology*, 4:103–108, 2011.

[54] Erian FF, Corrsin S, and Davis SH. Maternal, placental blood flow: A model with velocity-dependent permeability. *Journal of Biomechanics*, 10:807–814, 1977.

[55] Serov AS, Salafia CM, Brownbill P, Grebenkov DS, and Filoche M. Optimal villi density for maximal oxygen uptake in the human placenta. *Journal of Theoretical Biology*, 364:383–396, 2015.

[56] Serov AS, Salafia CM, Filoche M, and Grebenkov DS. Analytical theory of oxygen transport in the human placenta. *Journal of Theoretical Biology*, 368:133–144, 2015.

[57] Gill JS, Salafia CM, Grebenkov D, and Vvedensky DD. Modeling oxygen transport in human placental terminal villi. *Journal of Theoretical Biology*, 291:33–41, 2011.

[58] Desforges M and Sibley CP. Placental nutrient supply and fetal growth. *The International Journal of Developmental Biology*, 54:377–390, 2010.

[59] Faber JJ. Review of flow limited transfer in the placenta. *International Journal of Obstetric Anesthesia*, 4:230–237, 1995.

[60] Lardner TJ. A model for placental oxygen exchange. *Journal of Biomechanics*, 8: 131–134, 1975.

[61] Costa A, Costantino ML, and Fumero R. Oxygen exchange mechanisms in the human placenta: Mathematical modelling and simulation. *Journal of Biomedical Engineering*, 14:385–389, 1992.

[62] Curran PF, Schultz SG, Chez RA, and Fuisz RE. Kinetic relations of the Na-amino acid interaction at the mucosal border of intestine. *Journal of General Physiology*, 50:1261–1286, 1967.

[63] Stein WD and Lieb WR. *Transport and diffusion across cell membranes*. Academic Press, San Diego CA, USA, 1986.

[64] Parent L, Supplisson S, Loo DD, and Wright EM. Electrogenic properties of the cloned $Na^+$/glucose cotransporter: II. A transport model under nonrapid equilibrium conditions. *Journal of Membrane Biology*, 125:63–79, 1992.

[65] Barta E and Drugan A. Glucose transport from mother to fetus – a theoretical study. *Journal of Theoretical Biology*, 263:295–302, 2010.

[66] Meier C, Ristic Z, Klauser S, and Verrey F. Activation of system L heterodimeric amino acid exchangers by intracellular substrates. *The EMBO Journal*, 21:580–589, 2002.

[67] Segawa H, Fukasawa Y, Miyamoto K-i, Takeda E, Endou H, and Kanai Y. Identification and functional characterization of a $Na^+$-independent neutral amino acid transporter with broad substrate selectivity. *The Journal of Biological Chemistry*, 274:19745–19751, 1999.

[68] Jansson N, Pettersson J, Haafiz A, Ericsson A, Palmberg I, Tranberg M, Ganapathy V, Powell TL, and Jansson T. Down-regulation of placental transport of amino acids precedes the development of intrauterine growth restriction in rats fed a low protein diet. *The Journal of Physiology*, 576:935–946, 2006.

[69] Carruthers A, DeZutter J, Ganguly A, and Devaskar SU. Will the original glucose transporter isoform please stand up! *American Journal of Physiology Endocrinology and Metabolism*, 297:E836–E848, 2009.

[70] Zhao B, Diraviyam T, and Zhang X. A bio-mathematical approach: Speculations to construct virtual placenta. *Applied Mathematics and Computation*, 256:344–351, 2015.

[71] Sibley CP, Brownbill P, Dilworth M, and Glazier JD. Review: Adaptation in placental nutrient supply to meet fetal growth demand: Implications for programming. *Placenta*, 31:S70–S74, 2010.

[72] Paolini CL, Marconi AM, Ronzoni S, Di Noio M, Fennessey PV, Pardi G, and Battaglia FC. Placental transport of leucine, phenylalanine, glycine, and proline in intrauterine growth-restricted pregnancies. *The Journal of Clinical Endocrinology and Metabolism*, 86:5427–5432, 2001.

[73] Cleal JK, Glazier JD, Ntani G, Crozier SR, Day PE, Harvey NC, Robinson SM, Cooper C, Godfrey KM, Hanson MA, and Lewis RM. Facilitated transporters mediate net efflux of amino acids to the fetus across the basal membrane of the placental syncytiotrophoblast. *The Journal of Physiology*, 589:987–997, 2011.

[74] Philipps AF, Holzman IR, Teng C, and Battaglia FC. Tissue concentrations of free amino acids in term human placentas. *American Journal of Obstetrics and Gynecology*, 131:881–887, 1978.

[75] Wagner CA, Lang F, and Bröer S. Function and structure of heterodimeric amino acid transporters. *American Journal of Physiology – Cell Physiology*, 281:C1077–C1093, 2001.

[76] Jóźwik M, Teng C, Wilkening RB, Meschia G, and Battaglia FC. Reciprocal inhibition of umbilical uptake within groups of amino acids. *American Journal of Physiology – Endocrinology And Metabolism*, 286:E376–E383, 2004.

[77] Friedman MH. *Principles and Models of Biological Transport*. Springer-Verlag, New York NY, USA, 2008.

[78] Devés R and Krupka RM. A simple experimental approach to the determination of carrier transport parameters for unlabeled substrate analogs. *Biochimica et Biophysica Acta (BBA) – Biomembranes*, 556:524–532, 1979.

[79] Jacquez JA. The kinetics of carrier-mediated transport: stationary-state approximations. *Biochimica et Biophysica Acta (BBA) - Specialized Section on Biophysical Subjects*, 79:318–328, 1964.

[80] Segel LA and Slemrod M. The quasi-steady state assumption: a case study in perturbation. *SIAM Review*, 31:446–477, 1989.

[81] Blumenthal R and Kedem O. Flux ratio and driving forces in a model of active transport. *Biophysical Journal*, 9:432–446, 1969.

[82] Fotiadis D, Kanai Y, and Palacín M. The SLC3 and SLC7 families of amino acid transporters. *Molecular Aspects of Medicine*, 34:139–158, 2013.

[83] Glazier JD, Jones CJP, and Sibley CP. Purification and $Na^+$ uptake by human placental microvillus membrane vesicles prepared by three different methods. *Biochimica et Biophysica Acta (BBA) – Biomembranes*, 945:127–134, 1988.

[84] Mahendran D, Donnai P, Glazier JD, D′Souza SW, Boyd RD, and Sibley CP. Amino acid (system A) transporter activity in microvillous membrane vesicles from the placentas of appropriate and small for gestational age babies. *Pediatric Research*, 34:661–665, 1993.

[85] Kuruvilla AG, D′Souza SW, Glazier JD, Mahendran D, Maresh MJ, and Sibley CP. Altered activity of the system A amino acid transporter in microvillous membrane vesicles from placentas of macrosomic babies born to diabetic women. *The Journal of Clinical Investigation*, 1994:689–695, 1994.

[86] Ganapathy ME, Leibach FH, Mahesh VB, Howard JC, Devoe LD, and Ganapathy V. Characterization of tryptophan transport in human placental brush-border membrane vesicles. *The Biochemical Journal*, 238:201–208, 1986.

[87] Tsitsiou E, Sibley CP, D′Souza SW, Catanescu O, Jacobsen DW, and Glazier JD. Homocysteine transport by systems L, A and y+L across the microvillous plasma membrane of human placenta. *The Journal of Physiology*, 587:4001–4013, 2009.

[88] Harrison LI and Christensen HN. Simulation of differential effects on rates in membrane transport. *Journal of Theoretical Biology*, 49:439–459, 1975.

[89] Pineda M, Fernández E, Torrents D, Estévez R, López C, Camps M, Lloberas J, Zorzano A, and Palacín M. Identification of a membrane protein, LAT-2, that co-expresses with 4F2 heavy chain, an L-type amino acid transport activity with broad specificity for small and large zwitterionic amino acids. *The Journal of Biological Chemistry*, 274:19738–19744, 1999.

[90] Kanai Y, Segawa H, Miyamoto K-i, Uchino H, Takeda E, and Endou H. Expression cloning and characterization of a transporter for large neutral amino acids activated by the heavy chain of 4F2 antigen (CD98). *Journal of Biological Chemistry*, 273:23629–23632, 1998.

[91] Ganapathy V, Ganapathy ME, Tiruppathi C, Miyamoto Y, Mahesh VB, and Leibach FH. Sodium-gradient-driven, high-affinity, uphill transport of succinate in human placental brush-border membrane vesicles. *The Biochemical Journal*, 249:179–184, 1988.

[92] Bröer S. The SLC38 family of sodium-amino acid co-transporters. *Pflügers Archiv – European Journal of Physiology*, 466:155–172, 2014.

[93] Hatanaka T, Huang W, Wang H, Sugawara M, Prasad PD, Leibach FH, and Ganapathy V. Primary structure, functional characteristics and tissue expression

pattern of human ATA2, a subtype of amino acid transport system A. *Biochimica et Biophysica Acta (BBA) – Biomembranes*, 1467:1–6, 2000.

[94] Albers A, Bröer A, Wagner CA, Setiawan I, Lang PA, Kranz EU, Lang F, and Bröer S. $Na^+$ transport by the neural glutamine transporter ATA1. *Pflügers Archiv – European Journal of Physiology*, 443:92–101, 2001.

[95] Mackenzie B, Schäfer MK-H, Erickson JD, Hediger MA, Weihe E, and Varoqui H. Functional properties and cellular distribution of the system A glutamine transporter SNAT1 support specialized roles in central neurons. *Journal of Biological Chemistry*, 278:23720–23730, 2003.

[96] Mackenzie B and Erickson JD. Sodium-coupled neutral amino acid (system N/A) transporters of the SLC38 gene family. *Pflügers Archiv – European Journal of Physiology*, 447:784–795, 2004.

[97] Pradhan RK, Vinnakota KC, Beard DA, and Dash RK. *Carrier-Mediated Transport Through Biomembranes, in Transport in Biological Media.* Elsevier, Boston MA, USA, 2013.

[98] Yao D, Mackenzie B, Ming H, Varoqui H, Zhu H, Hediger MA, and Erickson JD. A novel system A isoform mediating $Na^+$/neutral amino acid cotransport. *The Journal of Biological Chemistry*, 275:22790–22797, 2000.

[99] Zhang Z, Gameiro A, and Grewer C. Highly conserved asparagine 82 controls the interaction of $Na^+$ with the sodium-coupled neutral amino acid transporter SNAT2. *The Journal of Biological Chemistry*, 283:12284–12292, 2008.

[100] Costa PF, Emilio MG, Fernandes PL, Ferreira HG, and Ferreira KG. Determination of ionic permeability coefficients of the plasma membrane of *Xenopus* laevis oocytes under voltage clamp. *The Journal of Physiology*, 413: 199–211, 1989.

[101] Lewis RM, Cleal JK, and Hanson MA. Review: Placenta, evolution and lifelong health. *Placenta*, 33:S28–S32, 2012.

[102] Avagliano L, Garò C, and Marconi AM. Placental amino acids transport in intrauterine growth restriction. *Journal of Pregnancy*, 2012:972562–972567, 2012.

[103] Panitchob N, Widdows KL, Crocker IP, Hanson MA, Johnstone ED, Please CP, Sibley CP, Glazier JD, Lewis RM, and Sengers BG. Computational modelling of amino acid exchange and facilitated transport in placental membrane vesicles. *Journal of Theoretical Biology*, 365:352–364, 2015.

[104] Jones H, Crombleholme T, and Habli M. Regulation of amino acid transporters by adenoviral-mediated human insulin-like growth factor-1 in a mouse model of

placental insufficiency *in vivo* and the human trophoblast line BeWo *in vitro*. *Placenta*, 35:132–138, 2014.

[105] Sibley CP. Understanding placental nutrient transfer – why bother? New biomarkers of fetal growth. *The Journal of Physiology*, 587:3431–3440, 2009.

[106] Cetin I, de Santis MS, Taricco E, Radaelli T, Teng C, Ronzoni S, Spada E, Milani S, and Pardi G. Maternal and fetal amino acid concentrations in normal pregnancies and in pregnancies with gestational diabetes mellitus. *American Journal of Obstetrics and Gynecology*, 192:610–617, 2005.

[107] Mayhew TM. A stereological perspective on placental morphology in normal and complicated pregnancies. *Journal of Anatomy*, 215:77–90, 2009.

[108] Konje JC, Kaufmann P, Bell SC, and Taylor DJ. A longitudinal study of quantitative uterine blood flow with the use of color power angiography in appropriate for gestational age pregnancies. *American Journal of Obstetrics and Gynecology*, 185:608–613, 2001.

[109] Acharya G, Wilsgaard T, Rosvold Berntsen GK, Maltau JM, and Kiserud T. Reference ranges for umbilical vein blood flow in the second half of pregnancy based on longitudinal data. *Prenatal Diagnosis*, 25:99–111, 2005.

[110] Birdsey TJ, Boyd RD, Sibley CP, and Greenwood SL. Microvillous membrane potential (Em) in villi from first trimester human placenta: Comparison to Em at term. *The American Journal of Physiology*, 273:R1519–R1528, 1997.

[111] Larsson A, Palm M, Hansson LO, and Axelsson O. Reference values for clinical chemistry tests during normal pregnancy. *BJOG: An International Journal of Obstetrics and Gynaecology*, 115:874–881, 2008.

[112] Madelin G, Kline R, Walvick R, and Regatte RR. A method for estimating intracellular sodium concentration and extracellular volume fraction in brain *in vivo* using sodium magnetic resonance imaging. *Scientific Reports*, 4:4763, 2014.

[113] Lee P, Ridout D, Walter J, and Cockburn F. Maternal phenylketonuria: Report from the United Kingdom Registry 1978–97. *Archives of Disease in Childhood*, 90: 143–146, 2005.

[114] O′Connor IA, Veltman K, Huijbregts MAJ, Ragas AMJ, Russel FGM, and Hendriks AJ. Including carrier-mediated transport in oral uptake prediction of nutrients and pharmaceuticals in humans. *Environmental Toxicology and Pharmacology*, 38:938–947, 2014.